Nature, age, and origin of the informal Lower Cenozoic Red Bank group, northern Belize

by

Sandor Ricketts

A thesis submitted to the Graduate Faculty of
Auburn University
in partial fulfillment of the
requirements for the Degree of
Master of Science.

Auburn, Alabama
August 8, 2020

Keywords: clay, Belize, karst, Corozal basin

Approved by

David T. King, Jr., Chair, Professor of Geology
Ashraf Uddin, Professor of Geology
Dr. Stephanie Rogers, Assistant Professor of Research

ABSTRACT

The informal[i] Lower Cenozoic Red Bank group of Belize crops out in several areas of the northern part of the country and is comprised mainly of clay with relatively minor amounts of carbonate and rare evaporite beds. The Red Bank group is of geologic importance because of its relationship to petroleum exploration, specifically the presence of this clay unit causes processing problems in seismic exploration for potential oil accumulations in underlying strata. Previous literature about the geologic nature and origin of the Red Bank group is limited due to earlier proprietary restrictions on publications. It was previously assumed that this stratigraphic unit was a relatively thin, widespread clay deposit across most of northern Belize, but recent research indicates otherwise. Thus, the objectives of this study were to better understand the dimensions of the Red Bank group and its nature and origin. These objectives were achieved using petrographic and cartographic methods. Results indicate that the Red Bank group is much thicker than previously known, is of a different age than assumed before, and has a significantly different depositional environment than was previously suggested. In conclusion, we now know that the Red Bank group is a more complex stratigraphic unit, which has a depositional history linked to global events such as sea-level high-stand.

Subsurface correlation of well log shows that the Red Bank group ranges in thickness from zero to 1800 ft (549 m), as determined from well logs taken in and around the Spanish Lookout and Never Delay oil fields. Further, an analysis of well logs in the study area of northern Belize, showed that the Red Bank has an unconformable relationship with underlying formations, particularly the informal Upper Cretaceous Barton Creek formation. Correlations of

the Red Bank also indicate that the nature of that basal stratigraphic contact is karstic and the Red Bank clay also fills caverns within the Barton Creek. Further, surficial studies of outcrop areas indicate that the Red Bank group itself occurs mainly in a north-west trending, fault-bounded karstic plain (a low-lying area during deposition), and occurs also within thinner, clay-filled Red Bank channel deposits atop the karstic limestone.

Based on stratigraphic analysis of Red Bank nannofossils from outcrops and drill cuttings, the present study identified the chronostratigraphic position of the group as late Paleocene to early Eocene, not Miocene as earlier reports suggested. Late Paleocene to early Eocene period was a time interval of several notable global events, including the PETM (Paleocene-Eocene Thermal Maximum) global climatic event and significant high and low sea-level stands. Potential evidence of the PETM can be seen in the Red Bank group as evaporite-rich beds within the clay. Whereas, low sea-level stand likely was related to karst development in the underlying limestone; high sea-level stand likely was related to transgressive sedimentation of the Red Bank clays, which is interpreted here to have occurred within an estuarine setting, based on the Red Bank's clay mineralogy and microfossil content.

Information gleaned from the present study of the Red Bank group will help in future petroleum exploration activity in northern Belize because the dimensions and characteristics of the Red Bank group can be better accommodated in seismic processing and modeling of that area. Future work in this area would be to more thoroughly map the Red Bank group in outcrop and correlate it more widely in the subsurface.

ACKNOWLEDGMENT

The accomplishment of this project was both difficult and exciting, and I could not have succeeded without the help of faculty staff and students of the Auburn Geoscience department, for which I am most grateful. I would also like to extend thanks to the staff of the Geology and Petroleum Department of Belize for all their assistance in obtaining samples and data used in this research.

To analyze my samples, I enlisted the assistance of:

1. Nicholas R Myers, Sr., at Paleo-Data, Inc, for his expertise as a nannofossil paleontologist and biostratigrapher for biostratigraphic analysis of samples.
2. Dr. Dan Larsen, Chair of Earth Science at the University of Memphis for his expertise in X-ray powder diffraction analysis.

Special thanks to Dr. David King, Jr., for inviting and involving me in the project.

To all friends and family who played a part in me accomplishing my goal, I am extremely grateful.

Though things may seem difficult,

dedication, strength, and encouragement

can help you along your journey.

Table of Contents

List of Figures

1 INTRODUCTION

The geology of Central America is complex and composed of a variety of lithologies, including volcanic and sedimentary rocks, which exhibit various degrees of alteration, from mountain ranges, and comprise multiple sedimentary basins (Figure 1) (Rica et al., 2007). Belize (formerly British Honduras), the focus of this study, is located on the eastern coast of the Yucatan peninsula and is south of Mexico and east of Guatemala. The Geology of Belize is as diverse as the rest of the region, including the Maya Mountains. These mountains are a tectonic, igneous/metamorphic mountain range (Figure 2A), protruding approximately 3,688 ft (1,124 m), above a relatively flat topography. The Maya Mountains are situated along the western border of Belize and extend to the southern region of the country. The remaining topography of Belize is much lower with a maximum elevation of approximately 344 ft (144 m). This lower elevation of the country is divided into two main sedimentary basins, the Corozal basin to the north and the Belize basin to the south (Figure 2A). These two basins along with the Maya Mountains constitute the more significant structural features of the country (Purdy et al., 2003). The Corozal Basin is divided into the Blue Creek sub-basin, the Orange Walk

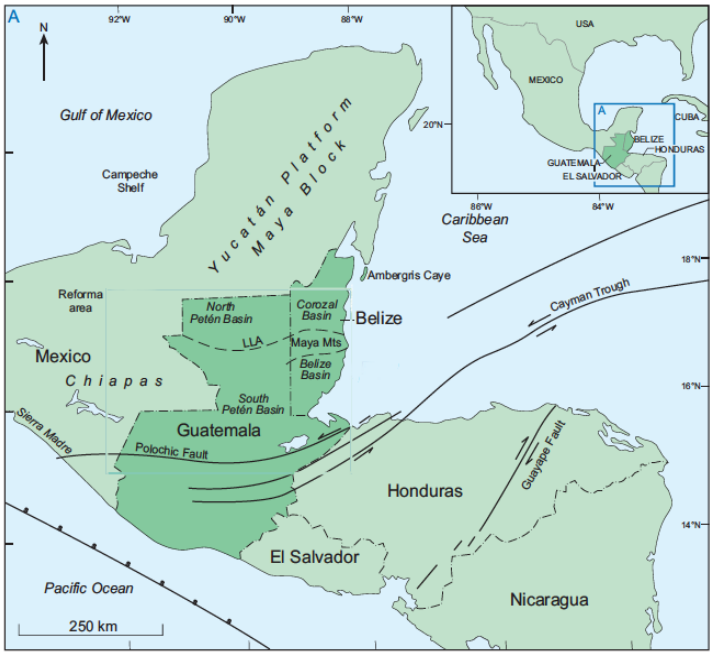

Figure 1. Regional tectonic setting of Central America showing the sedimentary basins of Guatemala and Belize (from Petersen et al., 2012)

sub-basin, and the Belmopan-Shipstern Ridge are considered less significant structures (Figure 2B) (Aitken and Stewart, 2002).

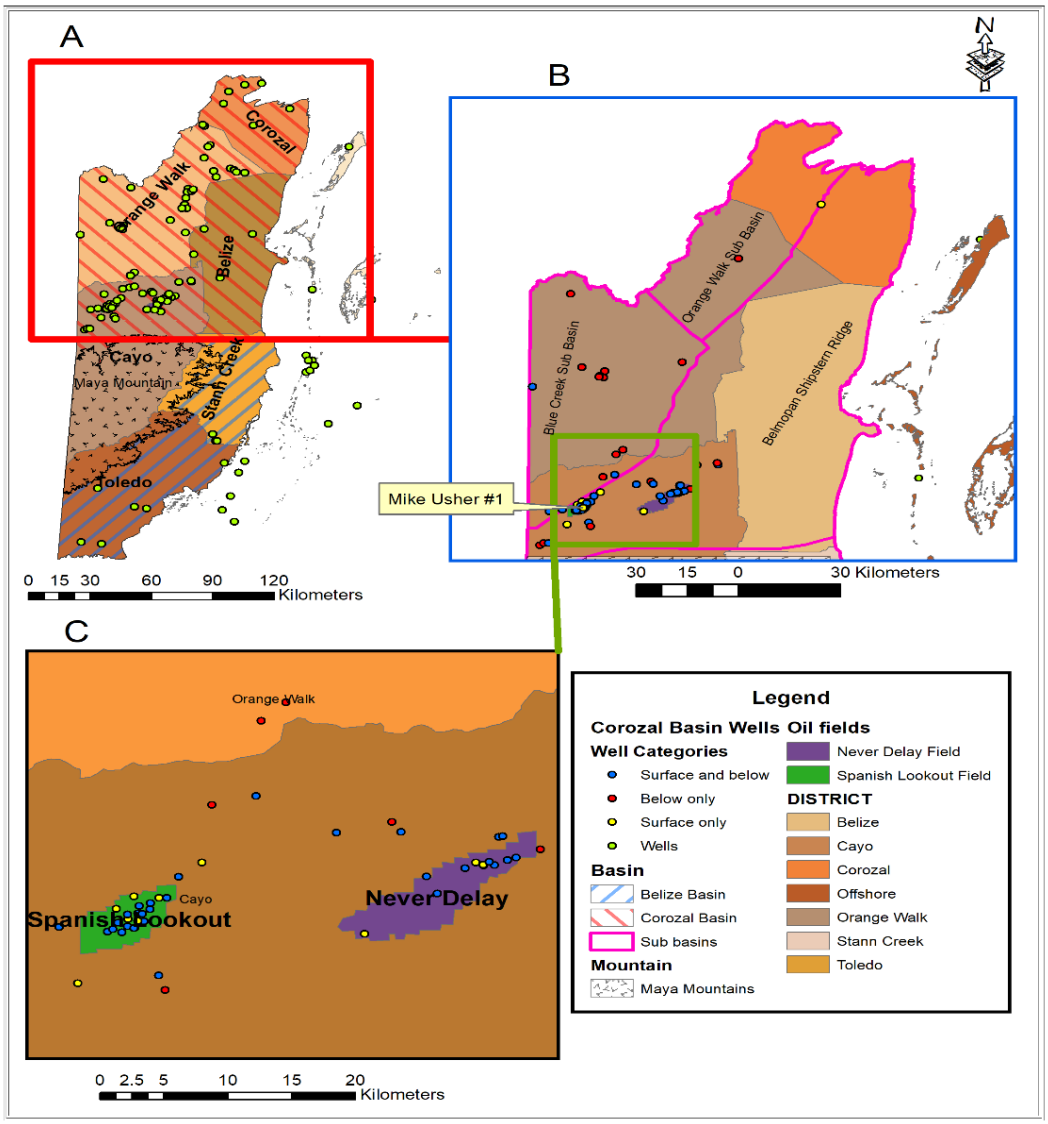

Figure 2. Map of Belize showing, A) the six districts and the wells drilled to date. B) Close-up view of the Corozal basin, showing the recent wells drilled and the location of Mike Usher #1. C) Location of the oil fields and wells in the Corozal basin[ii].

Numerous expeditions (starting 1878, pre-independence) attempted to map the Maya Mountains along with the juxtaposed basins (Ower, 1927) and continued after 1981 with the country's independence (Lewis, 2000). Despite the previous mapping projects many aspects of

the country's geology are still unknown or inaccurately portrayed, and all the stratigraphic units in Belize are informal (King et al., 2004). Inconsistencies aside, there is considerable knowledge about Belize's geology and geological history. Most of the information acquired on the geology up until the 1930s was based solely on outcrops. A shift from predominantly outcrop mapping occurred with the start of hydrocarbon exploration in the 1930s heralding a new era of exploration to now include a subsurface dimension to the study of the geology in Belize. This exploration period included the drilling of 59 wells between 1955 and 1997. Even though no hydrocarbons were discovered, a plethora of information was unearthed. This greatly enhanced the information of the country's geology including work done by Purdy et al. (2003), with a focus on the geology of the Belize Basin and offshore Belize.

The first commercially successful petroleum well was drilled in 2005, Mike Usher #1 (Figure 2B). This well was drilled north of the Maya Mountains in the Corozal basin to a depth of 1054 m (3459 ft). During drilling, lithologic samples were collected, identified, and analyzed. Samples collected included clays, carbonates, anhydrite, sands, and sandstones. An additional eighty-one wells were completed by 2016, mostly in the Corozal basin. Of these, twenty-six wells were successful for petroleum, thus resulting in the development of two oil fields, Spanish Lookout and Never Delay (Figure 2C). The geology of the fields is similar but key differences include formation thicknesses, units pinching out, and missing stratigraphic sections. There was one distinctive difference however, the presence of a thick clay deposit atop the Spanish Lookout field, not previously discussed. These clay deposits are known as the Red Bank group (RBG). They overlie the other formations in several wells, lack economic hydrocarbons, and were deemed 'unimportant' and thus were not investigated or studied in detail.

Though it lacked economic value for hydrocarbon exploration, knowledge of the clay deposit is of great scientific and educational importance for the country's geologic history. One such study involved investigating how mainland lithologies influenced the offshore distribution of clay on the Belize shelf. With regards to the country's climate and drainage (Scott, 1975). The Belizean geologic records contained very little onshore information on clay in particular the Red Bank Clay, (Ower, 1927; 1928; Flores, 1952) until recently. King et al. (2018) undertook a study to determine the age of the sections of the Red Bank clay deposits of the Spanish Lookout area using outcrop observations and some limited nannofossil studies.

Building on the initial study, this project utilizes subsurface samples of the Red Bank clay from various well-bores located within the Corozal basin. The samples were analyzed based on biostratigraphy to establish an age of the deposit. The origin and composition of the deposit were established using petrographic and mineralogical analysis. While the depositional environment and the factors affecting the deposition of the Red Bank clays were analyzed based on local tectonic events, erosional events, and global sea-level changes. Information obtained from this study can be applied to other such deposits, not previously studied, in the country, and compared to similar regional karst clay deposits (Lary et al., 2018).

2 OBJECTIVES

The project focused on expanding the work started by King et al. (2018) undertaken on outcrop samples of the informal[i]. RBG. In their study, King et al. (2018) established the chronostratigraphic period of the clay (Figure 3). This project correlated the biostratigraphic age established by King et al. (2018) from outcrop samples with the analysis of well-bore samples previously collected within the Corozal basin (Figure 4), to determine the time period of deposition for both the outcrop and subsurface samples thus the depositional age range. Along with establishing the age range of the deposit this study will:

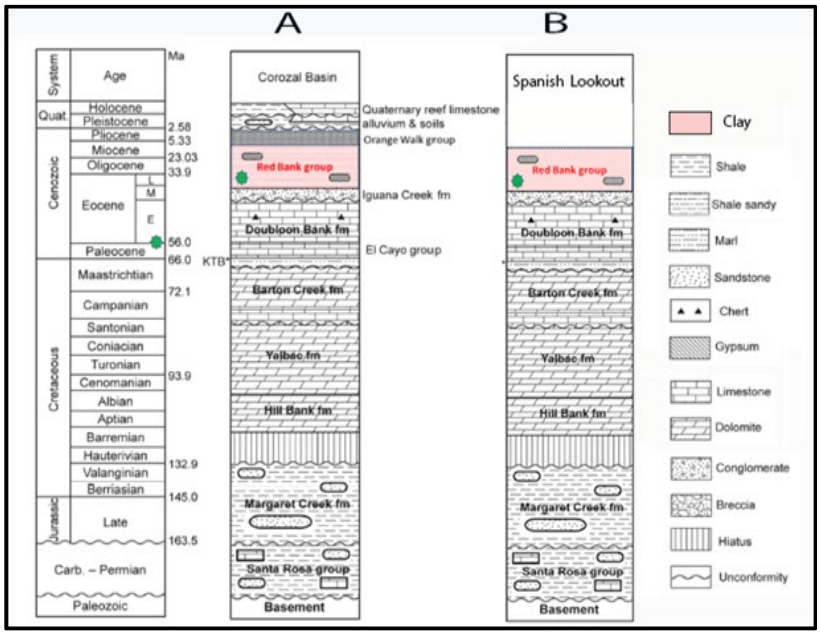

Figure 3. Stratigraphic columns of Corozal basin (A) and Spanish Lookout (B) showing the stratigraphic position and previously accepted age (based on nannofossil biostratigraphy) of the Red Bank group and other units. King et at (2018) sampled Red Bank outcrops in the Spanish Lookout area at the approximate location of the green dots; finding Early Cenozoic nannofossils (see dot at left), thus indicating for the first time that the age of the Red Bank is incorrect. Modified from King et al. (2018).

1. Define the extent and distribution of the deposit, based on lithologic log analysis.
2. Identify facies changes within the clay, using petrographic and mineralogical analysis.
3. Determine the sea level at the time of deposition, based on the biostratigraphic age of the deposit combined with existing sea-level records.

4. Define the depositional environment of the Red Bank deposit based on the petrographic and mineralogical analysis.

The information obtained from this study will create a framework for identifying such thick deposits of clay that were never previously identified. The knowledge can then be incorporated into future hydrocarbon exploration, to reduce errors during seismic interpretation. Unanticipated karst and thick clay deposits tend to deflect the seismic waves, resulting in multiple reflections which can be misinterpreted as formation changes leading to an inaccurate prognosis.

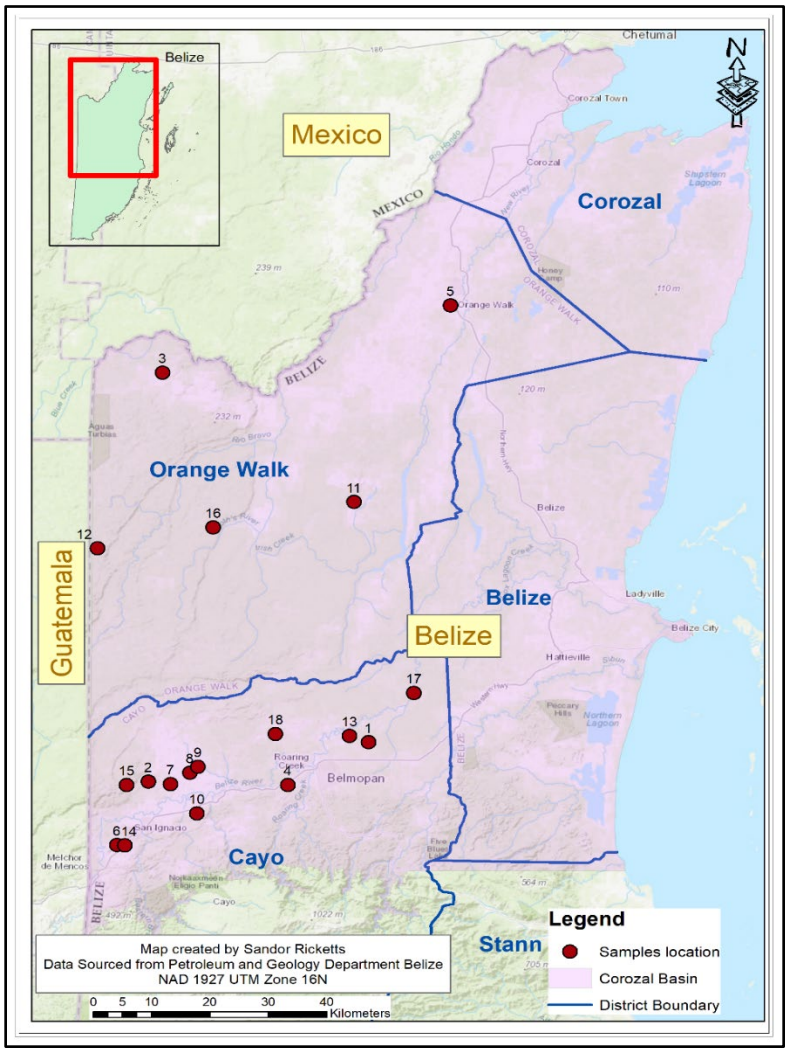

Figure 4. Map showing location of drilled wells from which subsurface samples were requested to be used in this study. Wells numbered 1-18, names listed in Table 2.

3 PREVIOUS RESEARCH

Geological surveys of the British colony of British Honduras (Belize) began in the mid-late 1800s. Fowler (1878-1879), contained erroneous information attributed to bad weather, while G. H. Wilson (1886) died before being able to complete his work (Ower, 1927), both projects generated maps though flawed or incomplete. Several other surveying attempts were made between 1886 and 1921, though none of them were able to give a complete account of the geology of the country (Ower, 1927).

In the mid-late 1920s, Leslie H. Ower completed an extensive survey of the country, from which he generated a map (Appendix I) and published four papers (Ower, 1927), within which he discussed the geomorphology and geology of the country along with vegetation and native people (Flores, 1952). An account was given of the mountainous region with the highest peak, Cockscomb Peak, approximately 3800 ft (1.158 km) above sea level as part of the Maya Mountains range. His report indicated outcrops of rocks of varying biostratigraphically from Upper Carboniferous to post-Pliocene (Table 1). Throughout his papers, Ower makes rare note of clay outcrops; he describes sandy clay in some places and ferruginous sandy clay in other places, all constituting portions of the coastal alluvium. Throughout Ower's writing, there was no mention of the unit that would become Flores' Red Bank group.

Table 1. Lithologies and respective interpreted time-stratigraphy from Ower's (1928) report.

Lithology	Time-stratigraphy
Coastal alluvium	Post Pliocene
Toledo beds	Miocene
Rio Dulce limestone and chalky marl	Oligocene
	Miocene
Acid igneous intrusions	Permo-Carboniferous
Slate series	Late Carboniferous

Giovanni Flores work during the early 1950s studied the northern portion and the coastal plain of Belize. This study was part of his work for the Bahama Exploration Company, Ltd. in which he reviewed previous work completed by Ower and others. In his review of Ower's reports, he noted two significant inconsistencies: (1) outcrops described in the text were not properly represented on the map, and; (2) the age of outcrops discussed in the reports had no good supporting paleontological evidence (i.e., they seemed only to have been inferred by stratigraphic position). As part of his fact-finding mission, Flores collected a variety of fossils from different localities. From his analysis, no samples that could be assigned to Oligocene were noted, and none matched the localities described by Ower. The fossils collected (mainly from limestones) represented taxa that were then assigned to Upper Cretaceous, Paleocene-lower Eocene, middle Eocene, and Miocene-Pleistocene strata. Flores went on to explain that the map presented by Ower displays limestone across much of northern Belize. He found this to not be the case as his field mapping identified other strata, including a series of clays deposited across wide areas. Flores (1952) described the new RBG as a sandy clay forming the old coastal plain east of the Maya Mountains, which overlies a limestone unit (the Barton Creek formation). He described some outcrops of clay in northern Belize as a "sequence of mottled bentonitic pelites with gypsum-crystal inclusions and layers and an admixed component of volcanic ash". King et al. (2018) investigated the depositional environment of the RBG describing it as "a very low coastal tidal flat area, akin to the modern Waddenzee of the Netherlands' coast". The informal 'type locality'[iii] for Red bank was an exposure that Flores found (but that no longer exists) near the town of Red Bank on the Belize River. The town is not existing today but was included on the map within Owers' (1927) (Appendix I). Flores (1952) interpreted that the age of Red Bank ranged

from Miocene to Pleistocene, using predominantly long-ranging megafossils (Appendix II, and II). Several other studies have since been completed on Belize, including E. G. Purdy (1952) and Jean Cornec (2004) both producing geology maps of the country. The map generated by Cornec is the most recent being published in 2004 (updates have been published online since 2004) (Appendix IV). This map has formed the foundation for various other studies. One such study focused on the stratigraphy of northern Belize and its various informal stratigraphic units (King et al., 2004). Other surficial geological studies on northern Belize include those on the Margaret Creek formation (King and Petruny, 2012), the Barton Creek formation (King and Petruny, 2012), and the Orange Walk group (King et al., 2003). As noted earlier, all formations and groups in Belize are informal, hence the lower-case rank terms. Subsurface studies published in the open literature on northern Belize strata are very few (e.g., Purdy et al., 2003, Gill et al., 2018).

Several focused studies on clay in Belize have been published over the years including a general overview of the distribution of clay minerals by Scott, (1975). In a more specific report on the Red Bank group of clays since Flores' work, King et al. (2018), also using outcrop samples, investigated the variations of this group of clays. In this paper, the group is described as a series of clayey sedimentary facies containing gypsum, silica-rich sections, and some micritic limestone

(Figure 5). An initial paleontological study undertaken on the nannofossils (King et al., 2018) indicated that they were Early Cenozoic and were index species ranging from late Paleocene to early Eocene (Figure 3). The fossils analyzed were all from outcrops (Appendix V) because subsurface samples were not available for that study. That initial study on the Red Bank group identified three distinct facies differentiated by color: tan, red and black clay, two of which contained fossils. Unfortunately, no fossils were found in the black clay. The tan sections of clay contained fossils of *Prinsius bisulcus*, an early Eocene index fossil, along with *Toweius tovae*, a late Paleocene index fossil. In contrast, the reddish sections of clay contained *Toweius tovae*, relating to late Paleocene. This nannofossil work by King et al. (2018) suggested an age range for the Red Bank group from the late Paleocene to early Eocene.

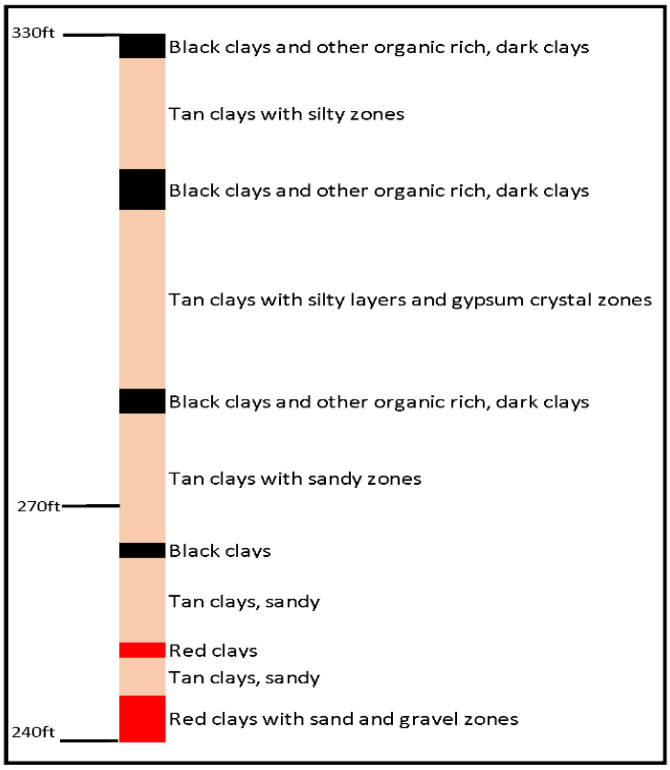

Figure 5. Stratigraphic sketch of a 90 ft thick Red Bank clay section based on outcrops along road cut in Spanish Lookout, Belize. Color changes depict possible facies changes. Modified from King et al. (2018).

Even with hydrocarbon exploration and development, little has been written on the Corozal basin, especially the type of basin and its specific origin concerning the geological history of Belize. This basin has been compared to a thermal subsidence basin (Fisher and King, 2015), with a thickening upward stratigraphic profile (Mann, 1999), though it has not been formally classified as such. The physiography of the basin is described as being divided into two sub-basins, juxtaposed against the Belmopan-Shipstern Ridge (Aitken and Stewart, 2002) (Figure 6). It is within the southwestern region Belmopan-Shipstern Ridge area that the thickest deposit of Red Bank clay was identified based on well log analysis (Figure 6).

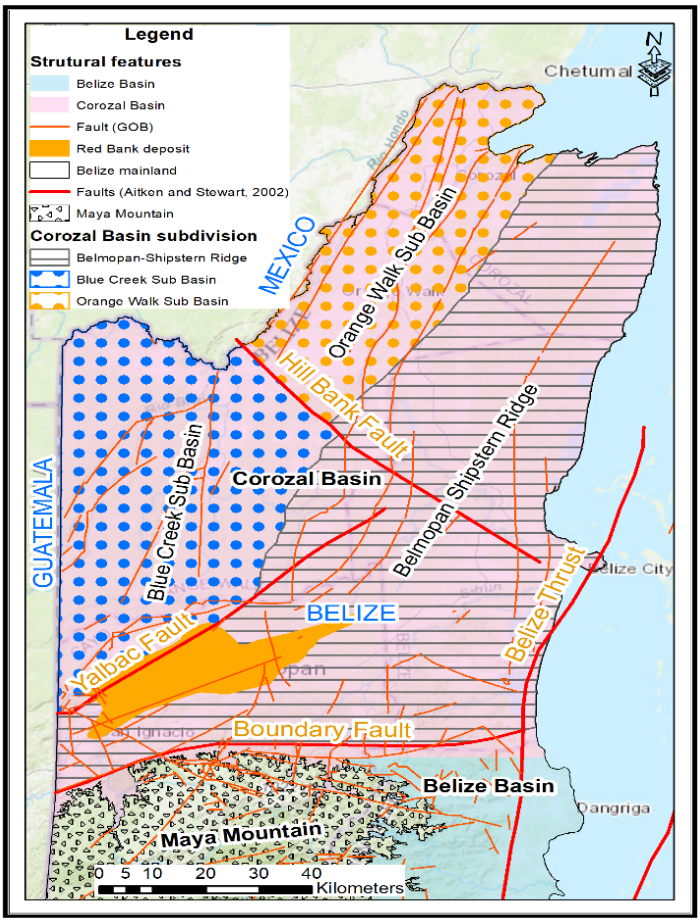

Figure 6. Corozal Basin subdivision, major faults indicated by think red lines.

4 METHODOLOGY

To achieve the objectives of the study, previously recorded information was analyzed for data relevant to the study area, and combined with results of sample analysis (Table 2). This was done using lithologic logs of recent wells in the Corozal Basin. The wells were then categorized based on the thickness of clay and proximity of the deposit to the surface. Samples were then selected from the identified wells to use in the study. Next was determining the age of the subsurface samples based on nannofossil identification. Other analyses used on the samples used include petrographic analysis to determine mineralogical and lithological variations that would constitute facies changes. While mineralogical analysis had a dual component, a) quantifying sediments, obtained while separating clay for XRD analysis, and b) identification of clay groups by XRD analysis. Determination of the sea level during the deposition of the clay was next, obtained by using the biostratigraphic age combined with sea-level records. The final step was determining the depositional environment, obtained using mineralogical and sea level data. The steps listed will be explained in more detail below.

Table 2. List of data sources and studies executed on samples illustrating the expected results

Data Analysis			Paleo-environment	Sample Analysis		
Mudlog	**E-log**	**Seismic Survey**	**Sea level records**	**Biostratigraphy**	**Petrography**	**X-ray Diffraction**
Well and sample	Variations in reading	Reflectors	Karst formation	Age from nannofossils	Mineral identification	Clay identification
Contact depth	Changes in lithology	Lithology changes	Clay deposition	Facies changes	Lithology Identification	Paleoenvironment
Facies changes	Facies changes	Facies changes	Facies changes	Sea level changes	Sedimentary characteristics	Sea-Level Changes
GIS Model						

Nature, age, and origin of the informal Lower Cenozoic Red Bank group

4.1 Well and Sample selection

This study expands on all previous work on the Red Bank by analyzing subsurface samples (cuttings) previously collected from various wellbores during hydrocarbon exploration between 2006 and 2013 (recent wells) (Figure 7). Relevant cuttings along with supporting documents for the study wells were obtained with permission from Geology and Petroleum Office (GPO) in Belmopan, Belize, (including mud logs and available e-logs). The wells used in the study represent 12.7% of the wells drilled since 1955 and samples requested were based on the occurrence of clay within the wellbore (Figure 7). Clay in the wellbore was determined by the interpretation of mud logs (i.e., the graphical representation of vertical lithology). The mudlog analysis identified sixty-eight viable wells that were subdivided into three categories (Figure 8). Included wells containing: (1) clay from the surface only; (2) clay from the surface and within limestone; and (3) clay only within limestone all identified as different locations across the study area (Figure 9).

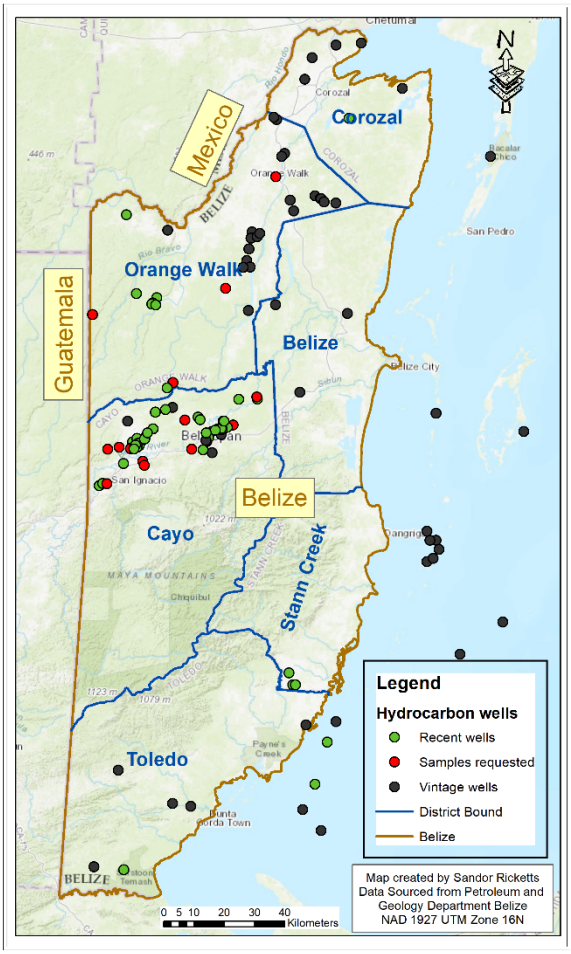

Figure 7. Location of Hydrocarbon exploration wells and requested sample locations.

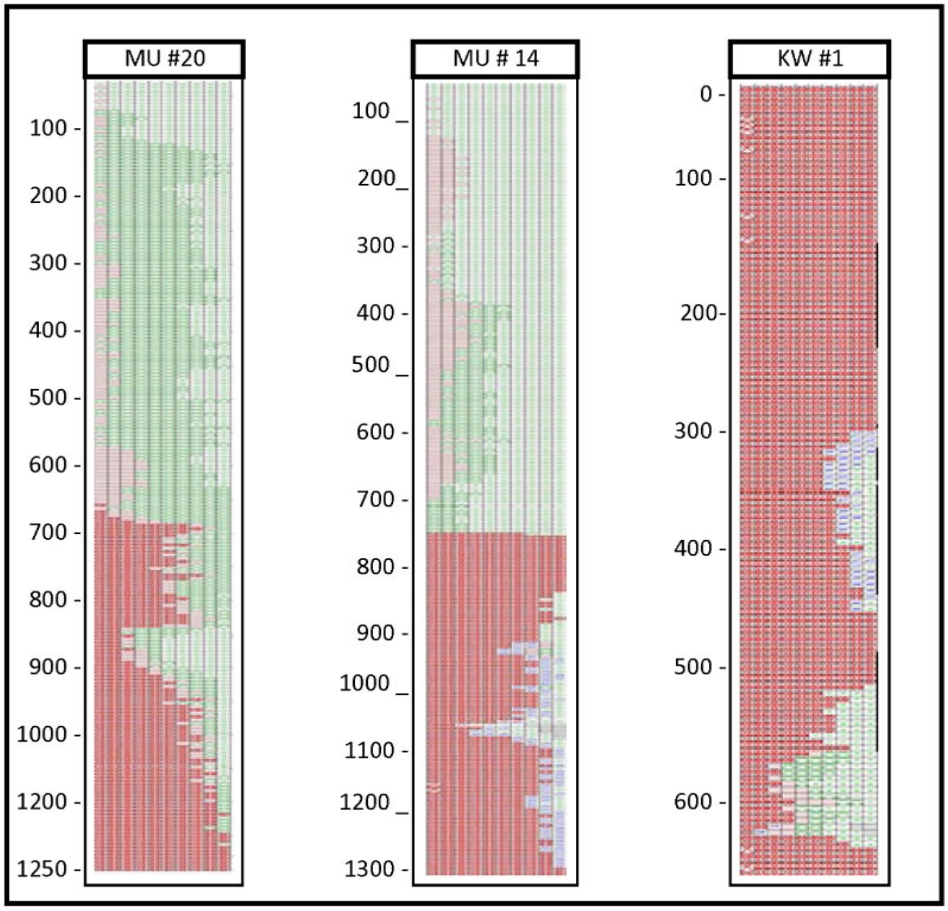

Figure 8. Lithic log segments from Mike Usher (MU) and Kay Works (KW) wells, located in northern Belize, illustrated in figure 9. Wells show clay and claystone (green), gypsum (pink), and limestone (red) in an interval from the karstic top of underlying Upper Cretaceous carbonates and overlying Red Bank group clays. Well logs (Horizon Well Logging Inc., 2016) *are from Geology and Petroleum Department, Belmopan, Belize, used with permission.*

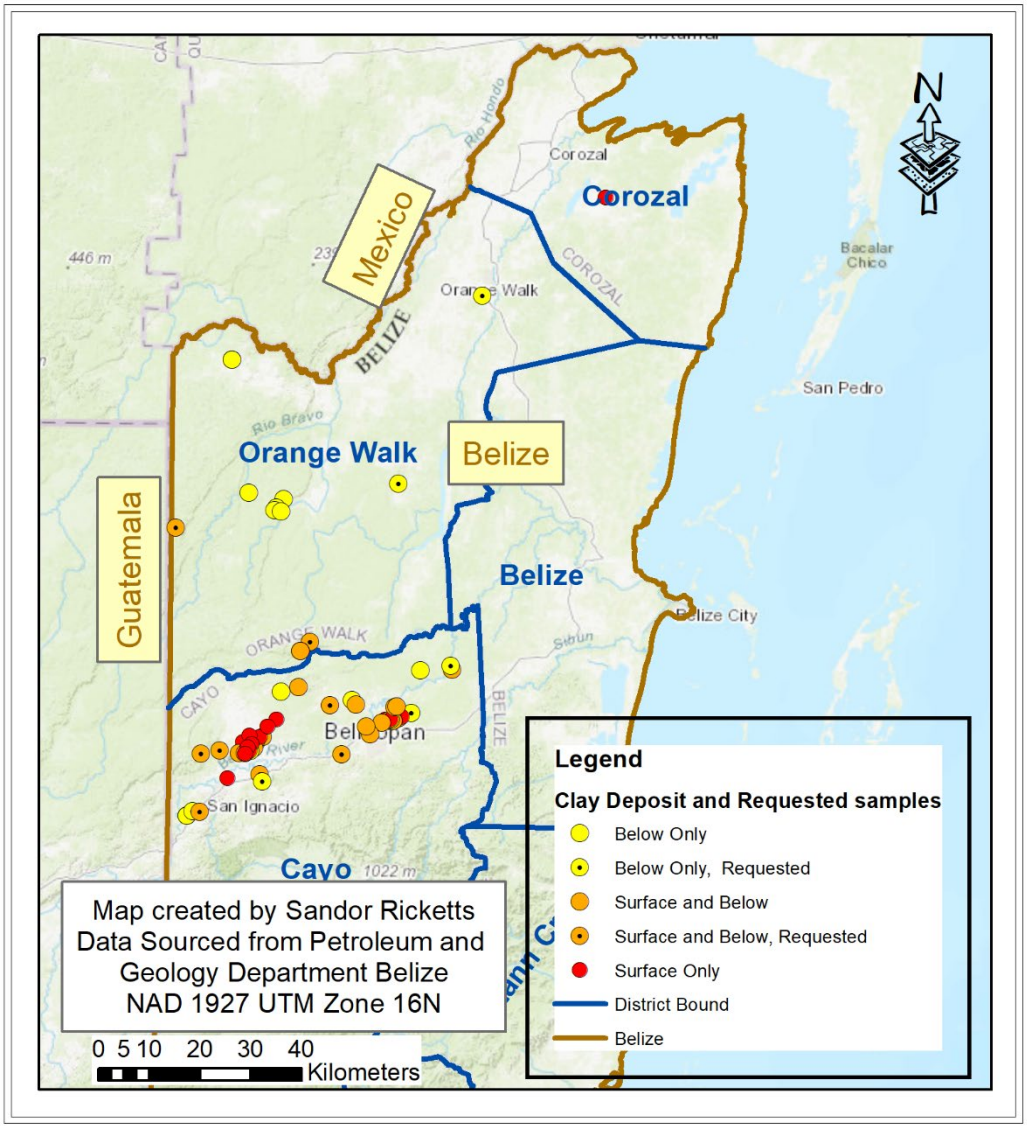

Figure 9. Hydrocarbon wells plotted and categorized based on the location of clay deposits lying upon Upper Cretaceous bedrock (i.e., Red Bank group), as interpreted from mudlogs.

Though sixty-eight wells were identified as containing clay, only twenty were selected for use in the study based on the frequency of samples per well containing more than fifty percent clay as noted from the mudlogs. Fifty-three samples (10 g / each) from the selected wells were requested from GPO. The samples were selected from various depths (Figure 10), the quantity and number of samples received were dependent on availability.

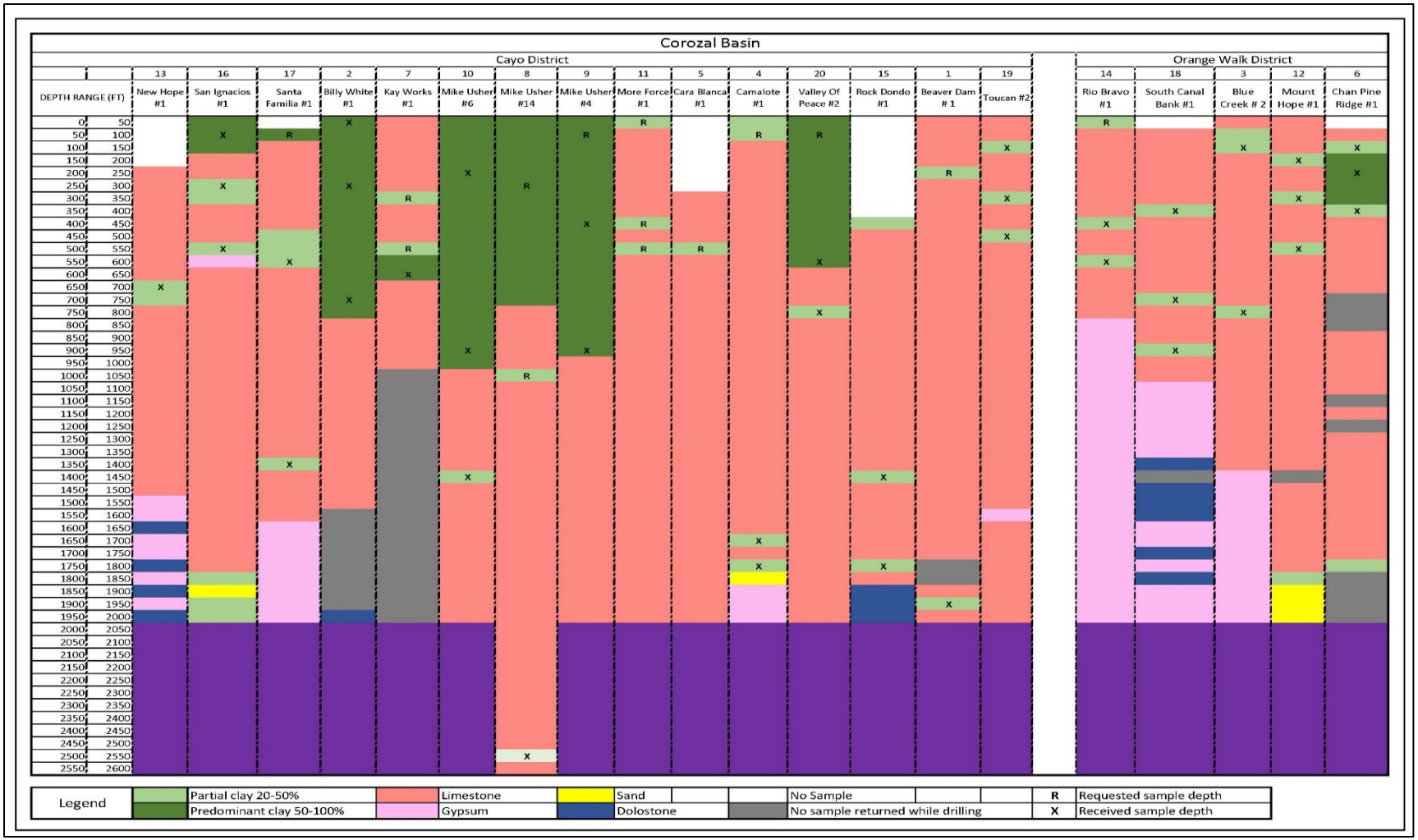

Figure 10. Non-correlated graphic representation of the well-logs (Horizon Well Logging Inc., 2016) *requested from the Geology and Petroleum Office, Belmopan, for the present study. Lithologies are color-coded, but formations are not marked. Generally, the Red Bank is the "predominantly clay" part of the drilled stratigraphic section. Vertical scale in feet, samples marked by R and X.*

4.2 Stratigraphic Analysis

The mudlogs (Figure 11) of the wells were analyzed, to determine which wells recorded clay at the surface and which had clay deposits within the limestone. Coordinates for the wells obtained from mudlogs allowed for the mapping of the surficial extent of the clay deposit. This was done by executing the aggregate point tool within ArcMap on wells with clay outcrops. The resulting image was then modified taking into consideration the distance from data points and the location of wells without outcrops of clay. The subsurface distribution was identified from the thickness of clay sections and occurrence. The depth data for clay to limestone contact was obtained from thirty nine mudlogs and transposed in a tabular form suitable for ArcMap to plot data by depth. This was then imported, plotted and the spatial analyst tool, nearest neighbor used to generate a raster layer representing the unconformity between the clay and underlying limestone. This raster layer was then mergered with the digital elevation model (DEM) of the area, provided by the GPO in Belmopan, to generate a 3D model of the RGB deposit with the 3D Analyst tool in ArcMap. This 3D model surface represents the unconformity between the RBG and limestone and provided a reference point for the rest of this study.

Based on the model, cross-sections were generated of the deposit using the cross-section tool within ArcMap. While seismic line data and shot point data collected during the oil exploration process and interpreted using Kingdom software by GPO, allowed for verification of the 3D model produced from mudlog analysis based on similarities noted from both methods.

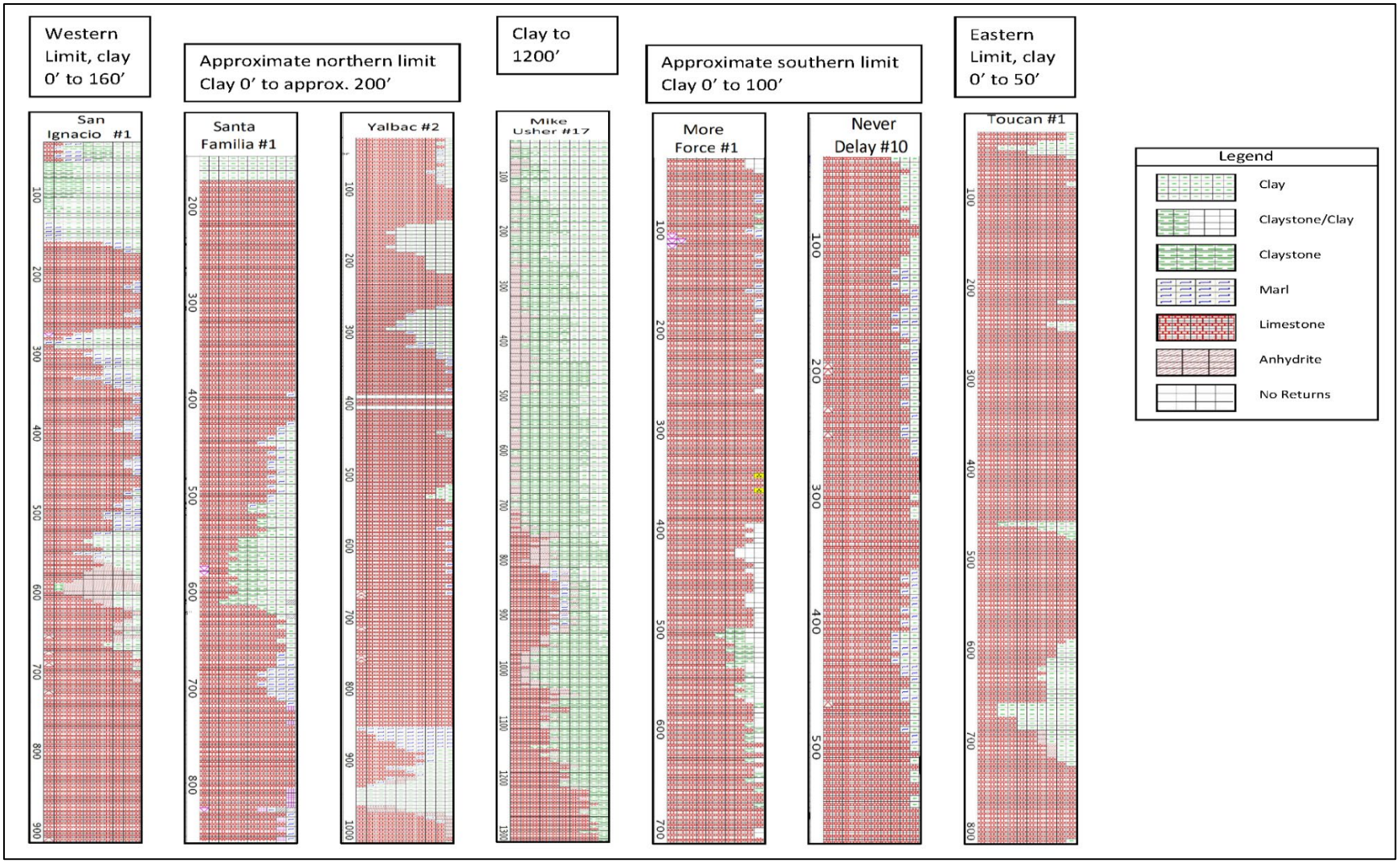

Figure 11. Well-log segments of boreholes (vertical scale in feet) identified in Figure 9 showing clay deposit of varying thickness, influenced by limestone bounded basin. Thickness varies from 20 ft (6 m) to approximately 1200 ft (366 m) in the deepest sections. Wells logs (Horizon Well Logging Inc., 2016) used with permission of GPO, Belmopan.

4.3 Biostratigraphy

To determine a relative age for the RBG approximately three grams of each sample obtained from GPO (Table 3; Figure 10) was shipped to Paleo-Data Inc. in New Orleans for biostratigraphic and biochronostratigraphic analysis. Before undertaking this nannofossil analysis, the team at Paleo Data separated a portion of the sample and placed it in a four-milliliter vial which was then filled with water and left to soak for approximately five minutes. The suspension was mixed with a wooden applicator resulting in a slurry of uniform consistency. Three to four drops of the slurry were then placed on a standard-sized microscope slide using a disposable glass capillary and spread to a uniform thickness. The slides were then dried on a hotplate at low heat, and a coverslip secured with two drops of NOA61 Optical Cement.

The slide with cement was then exposed to ultraviolet light for a minimum of five minutes allowing the cement to harden. Once hardened the excess coverslip and cement were trimmed away with a single-edge razor blade. The slides were then examined using a Leica/Wild stereozoom microscope. Identified nannofossils were used to make smear slides that were analyzed using a Zeiss Axioscop or Axiolab microscope to which a digital camera was attached. To obtain a complete assemblage, a minimum of 400 fields of view was used during the examination process at a magnification of 1,000x or 1,260x. The identified taxa were then digitally documented, counted, and assigned to one of the 13 abundant groups to determine the relative age of the samples (Williams et al., 2018).

Table 3. A list of 39 samples obtained, from 18 wells, illustrated in figure 7. Wells were drilled between 2006 and 2013, during which the samples were collected. Samples were obtained from the Geology and Petroleum Department, Belize.

Well Number	Well Name	Well ID	Quantity	Sample name	Depth range (ft)
1	Beaver dam # 1	BD #1	1	BD #1A	1890-1920
2	Billy White #1	BW #1	3	BW #1A	0-30
				BW #1B	270-300
				BW #1C	720-750
3	Blue Creek # 2	BC #2	2	BC #2A	90-120
				BC #2B	780-810
4	Camalote #1	Cam #1	2	Cam #1A	1680-1710
				Cam #1B	1770-1800
5	Chan Pine Ridge #1	CPR #1	3	CPR #1A	100-120
				CPR #1B	180-200
				CPR #1C	380-400
6	Kay works #1	KW #1	1	KW #1A	630-660
7	Mike Usher # 14	MU #14	1	MU #14	2520-2550
8	Mike Usher #4	Mu #4	2	MU #4A	410-440
				MU #4B	920-950
9	Mike Usher #6	MU #6	3	MU #6A	200-230
				MU #6B	890-920
				MU #6C	1400-1430
10	Mount Hope #1	MH #1	3	MH #1A	190-200
				MH #1B	330-340
				MH #1C	540-550
11	New Hope #1	NH #1	1	NH #1A	690-720
12	Rio Bravo #1	RB #1	2	RB #1A	420-480
				RB #1B	570-600
13	Rock Dondo #1	RD #1	2	RD #1A	1420-1450
				RD #1B	1750-1780
14	San Ignacios #1	SI #1	3	SI #1A	120-140
				SI #1B	280-300
				SI #1C	540-560
15	Santa Familia #1	SF #1	2	SF #1A	570-600
				SF #1B	1390-1400
16	South Canal Bank #1	SCB #1	3	SCB #1A	390-420
				SCB #1B	720-750
				SCB #1C	930-960
17	Toucan #2	Tou #2	3	Tou #2A	30-60
				Tou #2B	330-360
				Tou #2C	480-510
18	Valley Of Peace #2	VP #2	2	VP #2A	540-570
				VP #2B	750-780
	Total samples obtained		39		

4.4 Petrographic Analysis

Petrographic analysis of the samples was undertaken using grain-mount thin sections, created by Wagner Petrographics, LLC in Utah. Approximately 2 grams of each sample was shipped to Wagner for them to create standard thin sections (27 x 46 mm). This was done using vacuum impregnation with blue epoxy and mounted to the thin section glass using blue epoxy (Figure 12). The slides were then ground with an oil lubricant instead of water to prevent swelling of any clay particles.

Figure 12. Picture of sample of standard thin section created by Wagner Petrophysics

Analysis of the thin sections was done using photographs taken with a Nikon DS-Fi1 camera mounted on a Nikon LV-UEPI Illuminator and petrographic microscope set to a magnification of 4x/0.10 using Nikon Polarized lenses. A higher magnification was not required as the main purpose of this analysis was to identify and determine the lithology and percentages of each of the grains, to identify any possible facies changes within the deposit. The NIS Element imaging software (V 4.60.00, build 1171) was used to take the pictures. To obtain a complete image of the slides, individual field of view (fov) pictures were taken using the NIS Element, set to scan large images with a 10% overlap. This allowed for individual fov images to be stitched

together to generate panoramic picture strips. The strips were then merged using photomerge feature in Photoshop 2020 (Figure 13).

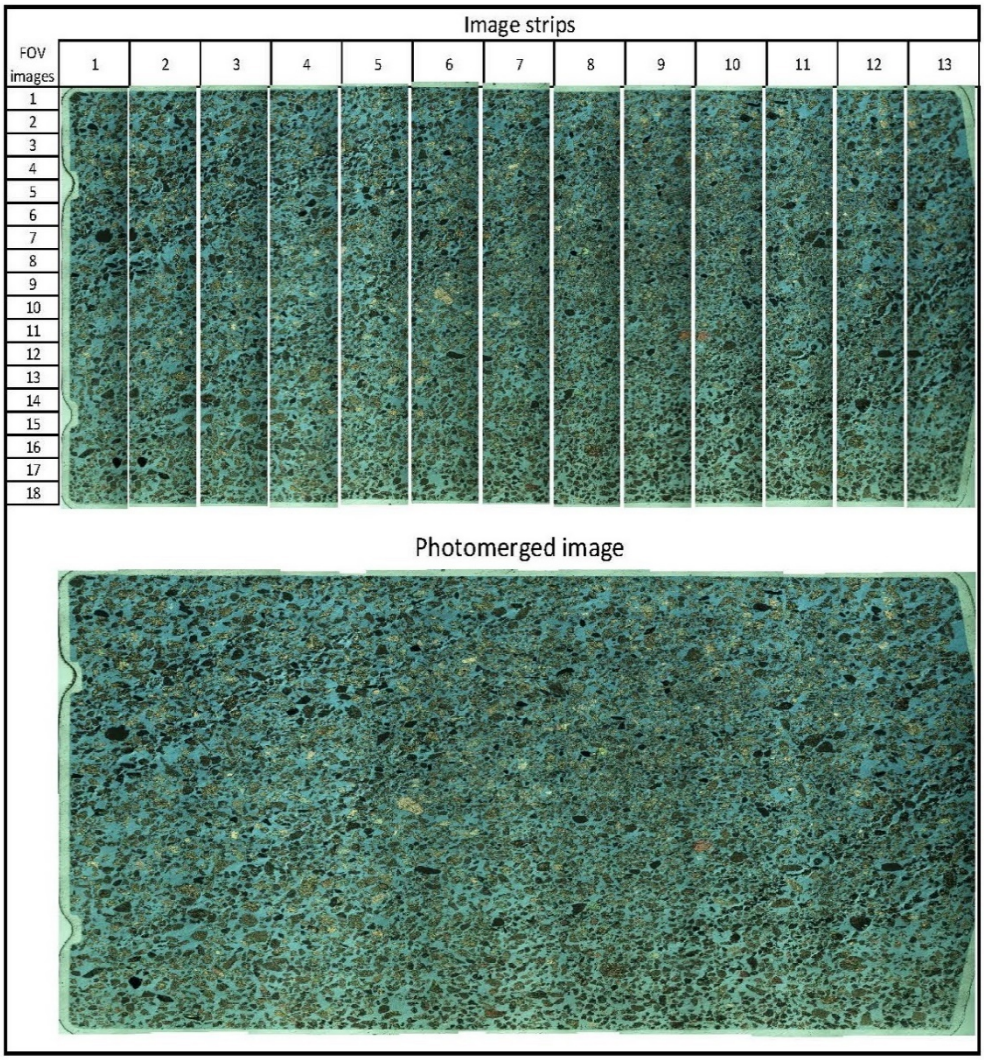

Figure 13. Image stitching and phot-merging of the field of view pictures to create a picture of thin sections, for petrographic analysis.

On compilation of all images, it was noted that the outer fringes of several slides were thinner, due to the grinding process of thin section manufacturing. A rectangle of 16 x 25.5 mm within the center portion of the slides was selected for analysis (Figure 14). This rectangle allowed for some quality control with regards to grain sample quality and area for analysis. An average of 300 grains within the rectangles was then manually identified and classified using the object

extraction feature of the J Microvision software, version 1.3.2 (Figure 15). Grains composed of dolomite, micrite, or limestone were all classified as carbonates, while feldspars, plagioclase, and quartz grains were grouped as framework silicates. The result was then computed and analyzed to identify lithological and mineralogical variations concerning sample depth and well location.

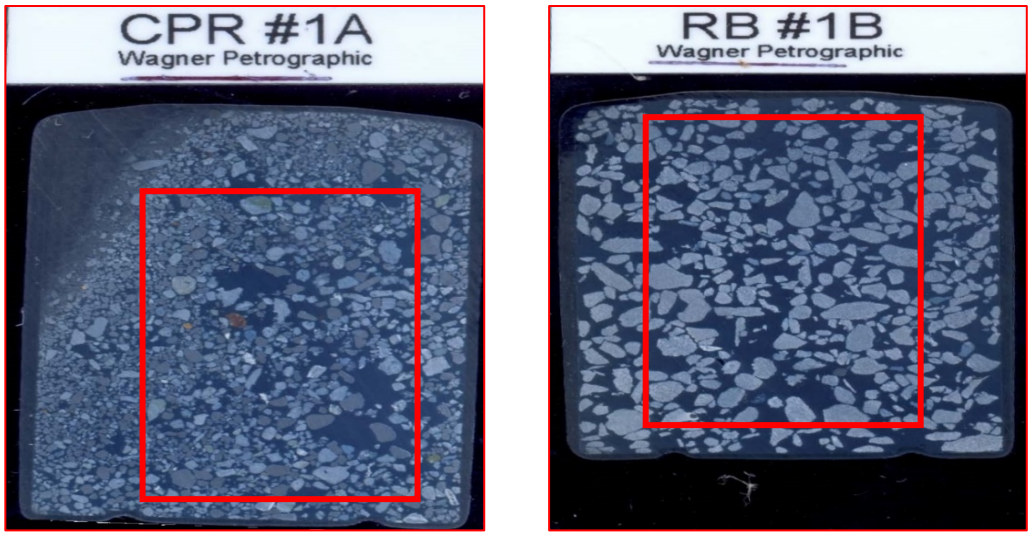

Figure 14 Thin sections with illustration of representative quality control boxes in red (not drawn to scale)

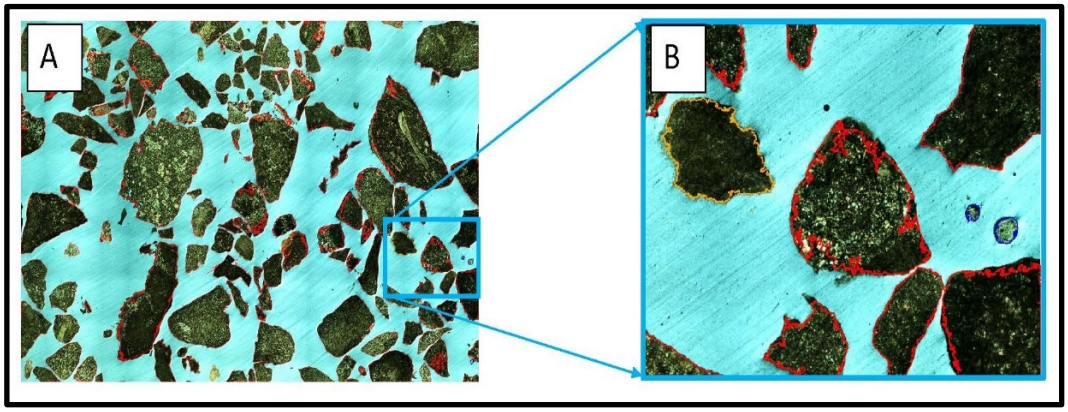

Figure 15. Example of an image not to scale, used for petrographic analysis, A is a cropped image of grain mount thin section, B is a zoomed-in section of an image showing colors around grains. Each color is used to identify a different lithology or mineral group.

4.5 Mineralogy: XRD

The clay-type/mineralogy was investigated using X-ray powder diffraction (XRD) to determine the chemical composition of the clay. Two independent studies (Figure 16) were undertaken, one done on the outcrop (bulk) samples (Appendix V) used in the preliminary study by King et al. (2018), while the other analysis was completed on the subsurface samples obtained from the GPO in Belmopan that were previously mentioned in this study. The subsurface samples were chosen from five wells across the study area to obtain representative mineralogy of the deposit (Figure 17).

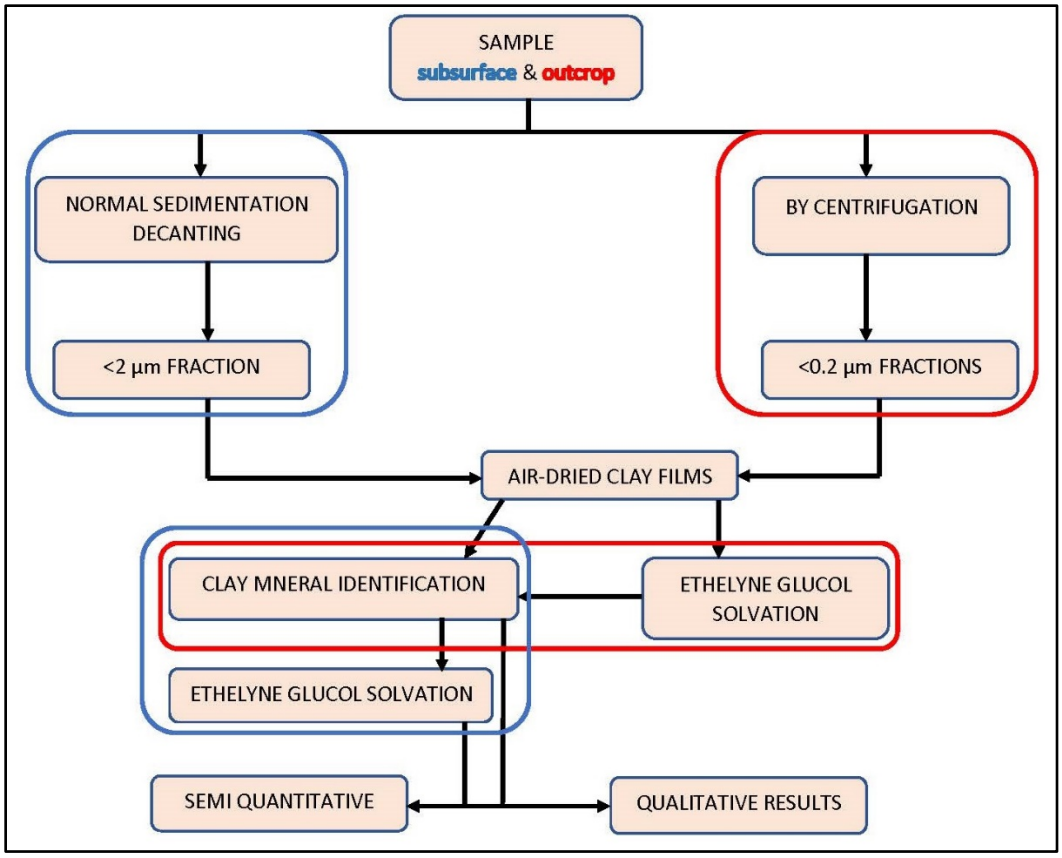

Figure 16. Flow chart of XRD preparation and analysis undertaken on samples. Modified from, Al-Ani and Sarapaa (2008*). Blue boxes indicate the process done on the subsurface sample while the red boxes highlight process applied to outcrop samples.*

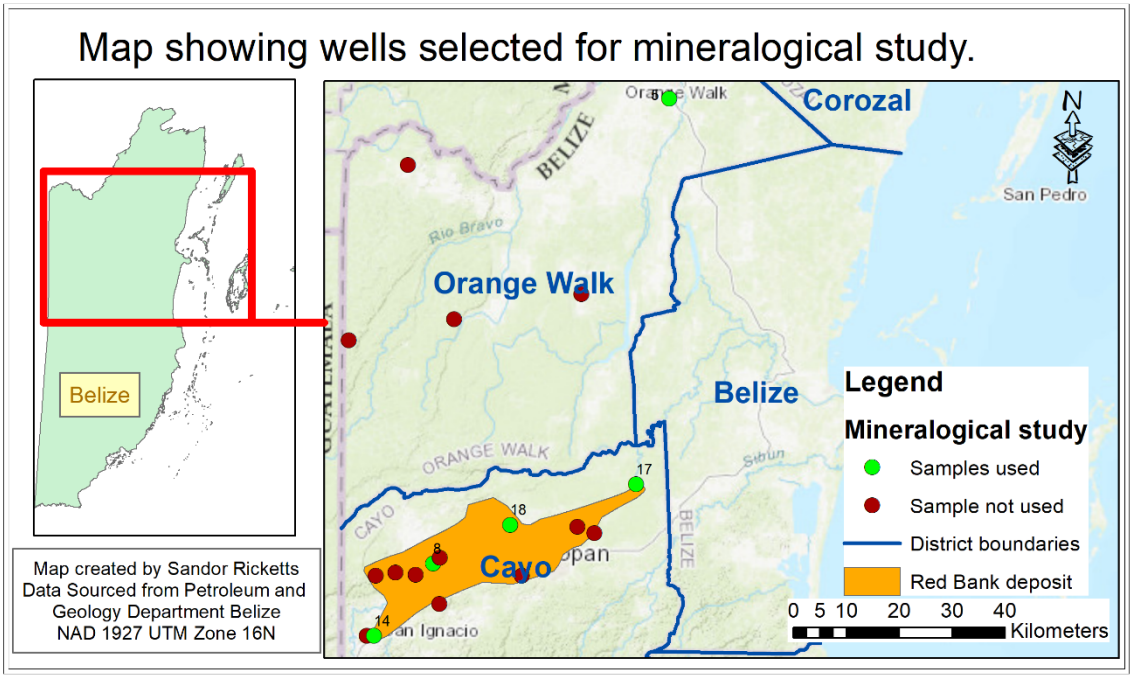

Figure 17. The map indicates the location of wells from which samples were chosen for mineralogical analysis

Both studies utilized two of the three recommended methods for analyzing clay (Moore and Reynolds, 1997). Initial XRD was completed on air-dried samples, followed by an analysis of glycolated samples.

The first study was undertaken by using the guidelines outlined in U.S. Geological Survey Open-File Report 01-041 (Poppe et al., 2001). For this, approximately 2 g from each of thirteen samples (Table 4) were separately mixed with dilute Acetic Acid (1 acid to 4 parts water) and left for 48 hours allowing for the removal of carbonates from the sample. The remaining sediments were then washed with de-ionized water and screened using 2.5 µ filter paper, dried, and weighed. The difference in weight was used to calculate an approximate percentage by weight of the carbonate portion of the sample. The decarbonated samples were then left to soak in 3% hydrogen peroxide solution to remove any organic matter, after which the remaining samples

were again washed, and left to dry on 2.5 μ filter paper. The dry samples were then transferred to graduated plastic centrifuge tubes for decanting to separate any silt and sand from the clay.

The separation was accomplished by decantation based on the small quantity of subsurface clay. This involved soaking the samples in 25 ml of de-ionized water for 12 hours and the tubes subjected to a sonic cleaner, to ensure the clay clumps were disaggregated. The samples were then left to stand for approximately an hour to allow sand and silt particles to settle out of suspension. A plastic pipette was then used to extract 20 ml clay-saturated suspension and put in an 80 ml beaker. An additional 20 ml of deionized water was added to the sample in the pipette and mixed.

Table 4. Samples selected for second independent XRD analysis

Well Number	Well Name	Quantity	Sample number	Initial Weight (g)	Sample pictures
5	Chan Pine Ridge #1	3	CPR #1A	2.0314	
			CPR #1B	2.0338	
			CPR #1C	2.03	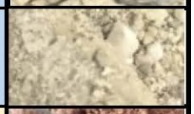
9	Mike usher # 4	2	MU #4A	2.0445	
			MU #4B	2.0053	
14	San Ignacio #1	3	SI #1A	2.0381	
			SI #1B	2.0368	
			SI #1C	2.0359	
17	Toucan #2	3	Tou #2A	2.0279	
			Tou #2B	2.0228	
			Tou #2C	2.0359	
18	Valley of Peace #2	2	VOP #2A	2.0645	
			VOP #2B	2.0738	

The suspension was then left to settle for an hour and clay suspension siphoned out with a pipette. This mixing, settling, and siphoning process was repeated until the suspension in the pipette remained relatively clear. This repeated process maximized clay recovery (Figure 18).

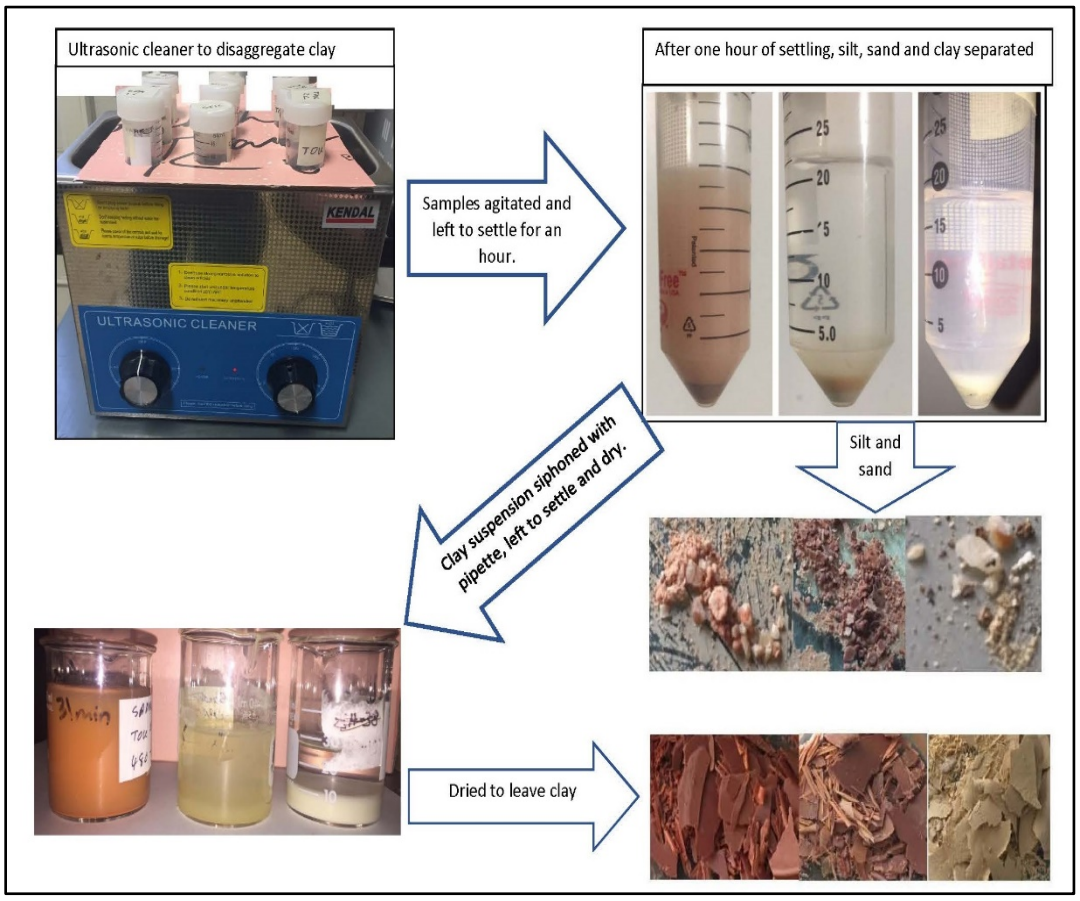

Figure 18. Images of Sequences for sample preparation for XRD.

The recovered clay samples were then crushed/mixed in a small agate mortar and pestle with approximately 4ml of iodized water. The Millipore method was then used to transfer the slurry to a glass slide (Figure 19), to obtain an oriented aggregate mounting of the clay (Moore and Reynolds, 1997). The slides were then left to dehydrate, after which they were placed in on the XRD specimen holder and placed into the Bruker D2 Phaser XRD machine for analysis (Figure 20). Samples were then subjected to Cu Kα radiation from 2° to 45° 2θ using a step of 0.02° 2θ at 2128 steps per second, and the results recorded. The results were then interpreted using DIFFRAC.EVA SUITE version 4.2 software, based on d-values.

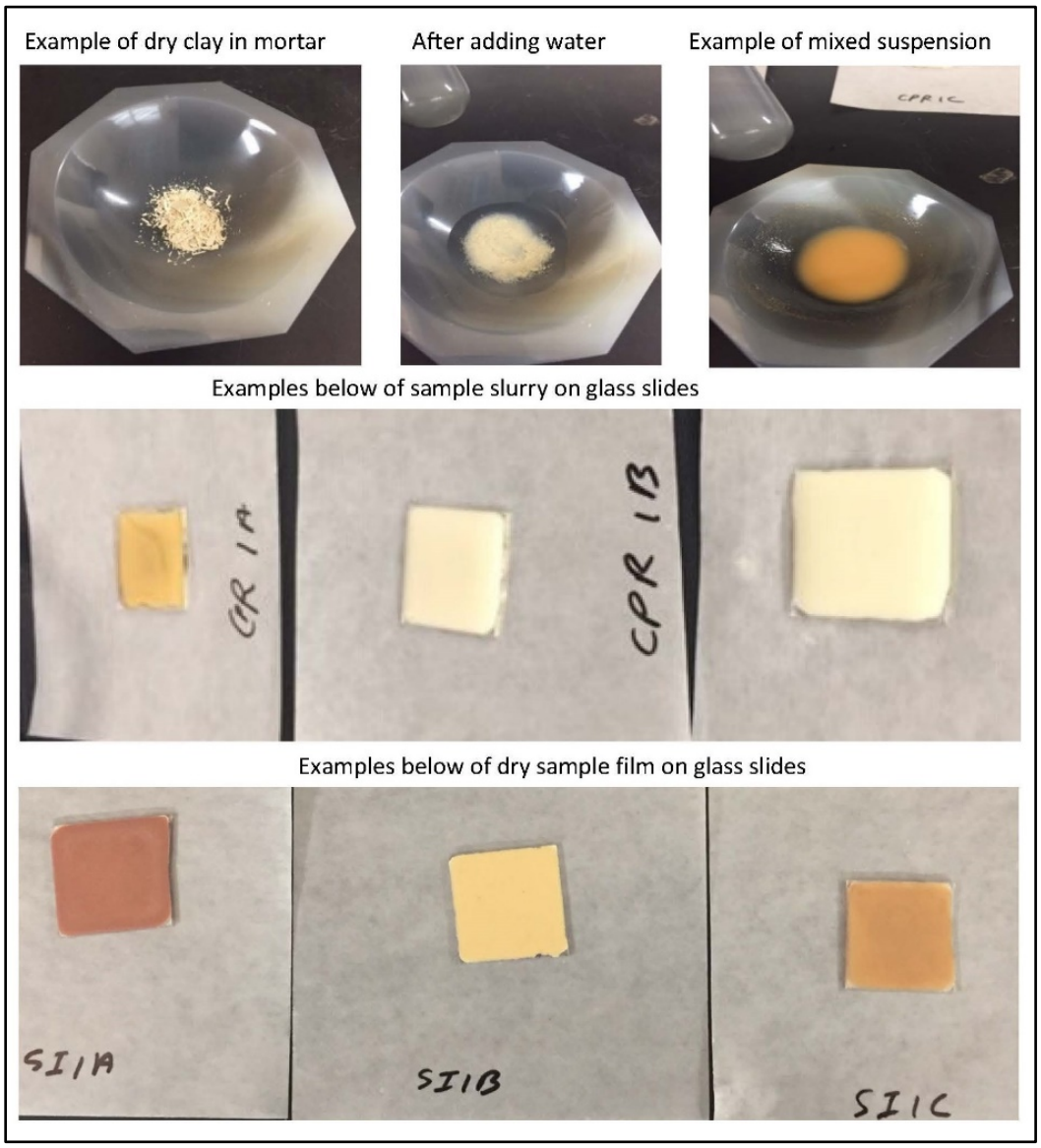

Figure 19. Images of clay sample before initial XRD analysis. The top row shows dry clay to the left, middle after the water had been added, right; clay slurry. The middle row of pictures of clay slurry on a glass slide. Bottom row, pictures of dry sample ready for XRD.

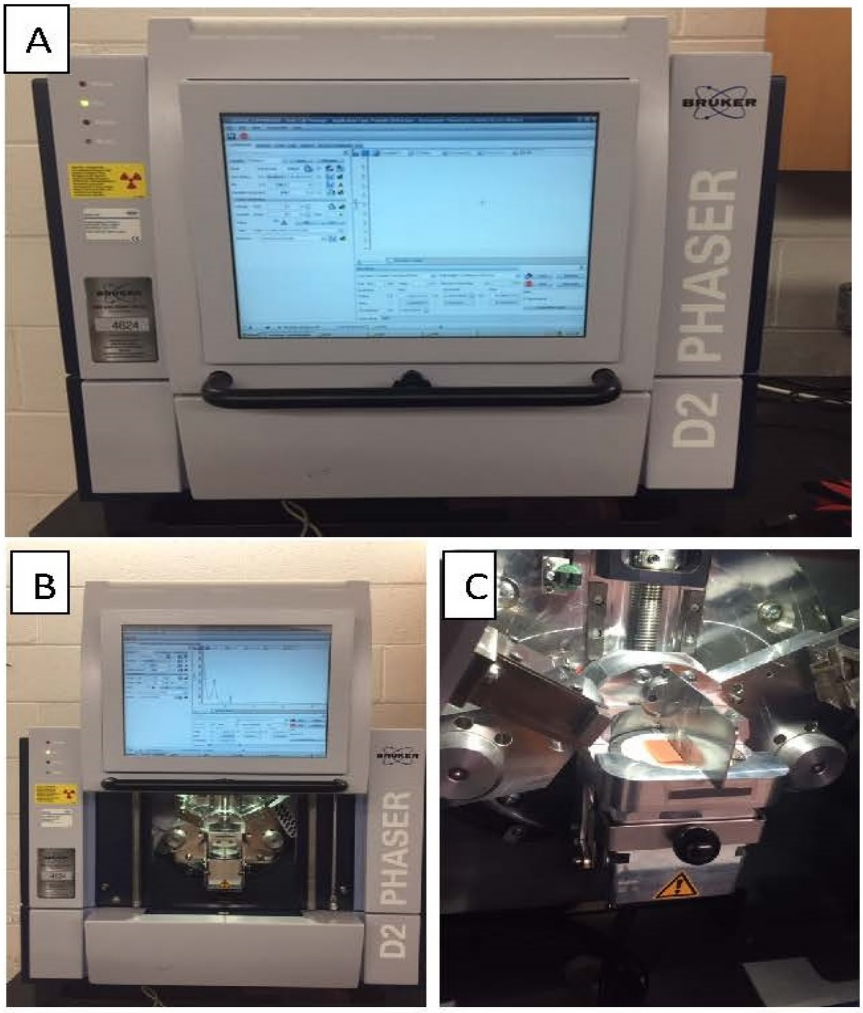

Figure 20. Pictures of the Bruker D2 Phaser XRD machine. A-external view of the machine: B, View of the machine open before loading sample: C, sample loaded in the machine ready for processing.

The final stage in the analysis process was to glycolate the sample by applying 1 to 2 drops to the slide coated with clay. Care was taken not to over-apply glycol with this rapid method. The samples were then left for 24 hours allowing the clay to absorb the oil resulting in swelling of the clay. (Figure 21). The glycolated samples were then analyzed with the XRD machine and the results recorded and interpreted with the aid of the DIFFRAC.EVA SUITE version 4.2 software.

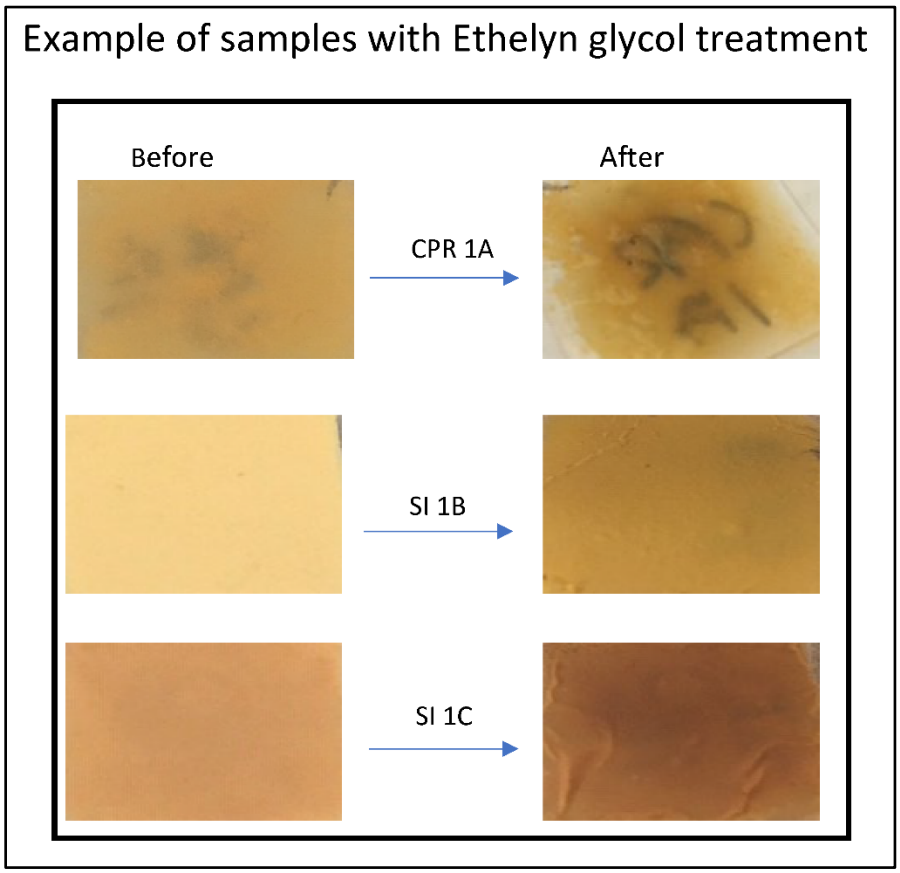

Figure 21. Pictures of samples on a slide before and after Ethylene glycol treatment for XRD analysis.

For the second study, approximately 80 g of each outcrop sample was packed and shipped to Dr. Dan Larsen in the Earth Science department at the University of Memphis for analysis. These samples were then put through multi-part analysis to determine the clay chemistry (Larsen et al., 2015). This multi-part process as described in Larsen et. al. (2015) involved "describing the samples to determine the Munsell color index, grain size and texture, sorting, roundness and general grain shape, framework grain mineralogy, fossils, matrix and cement, and deformation structures. The samples were then disaggregated for powder XRD analysis by crushing with a mortar and pestle, after which clay fraction (<2 mm) was separated by centrifuge, saturated with Mg^{2+} (1 M $MgCl_2$ solution), and mounted on glass slides using the Millipore method (Moore and

Reynolds, 1997). The next stage involved XRD of bulk (random orientation) mounts and oriented clay mounts and was done using a Bruker AXS D8 Advance X-ray diffractometer. Clay mounts were exposed to Cu Kα radiation from 3° to 40° 2θ using a step of 0.04° 2θ at 0.2 seconds per step. The clay mounts were first analyzed under air-dried conditions. The Mg-saturated clay mounts were then solvated at 60 °C for 24 hours or more in an ethylene glycol atmosphere and analyzed again to assess the presence of expandable clays. The abundance of clay mineral species was crudely quantified using peak height and reference intensity concepts (Moore and Reynolds, 1997). The clay abundance categories were defined based on relative peak intensity as follows: abundant, represents minerals with the highest intensity peaks in the pattern; minor, represents minerals with one or more low-intensity peaks; and trace, represents minerals with very low to low-intensity peaks." The intensity peaks were then plotted and interpreted.

4.6 Eustatic Sea Level

To determine the deposition of the RBG in Belize, relevant theories regarding regional (Rosenfeld and Pindell, 2002, 2003; Rosenfeld, 2016) and eustatic sea-level (Miller et al., 2005; Miller, 2009) were investigated and tested. Work by Miller et al., (2005) involved collecting and compiling information relevant to determing sea level change over time. This sea level depth data was used to generate elevations contours corresponding to the age of RBg clay. The contours were then used to clip the DEM raster image of northern Belize to generate illustrations of sea level relevant to the clay deposit.

Belize is located on the eastern coast of the Yucatan peninsula, with the Gulf of Mexico to the North of the peninsula. Petroleum exploration in the Gulf has identified several submarine paleo-canyons that have been attributed to a period of sea-level drawdown during Paleogene (Rosenfeld and Pindell, 2002, 2003; Rosenfeld, 2016). Such a drawdown is theorized to have occurred when the Cuban arc collided with the Yucatán and Bahamas carbonate platform, thus isolating the Gulf of Mexico from the rest of world's oceans (Figure 22).

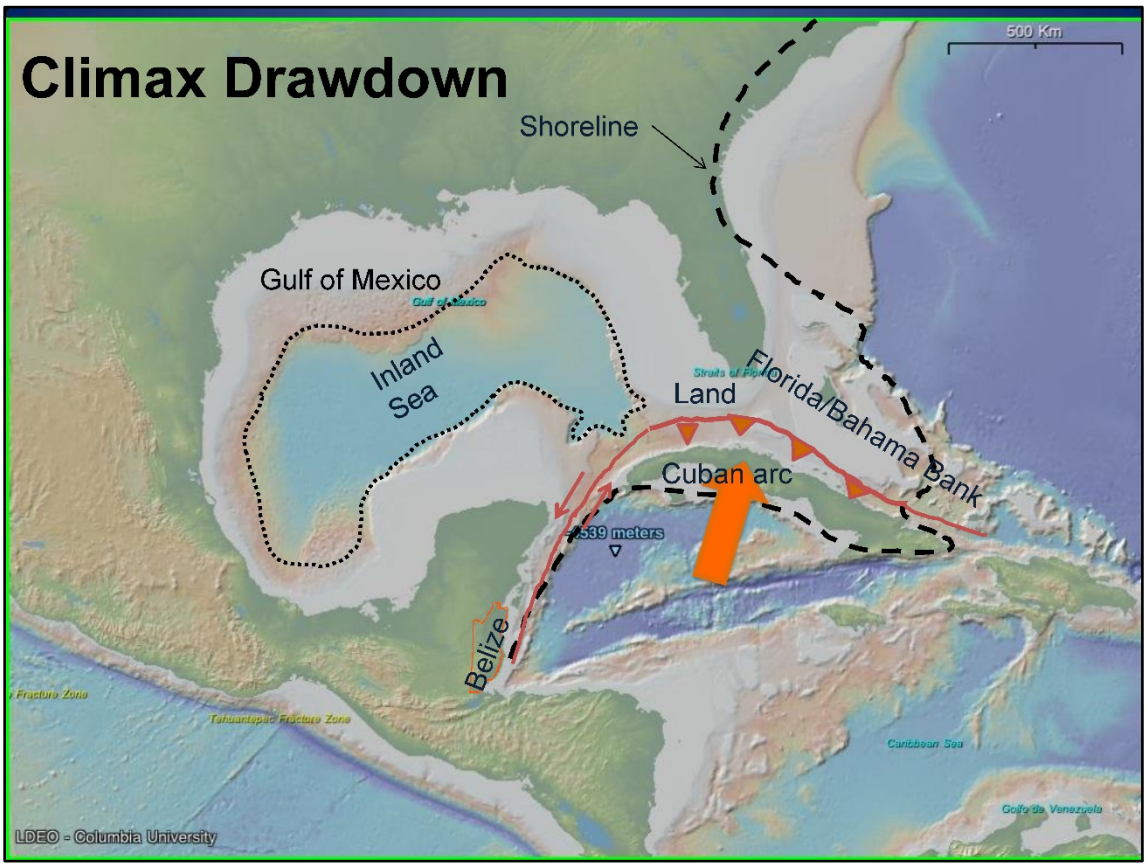

Figure 22. Map showing isolation of the Gulf of Mexico during the Paleocene-Eocene boundary, from the collision of the Cuban Arc with the Florida/ Bahama Block. Modified from (Rosenfeld, 2016).

4.7 Correlation

To achieve the goals of this study a variety of data correlations from various wells was executed including:

4.7.1 Well and Samples

Correlation of well data was based on the interpretation of descriptions of the mudlogs, e-logs, and seismic data. Mudlogs were analyzed for key phrases, “carbonate content”, “clay” along with color descriptions of the clay, the depth at which the phrases occurred were noted for comparison to other wells. The variation of e-logs curves was analyzed by the Geology Department of Belize using Kingdom software to identify lithological variations. Variations were inferred based on computed gamma-ray (CGR) data from spectral gamma-ray logs with a value of 15 as a cut-off for anhydrite, and a cut-off value of 7 for marine versus terrestrial influences (Kansas Geological Survey, 2017). The variations per depth for each well were compared to identify any facies changes, while e-logs were used to identify changes within the deposit. Seismic data were analyzed to identify and define the deposit using the proposed boundary as a guide.

4.7.2 Biostratigraphic

The results of the biostratigraphic analysis of the samples across the study area were correlated to determine the age and span of the episode of RBG deposition. Whereas the type of fossils was compared to previous interpretations of the depth and salinity of the key fossil species present, to determine the most likely paleoenvironment during RBG deposition.

4.7.3 Petrographic

Variation in vertical and lateral distribution of lithic types derived from the petrographic analysis was compared, particularly the lithological percentage changes by depth per well. The results of each well were then correlated to the other wells in the study, to identify any facies changes and any sedimentary packages that could aid in identifying fluctuations in sea level (Haq et al., 1987).

4.7.4 XRD preparation, sediment distribution

Carbonate percentages and variation plus sand/silt quantity and quality, obtained during the XRD sample preparation, were analyzed to determine any facies changes along with an indication of potential sea level variation. The results of the XRD analysis for each sample per depth were compared to the results from the other wells as a means of chemical correlation of the clay sections. Although samples were from different depths, the variations in the results were analyzed to identify any differences that may have resulted from depositional environmental changes, or variations in the source material.

4.7.5 Depositional Environment

Each of the four steps above generates parts of the puzzle to be used in understanding the nature of the RBG. Therefore, the results will be combined and correlated to establish depositional environments.

4.7.6 Sea Level

To establish the effects of sea level on the RBG, the eustatic sea level at the time of deposition was determined, using regional sea-level data from authors such as Rosenfeld (2016), Rosenfeld and Pindell (2003), and global studies of Miller et al. (2005) and Miller (2009). The purpose of this integration and interpretation of Red Bank data with global sea changes was

completed to help determine the effects that dynamic eustatic sea-level changes may have had on depositional processes and the specific depositional environments of the Red Bank group.

5 RESULTS

As described previously, wells selected were categorized for the study based on the presence of clay, as described in the mud logs (Figure 23). These samples obtained were then divided as required for analysis, including petrographic, biostratigraphy, and chemical analysis.

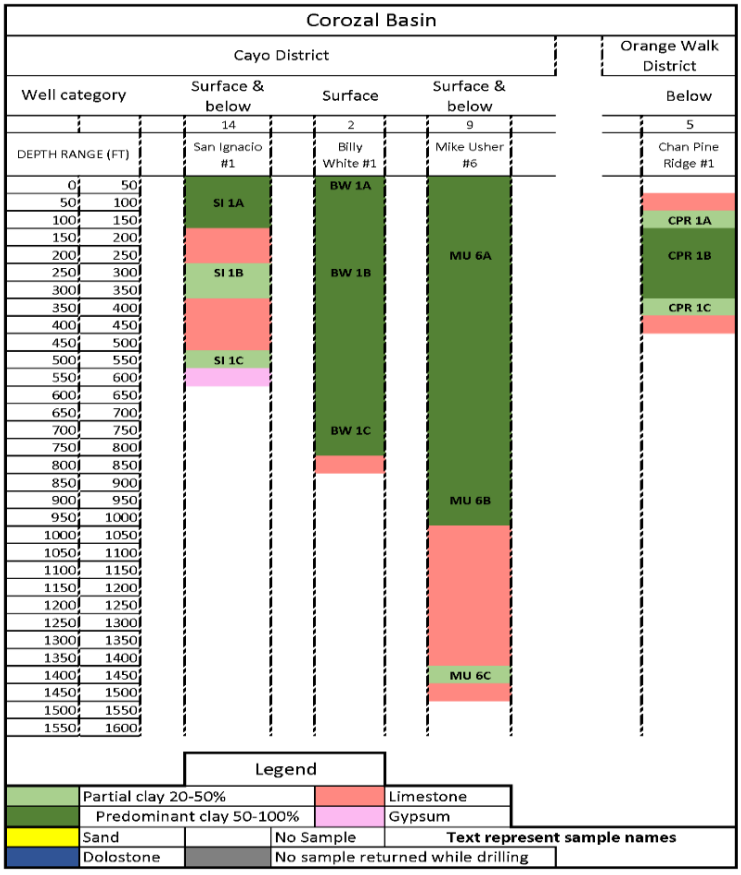

Figure 23. Location by depth of samples representing well categories shown in Figure 25. Vertical scale in feet (Horizon Well Logging Inc., 2016).

5.1 Well and sample selection

Though fifty-three samples (Figure 24) were requested from GPO, only thirty-nine were received and used in the study, selected from 18 wells (Figure 25). The reduction in the number of samples received was due to the availability of sufficient well cuttings.

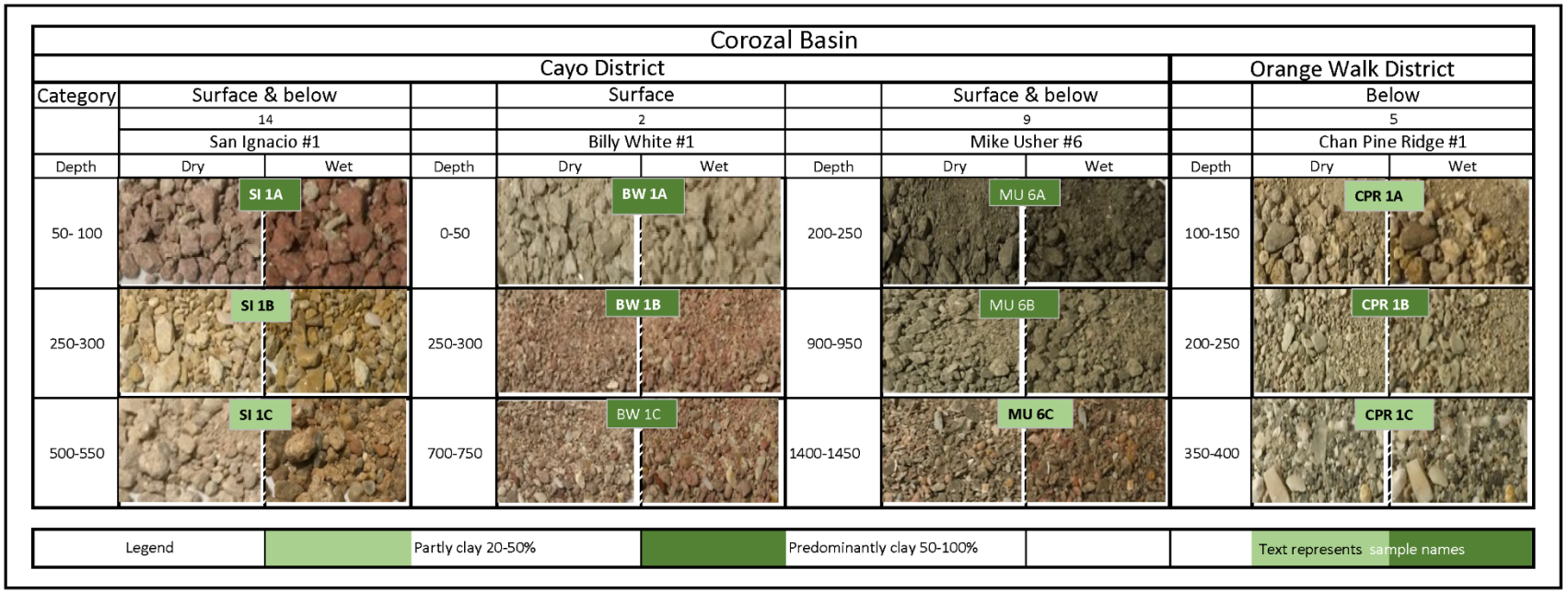

Figure 24. Pictures of samples (well cuttings) and their depth range in four wells, plus the clay percent in each. Sample depth in feet.

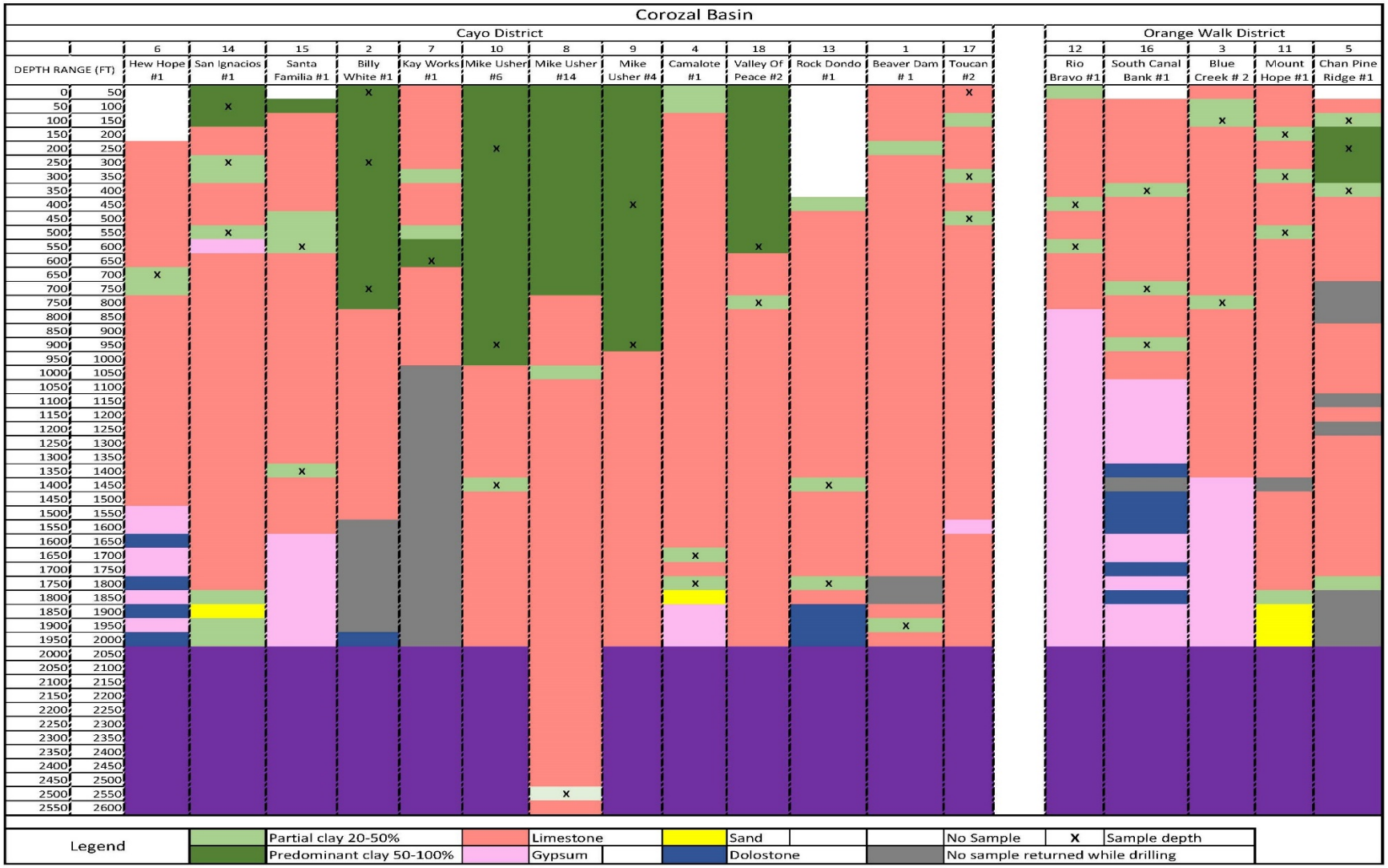

Figure 25: Non-correlated graphic representation of the well-logs available for study in the present report. Lithologies are color-coded, but formations are not marked. Generally, the Red Bank is the "predominantly clay" part of the drilled stratigraphic section. Vertical scale in feet[3] (Horizon Well Logging Inc., 2016).

5.2 Stratigraphic Analysis

This thick deposit of clay is located at the mouth of a regional valley, draining the surrounding Maya Mountain Ridge, which extends also into Guatemala (Figure 27A, and 29B). The RBG deposit extends to a maximum depth of approximately 1800 ft (548.6 m) within a long, linear depression within the limestone. This depression shows no surficial impression discernable on the most recent (2020) Digital Terrain Model (DTM) of Belize or in any 3D rendering (Figure 27C, and 29D). However, the deposit is shown by merging the DEM with the elevation raster of the unconformity surface between the RBG and the underlying limestone (Figure 28).

Multiple depressions and peaks can be identified within the limestone (Figure 28) based on the model generated for the unconformity, with the largest depression extrapolated from the western cluster of wells (Figure 28). The model gives a general overview of the deposit in 3D, however, to generate 2D representations of the unconformity cross-sections were generated (Figure 29) from which varying gradients can be observed. Steep gradients along the northwest and southeast of the deposit coincided with the location of previously reported faults with similar trends (Figure 29).

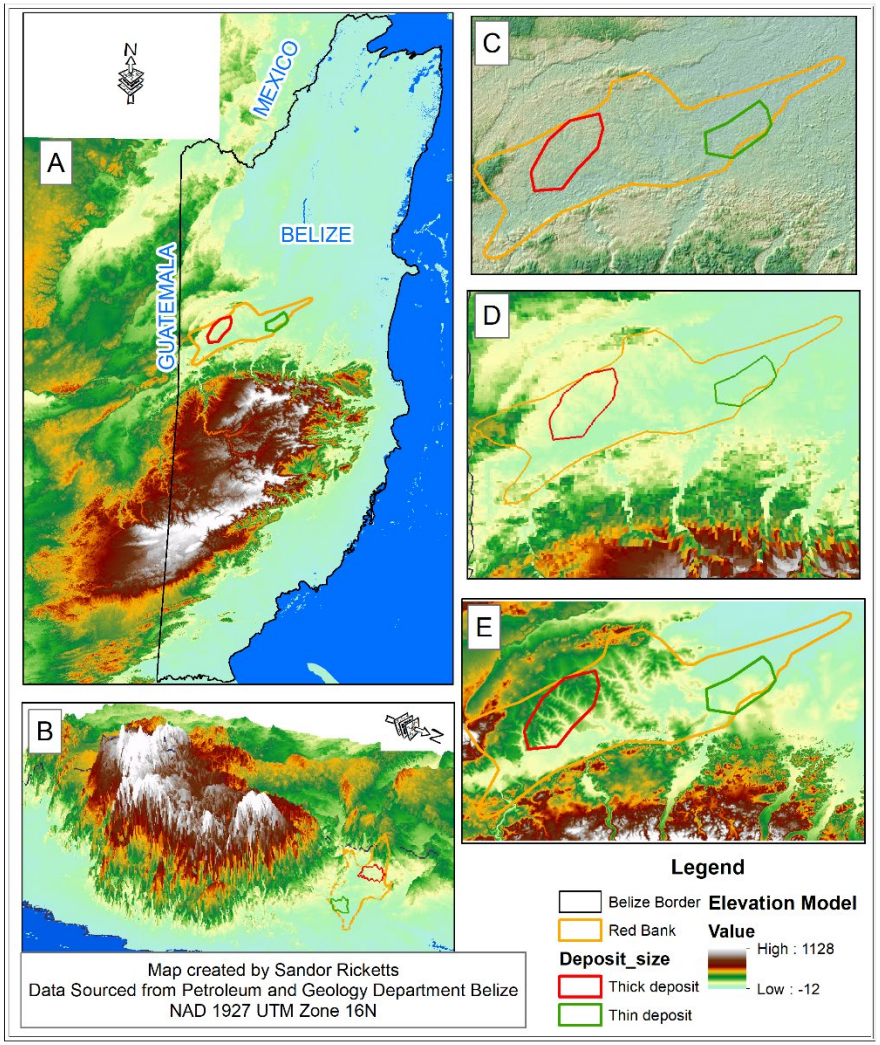

Figure 26 A, B regional topography showing location of Red Bank, at mouth of valley. C represent 2D DEM plot of deposit locality. D represents plan view of 3D Digital Elevation Model. E plan view of 2D Digital Terrain Model. Red polygon outlines the thicker clay deposits; green polygon outlines the thinner clay deposits.

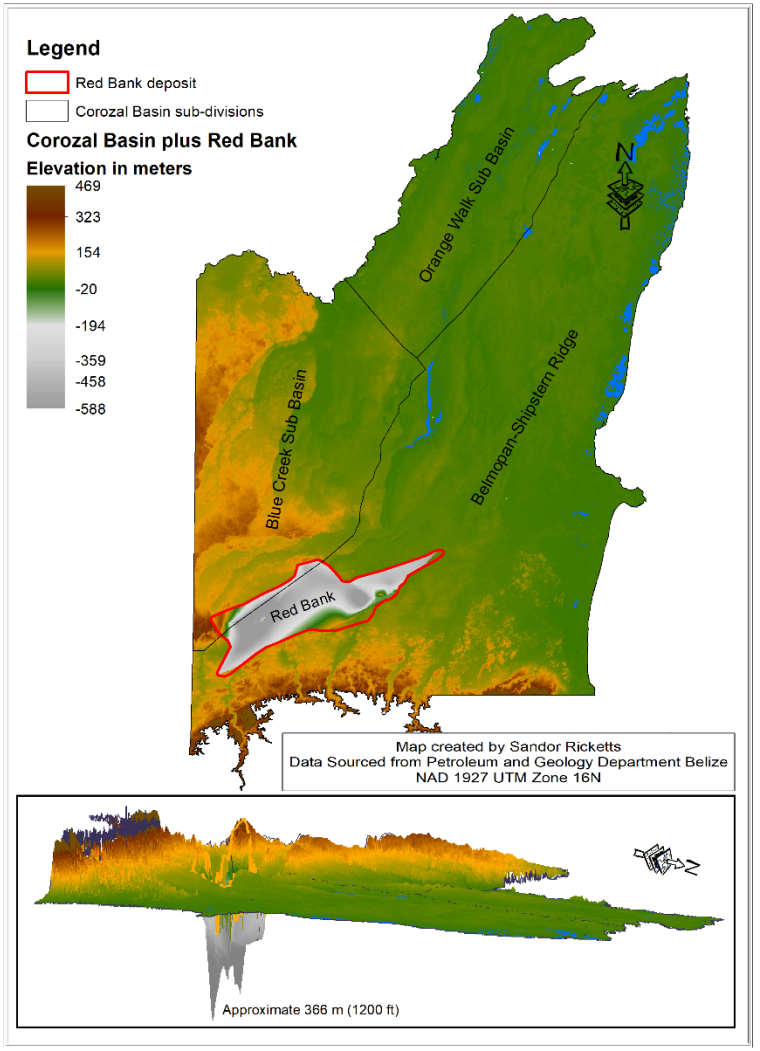

Figure 27. Digital Elevation Model showing Red Bank situated in the linear depression described in the text.

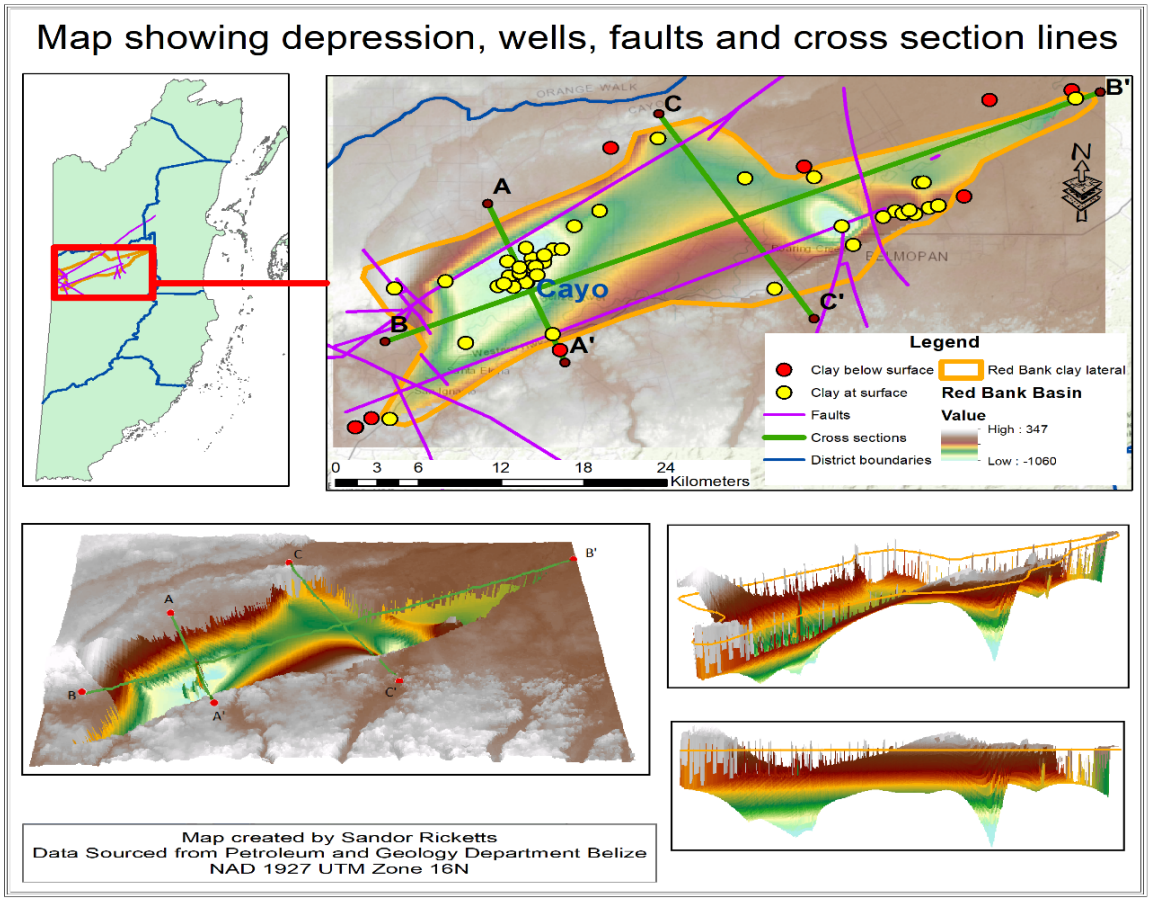

Figure 28. 3D model representation of Red Bank depression with wells, faults, and cross-section lines.

Based on the results of the modeling and maps created with data from GPO, the deposit appears to be bounded by faults. This was verified using seismic lines interpretation with the Kingdom Software package carried out by GPO (Figure 30). The images generated indicate that there are several faults in the vicinity of the deposit which may have influenced the location of the deposit. The varying depth of the deposit illustrated on the cross-sections (Figure 29) was also interpreted from seismic lines (Figure 30 andFigure 31) while facies changes were interpreted using gamma-ray and e-logs in which interbedded gypsum and regression/ transgression series were identified.

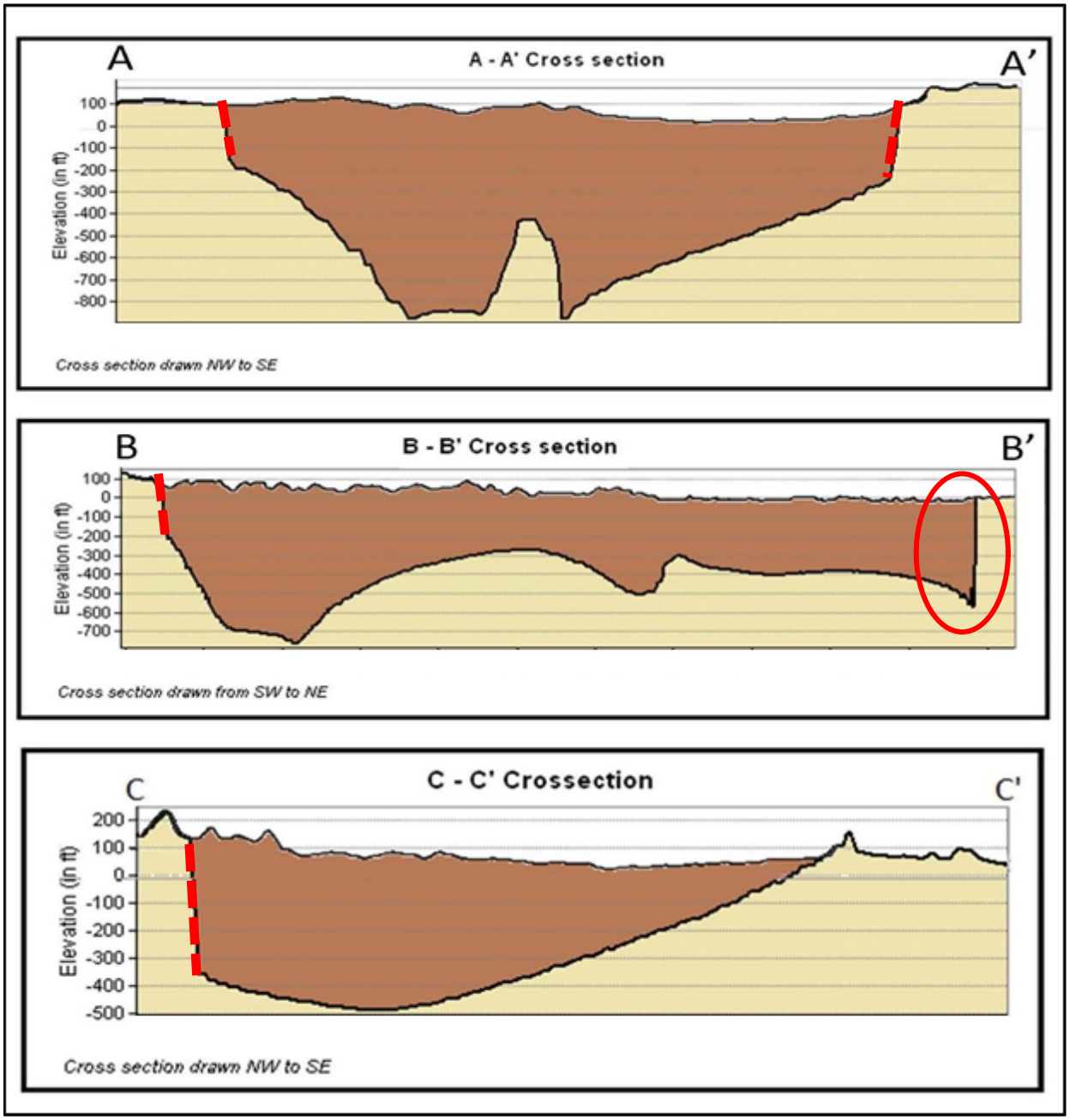

Figure 29. Cross-sections of the unconformity between clay (brown) filling a depression in limestone (tan). A possible faulted surface indicated by a red dashed line, and a red ellipsoid indicates insufficient data (B-B').

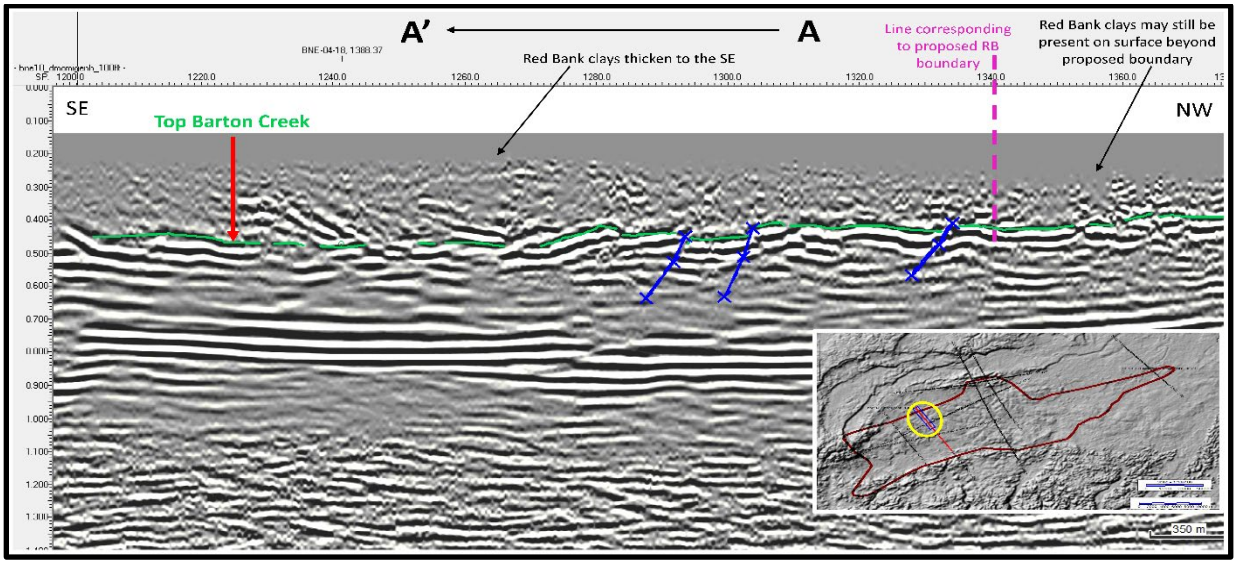

Figure 30. The image representing the interpretation of the seismic line intersecting the RBG deposit indicating a potential bounding fault. All work done on interpreting and generation of the image was done by Ashley Jones of the GPO, Belize[ii].

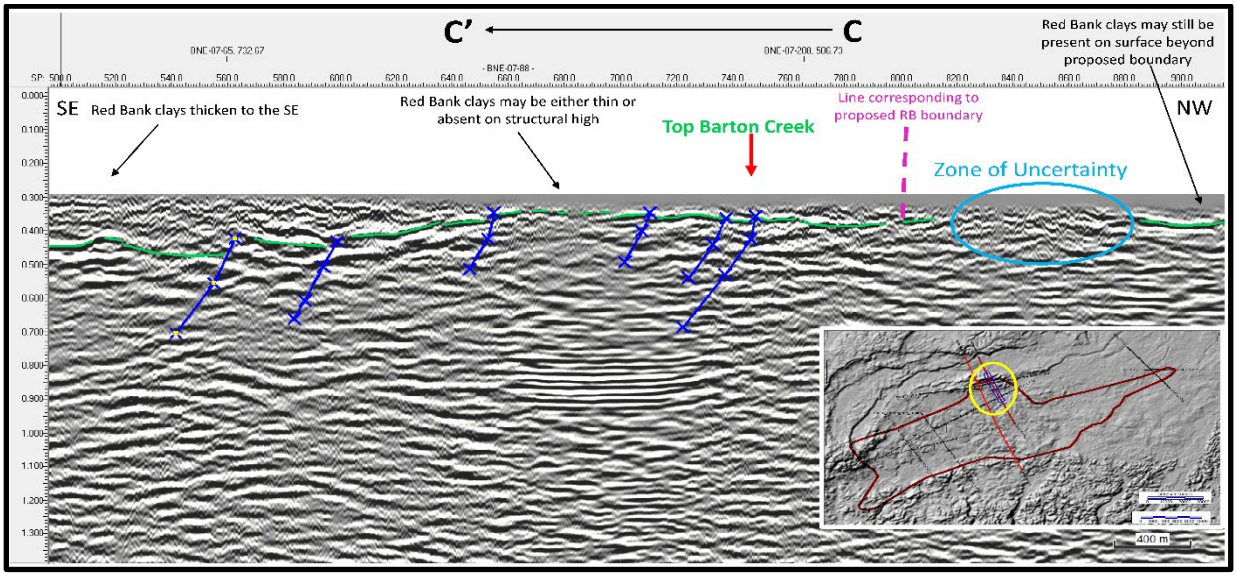

Figure 31. The image representing an interpretation of the seismic line intersecting the RBG deposit indicating varying unconformity contact with underlying limestone. All work done on interpreting and generation of the image was done by Ashley Jones of the GPO, Belize[ii].

5.3 Biostratigraphy

Of the 39 samples sent to Paleo Data for nannofossil analysis, twenty-eight were barren while the remaining eleven contained a variety of fossils (Appendix VII). The fossil abundance ranged from very rare to frequent and varied within each well and from well to well (Table 5). Of the fossils identified, *Coccolithus pelagicus,* which is extant and has

Table 5 List of samples used in the study. Those highlighted in green contain nannofossils. Underlined taxa represent the oldest diagnostic taxa.

Sample #	Sample Abbrev.	Sample Interval	General Abundance	Age-Diagnostic Taxa
1	CPR #1A	100-120	Barren	-
2	**CPR #1B**	**180-200**	**Numerous**	**Prinsius bisulcus, Prinsius matinii**
3	**CPR #1C**	**380-400**	**Low Numerous**	**Prinsius bisulcus, Prinsius matinii, Toweius eminens**
4	BC #2A	90-120	Barren	-
5	BC #2B	780-810	Barren	-
6	RB #1A	420-450	Barren	-
7	RB #1B	570-600	Barren	-
8	KW #1A	630-660	Barren	-
9	**SI #1A**	**120-140**	**Rare**	**Toweius eminens, Toweius callosus, Toweius pertusus**
10	SI #1B	280-300	Barren	-
11	SI #1C	540-560	Barren	-
12	MH #1A	190-200	Barren	
13	MH #1B	330-340	Barren	-
14	MH #1C	540-550	Barren	-
15	CAM #1A	1680-1710	Barren	-
16	CAM #1B	1770-1800	Barren	-
17	BD #1A	1890-1920	Barren	-
18	TOU #2A	30-60	Barren	-
19	TOU #2B	330-360	Barren	-
20	TOU #2C	480-510	Barren	-
21	NH #1A	690-720	Barren	-
22	SCB #1A	390-420	Barren	-
23	SCB #1B	720-760	Barren	-
24	SCB #1C	930-960	Barren	-
25	SF #1A	570-600	Barren	-
26	SF #1B	1390-1400	Barren	-
27	RD #1A	1420-1450	Barren	-
28	RD #1B	1750-1780	Barren	-
29	**VOP #2A**	**540-570**	**Numerous**	**Heliolithus cantabriae, Prinsius bisulcus, Prinsius martinii**
30	**VOP #2B**	**750-780**	**Very Rare**	**Prinsius bisulcus**
31	MU #14A	2520-2550	Barren	-
32	**MU #6A**	**200-230**	**Several to Numerous**	**Ericsonia subpertusa, Prinsius bisulcus, Toweius eminens**
33	**MU #6B**	**890-920**	**Numerous**	**Cruciplacolithus frequens, Prinsius bisulcus, Toweius callosus, Prinsius martinii**
34	MU #6C	1400-1430	Barren	-
35	**MU #4A**	**410-440**	**Numerous to frequent**	**Heliolithus cantabriae, Prinsius bisulcus, Discoaster multiradiatus, Toweius tovae**
36	**MU #4B**	**920-950**	**Numerous**	**Ericsonia subpertusa, Prinsius bisulcus, Toweius pertusus, Toweius callosus**
37	BW #1A	0-30	Barren	-
38	**BW #1B**	**270-300**	**Rare**	**Toweius eminens**
39	**BW #1C**	**720-750**	**Rare**	**Prinsius bisulcus, Toweius callosus**

been noted as far back as nannofossil biozone NP 2 (Varol, 1989), therefore, was not used in this study for age identification. Others with shorter ranges particularly late Paleocene to early Eocene (Figure 32) were identified as age-diagnostic taxa and were vital to the biostratigraphic study (Appendix VIII). Fossils identified during analysis were classified as calcareous nannofossil biozones NP9 and NP10, and planktonic foraminiferal biozones CP8 and CP9 (Martini, 1971; Okada and Bukry, 1980) (Figure 32, Table 6).

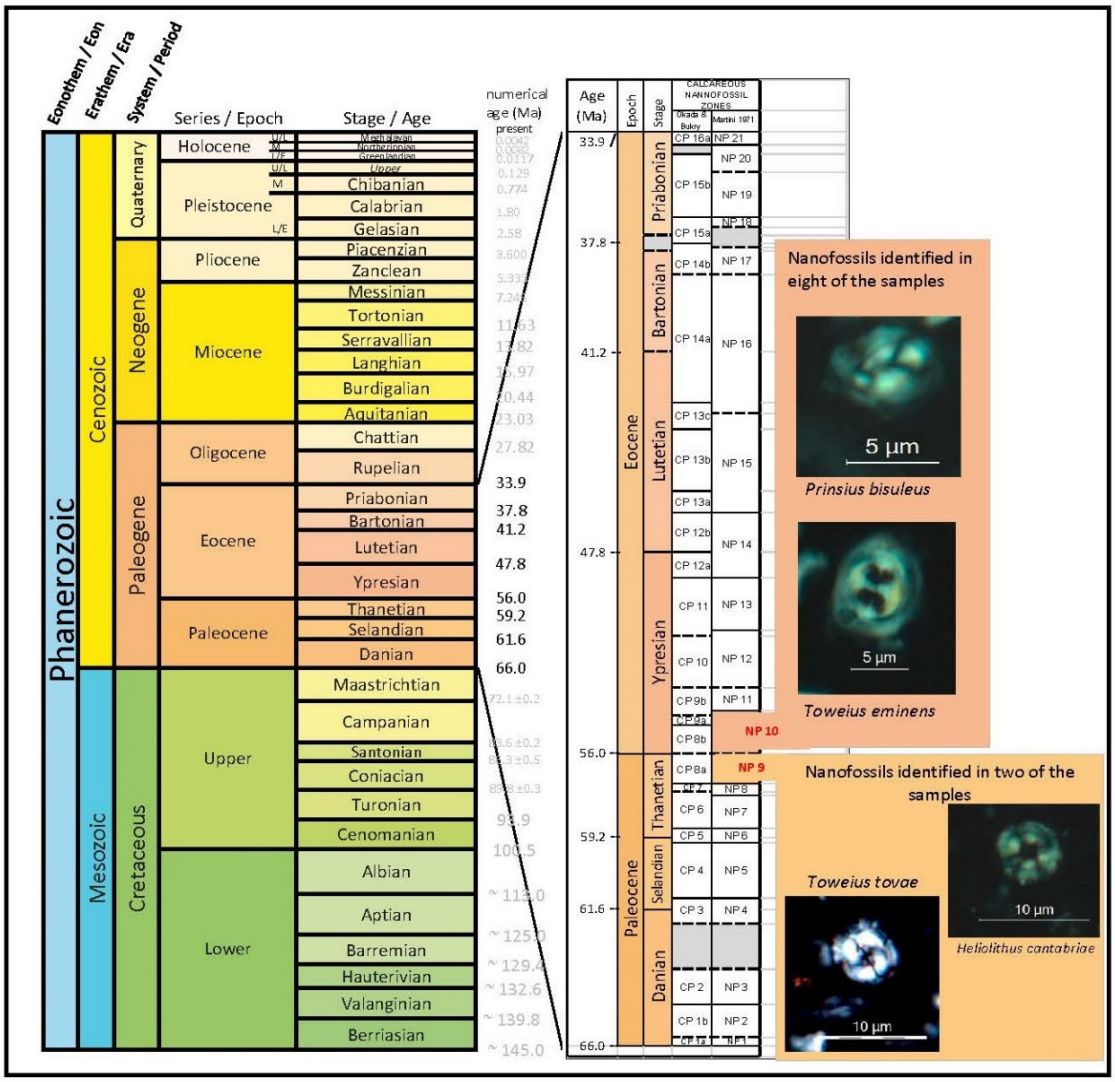

Figure 32. Nannofossil occurrence, highlighted by colored boxes with red text, along with pictures of fossils found in samples. Chronostratigraphic time scale modified from (Cohen et al., 2020) *and the plankton zone chart to the right modified from* Agnini et al., (2017).

Table 6 Nannofossils identified in samples, age-diagnostic taxa have been underlined. Age zones classified from using Martini (1971) zone and Okada & Bukry (1980) zone.

Sample #	Sample Abbrev.	Age-Diagnostic Taxa	Martini (1971) zone	Okada & Bukry (1980) zone	Sub-Epoch	Stage
2	**CPR #1B**	***Prinsius bisulcus*, *Prinsius matinii***	**NP10**	**CP9**	**Early Eocene**	**Ypresian**
3	**CPR #1C**	***Prinsius bisulcus*, *Prinsius matinii*, *Toweius eminens***	**NP10**	**CP9**	**Early Eocene**	**Ypresian**
9	**SI #1A**	***Toweius eminens*, *Toweius callosus*, *Toweius pertusus***	**NP10**	**CP9**	**Early Eocene**	**Ypresian**
29	**VOP #2A**	***Heliolithus cantabriae*, *Prinsius bisulcus*, *Prinsius martinii***	**NP9**	**CP8**	**Late Paleocene**	**Thanetian**
30	**VOP #2B**	***Prinsius bisulcus***	**As young as NP10, likely older**	**As young as CP9, likely older**	**Early Eocene**	**Ypresian**
32	**MU #6A**	***Ericsonia subpertusa*, *Prinsius bisulcus*, *Toweius eminens***	**NP10**	**CP8**	**Early Eocene**	**Ypresian**
33	**MU #6B**	***Cruciplacolithus frequens*, *Prinsius bisulcus*, *Toweius callosus*, *Prinsius martinii***	**NP10**	**CP8**	**Early Eocene**	**Ypresian**
35	**MU #4A**	***Heliolithus cantabriae*, *Prinsius bisulcus*, *Discoaster multiradiatus*, *Toweius tovae***	**NP9**	**CP8**	**Late Paleocene**	**Thanetian**
36	**MU #4B**	***Ericsonia subpertusa*, *Prinsius bisulcus*, *Toweius pertusus*, *Toweius callosus***	**NP10**	**CP8**	**Early Eocene**	**Ypresian**
38	**BW #1B**	***Toweius eminens***	**NP10**	**CP8**	**Early Eocene**	**Ypresian**
39	**BW #1C**	***Prinsius bisulcus*, *Toweius callosus***	**NP10**	**CP8**	**Early Eocene**	**Ypresian**

5.4 Petrographic Analysis

A variety of minerals and lithologies, along with fossils were noted from the thin sections (Figure 33). Petrographic analysis is an ideal method to determine the mineralogy of sample rock or the identification of lithologies. The samples used in this study had been cut, crushed, and ground during the drilling process, after which they were mixed as they were transported up the wellbore in the mud column, resulting in a mixing of lithologies (Figure 35).

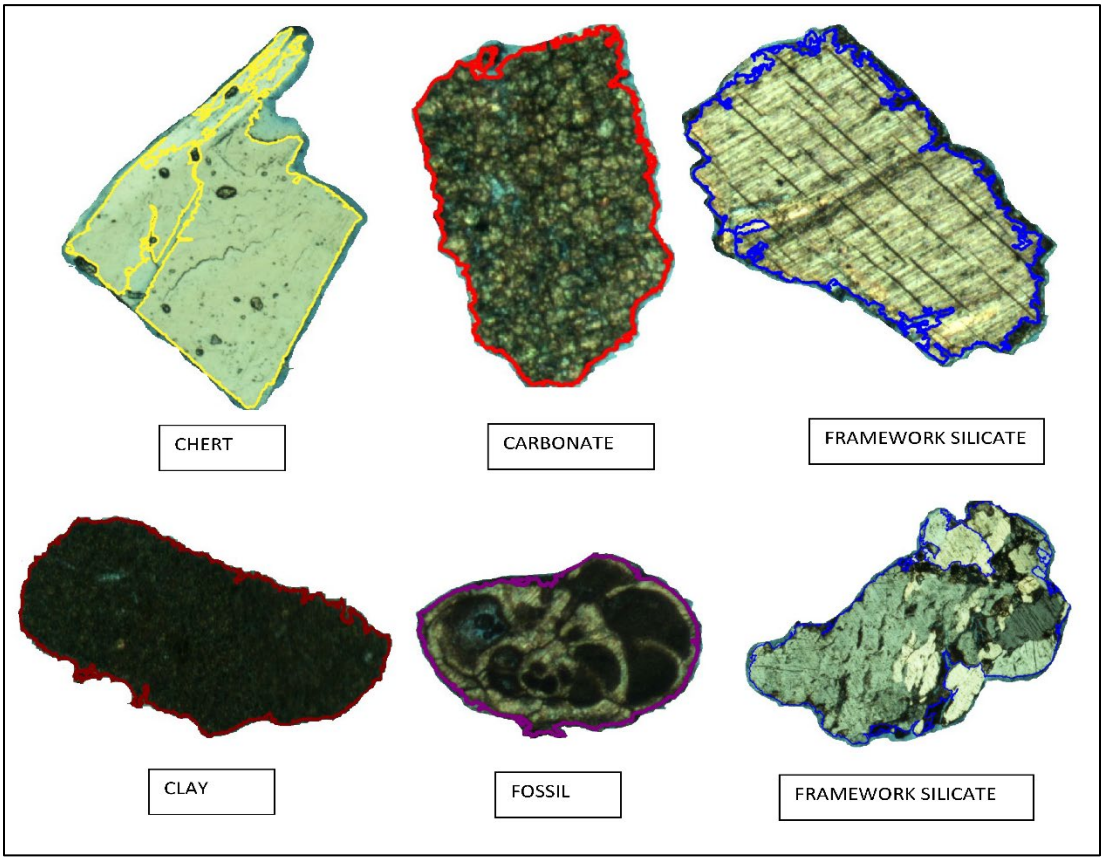

Figure 33. Photographic examples of minerals, lithology, and fossils identified during the petrographic analysis. Colors surrounding each grained used for identification and analysis of thin section by J Microvision software, not displayed to scale.

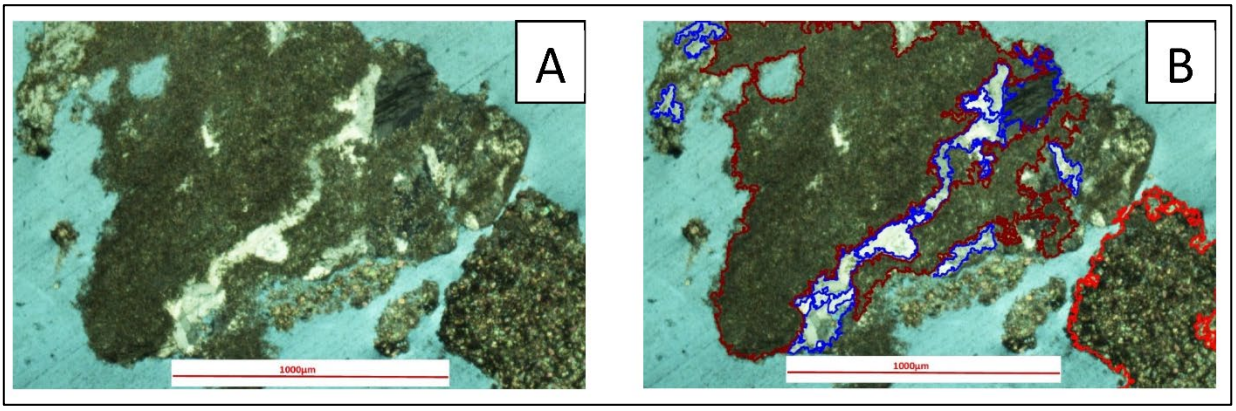

Figure 34. Picture A represents an example of grain composed of framework silicate (in blue) with silty-clay (in burgundy) crusting. Picture B grain with software identification of mineral and lithology for analysis.

The resulting grains which were used in this study are a combination making identifying specific lithology or minerals problematic. Therefore, results from the petrographic study are a representative quantitative analysis, that was used to identify variations in mineral and lithological content between samples within individual wells and across the study area (Figure 35 and Appendix V).

Analysis of the samples indicated that carbonates were dominant in most, followed by clay then framework silicate grains. However, clay is underrepresented in the analysis as many grains have a clay crust in part, but this crust was ignored on grains with less than 50% clay. Though most wells contained framework silicate, only Chan Pine Ridge (CPR) samples had a considerable percentage in all samples. Chan Pine Ridge samples also had notable quantities of miliolid foraminifera, which are bottom-dwelling (benthic) forms (Figure 36). Of all the samples analyzed only Billy White #1A (BW #1A) had chert fragments. This well (BW #1) also had considerable proportions of clay in two of its samples.

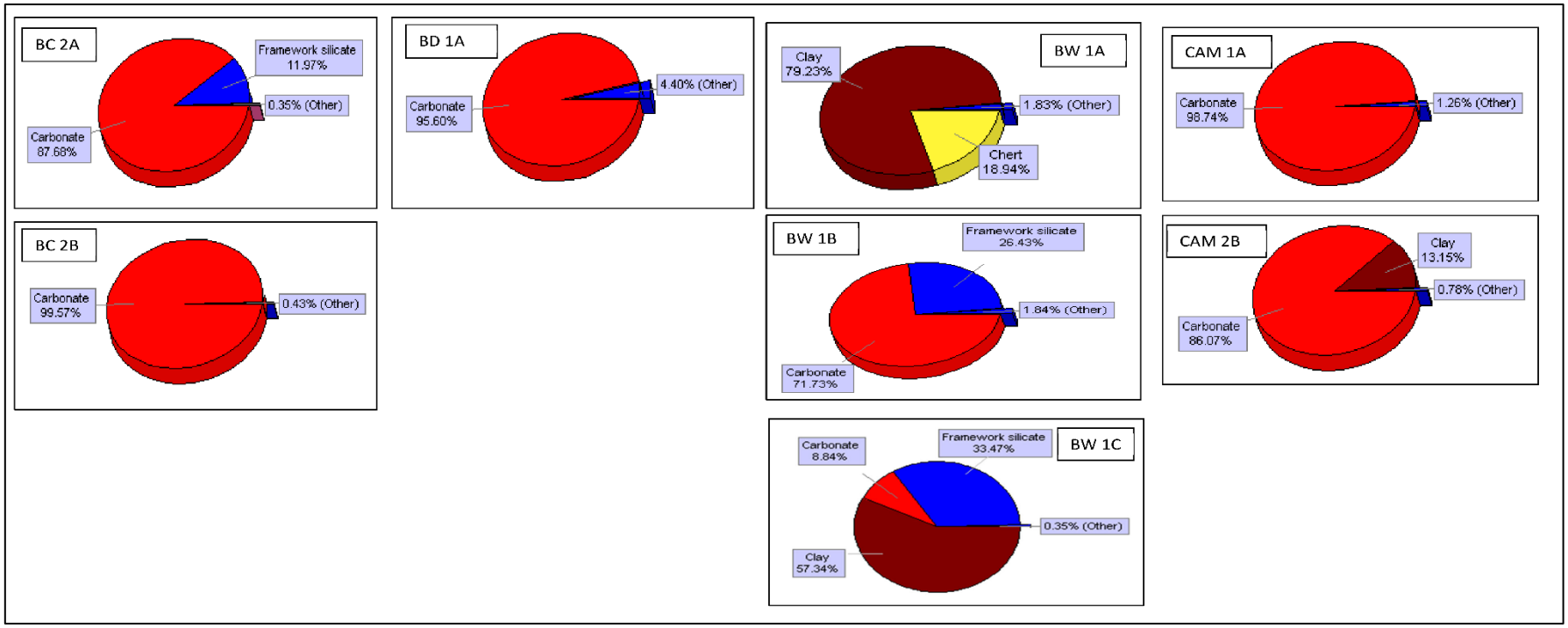

Figure 35. Examples of petrographic analysis of samples. proportions represented as percentages of the total samples selected for analysis.

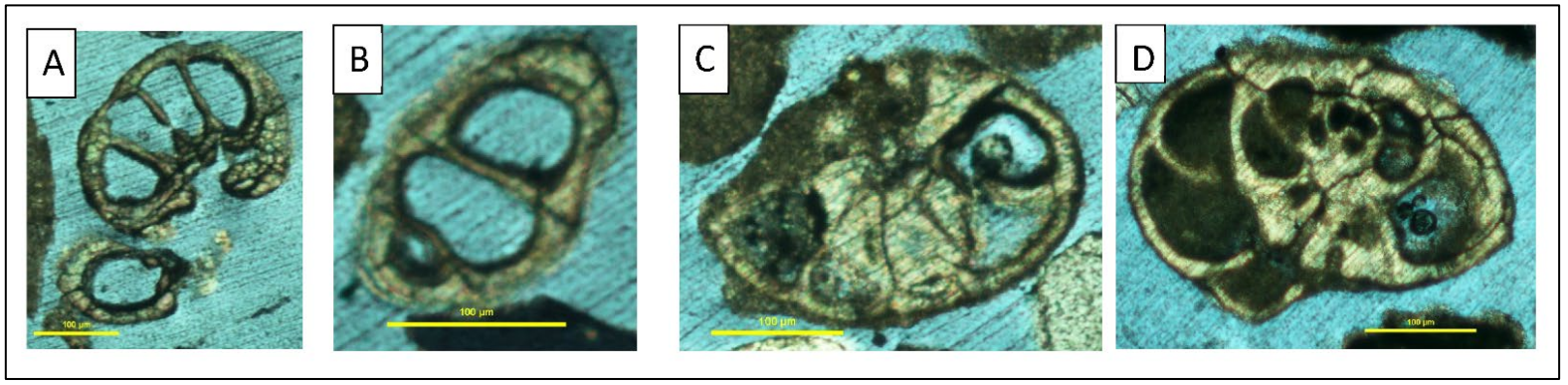

Figure 36. Pictures of miliolid (benthic) foraminifera noted in Chan Pine Ridge samples. Pictures A to C from CPR #1A and picture D from CPR #1B.

5.5 Mineralogy: XRD

The primary objective of the XRD mineralogical analysis was to determine the types/groups of clay comprising the RBG. During the preparation of the samples, other important information was gathered including calcium carbonate content and sand/silt content. The weight before and after the acid was recorded to determine an estimated percentage by weight of calcium carbonate in the samples (Table 7). Three of the wells had an overall increase in carbonate content with depth, one had a decrease in carbonate percentage with depth, while one of the wells showed a decrease followed by a slight increase in carbonate percentage of the samples.

Table 7. Weight of samples before and after an acid bath in preparation for XRD analysis. Color gradients used to depict carbonate concentration changes with darker color representing a higher percentage by weight. Lighter color indicates less carbonate in the sample.

Well Name	Number of samples	Sample number	Initial Weight (g)	Weight after Acid (g)	Percentage Carbonate	Carbonate Content change
Chan Pine Ridge #1	3	CPR #1A	2.0314	0.4571	77.50%	Decrease with depth
		CPR #1B	2.0338	1.0977	46.03%	
		CPR #1C	2.03	1.1642	42.65%	
Mike Usher # 4	2	MU #4A	2.0445	1.2995	36.44%	Increase with depth
		MU #4B	2.0053	0.5607	72.04%	
San Ignacio #1	3	SI #1A	2.0381	1.7232	15.45%	Increase with depth
		SI #1B	2.0368	0.7171	64.79%	
		SI #1C	2.0359	0.5797	71.53%	
Toucan #2	3	Tou #2A	2.0279	0.1717	91.53%	Decrease then increase with depth
		Tou #2B	2.0228	0.8135	59.78%	
		Tou #2C	2.0359	0.6869	66.26%	
Valley of Peace #2	2	VOP #2A	2.0645	1.3482	34.70%	Increase with depth
		VOP #2B	2.0738	0.4891	76.42%	

The next stage of sample preparation for XRD analysis involved the removal of the clay by sedimentation and decanting. Thirteen samples were selected for XRD analysis however, while decanting TOU #2A the clay yield was insufficient for analysis, as noted in table 7 above. This sample was composed of over 90% carbonate by weight. However, decanting all samples resulted in an aggregation of sand and silt with trace amounts of unremoved clay in some instances (Table 8). Examination of the remaining sediments indicated sand/silt trends in both quality and quantity within each well and throughout the deposit. Of the five wells, one (CPR#1), had a notable decrease in sediment content with depth with grains from fine to coarse and sub-round to angular. Three of the other wells indicated an overall increase in sand/silt with depth, though SI #1 indicated an initial decrease then an increase in sand/silt content for the three samples. The fifth well was stable with high sand/silt content for both sample depths.

The grain size and type of sediments varied also with depth in three of the five wells (CPR #1, SI #1, Tou #2) exhibiting an initial increase in grain size then a decrease with depth. The other two wells had opposite changes, with MU #4 demonstrating an increase in grain size with depth while VOP #2 had an overall decrease in grain size with depth.

The interpretation process that was carried out on the subsurface samples concerning grain size and carbonate content was not undertaken on the outcrop samples since they were more susceptible to the effects of weathering.

Table 8. Pictures of samples during the preparation for XRD along with results of decanting to remove clay. The term sand is used to represent framework silicate material.

Well Number	Well Name	Quantity	Sample number	Sample pictures	Extracted clay, on slide	Residual sediments	Relative Sediment Quantity	Sediment type	Average Sand Grade
5	Chan Pine Ridge #1	3	CPR #1A				high	sand	fine to med
			CPR #1B				medium	sand	fine to coarse
			CPR #1C				low	sand	fine to med
9	Mike usher # 4	2	MU #4A				high	sand to silt	fine to med
			MU #4B				high	sand & gypsum	med to coarse
14	San Ignacio #1	3	SI #1A				medium	silt to sand	fine to med
			SI #1B				low	sand to silt	med to coarse
			SI #1C				high	silt to sand	fine
17	Toucan #2	3	Tou #2A		No appreciable clay		low	sand to silt	fine to med
			Tou #2B				medium	silt to sand	fine to coarse
			Tou #2C				medium	silt to sand	fine to med
18	Valley of Peace #2	2	VOP #2A		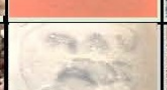		medium	silt to sand	fine to coarse
			VOP #2B				high	silt to sand	fine

Of the thirteen samples, twelve had significant quantities of clay (Table 8). These included chlorite, illite, kaolinite, montmorillonite (smectite), and vermiculite which have been identified for typical clay groups identified in the region (Scott, 1975; Thiry, 1993). XRD patterns were standardized to quartz (2-theta 26.66) (Table 9) and clay groups identified based on d-values for both air-dried and glycolated samples (Figure 37Figure 38, Figure 39,Figure 41Figure 41, and Appendix IX, and XI).

Table 9. XRD peak values for clay minerals used for identifying clay groups.

Test	Group	Peaks (A)		
		(001)	(002)	(003)
Air	Chlorite (Fe)	14.2	7.11	4.74
Glycol				
Air	Illite	10.1	5	3.38
Glycol				
Air	Kaolinite	7.15	3.58	
Glycol		7	3.5	
Air	Montmorillonite	15	5	3.75
Glycol		16.9	8.46	5.64
Air	Vermiculite	14.4	7.6	3.58
Glycol				

The two independent studies yielded similar results for clay groups (Figure 37). There were slight variations in their compositions, with the potential of mix layered clays. To verify the findings, the samples were subjected to Ethylene glycol allowing for the expansion of the clay resulting in a shift of the peak values for the respective mineral. These shifts were noted and used to confirm the presence of minerals such as smectite.

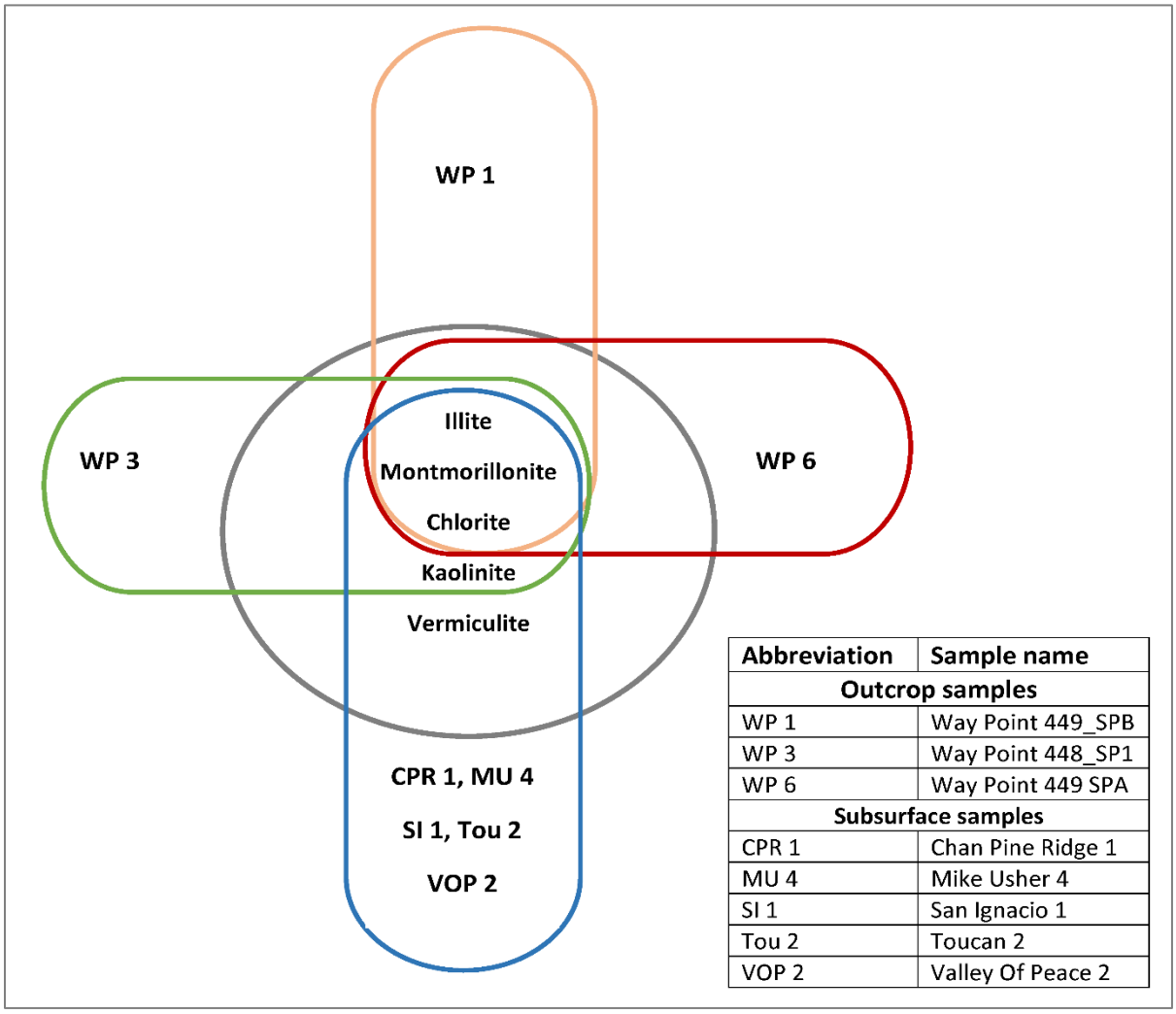

Abbreviation	Sample name
Outcrop samples	
WP 1	Way Point 449_SPB
WP 3	Way Point 448_SP1
WP 6	Way Point 449 SPA
Subsurface samples	
CPR 1	Chan Pine Ridge 1
MU 4	Mike Usher 4
SI 1	San Ignacio 1
Tou 2	Toucan 2
VOP 2	Valley Of Peace 2

Figure 37. Venn-type diagram showing results of XRD analysis on outcrop and subsurface samples, and thus indicating the respective groups that were identified in each sample.

XRD patterns outcrop samples.

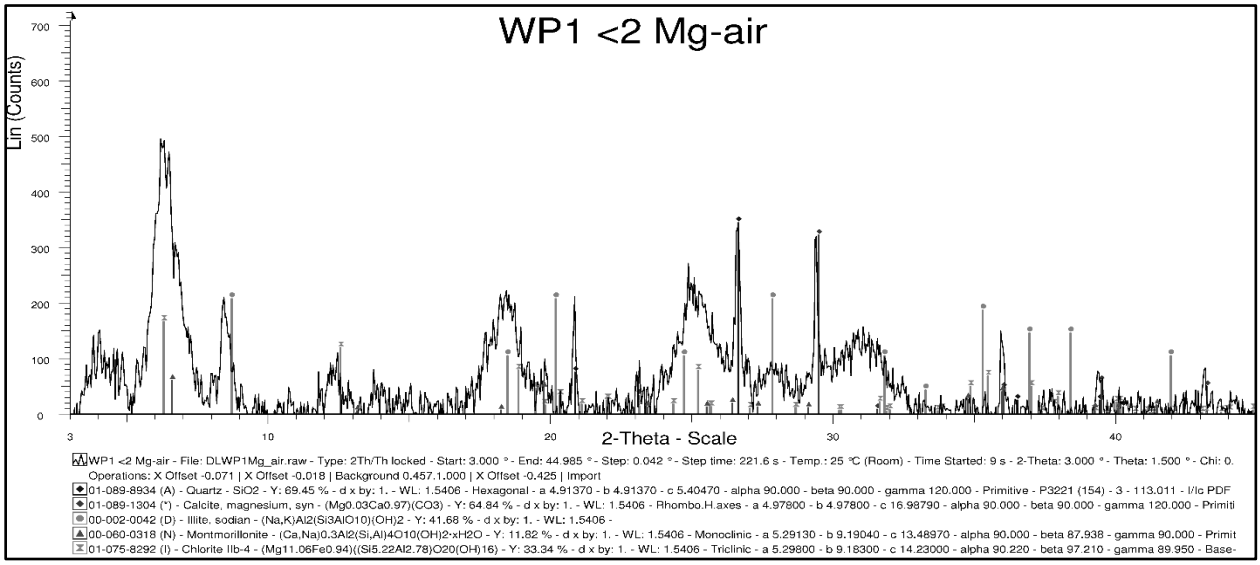

Figure 38. XRD pattern for air-dried samples WP1 (WP 488_SP1).

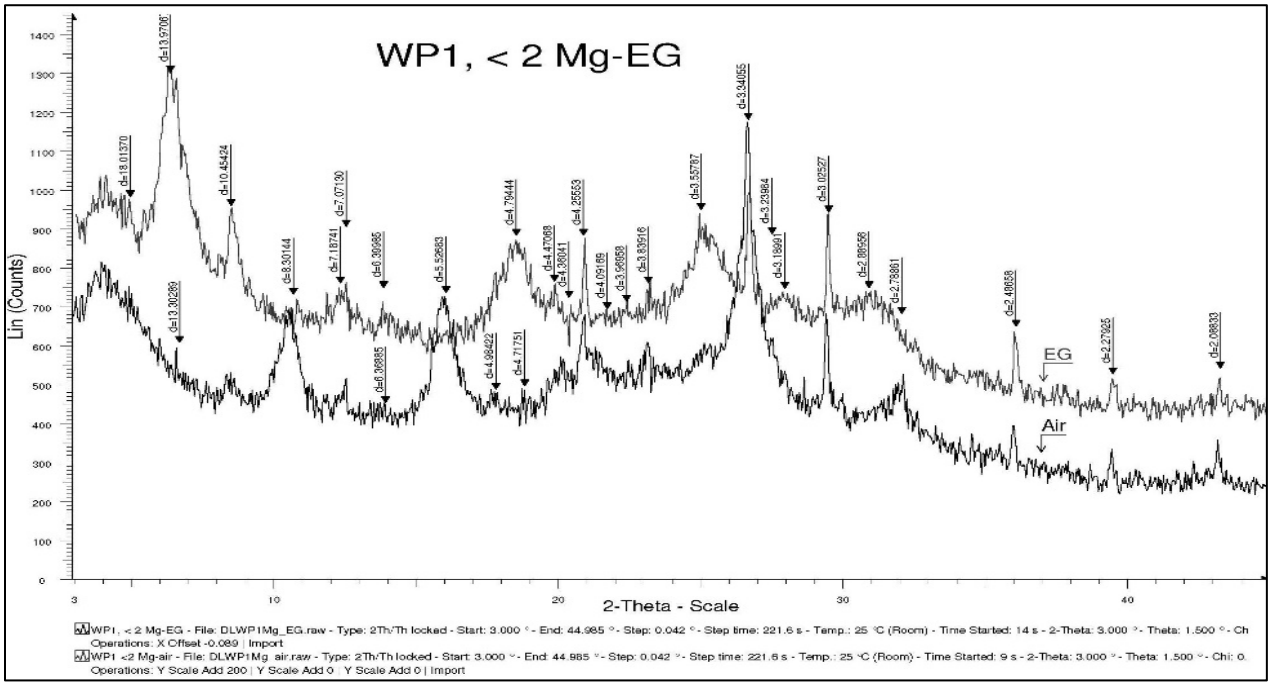

Figure 39. XRD pattern for air-dried versus glycolated sample WP1 (WP 488_SP1).

XRD patterns subsurface samples

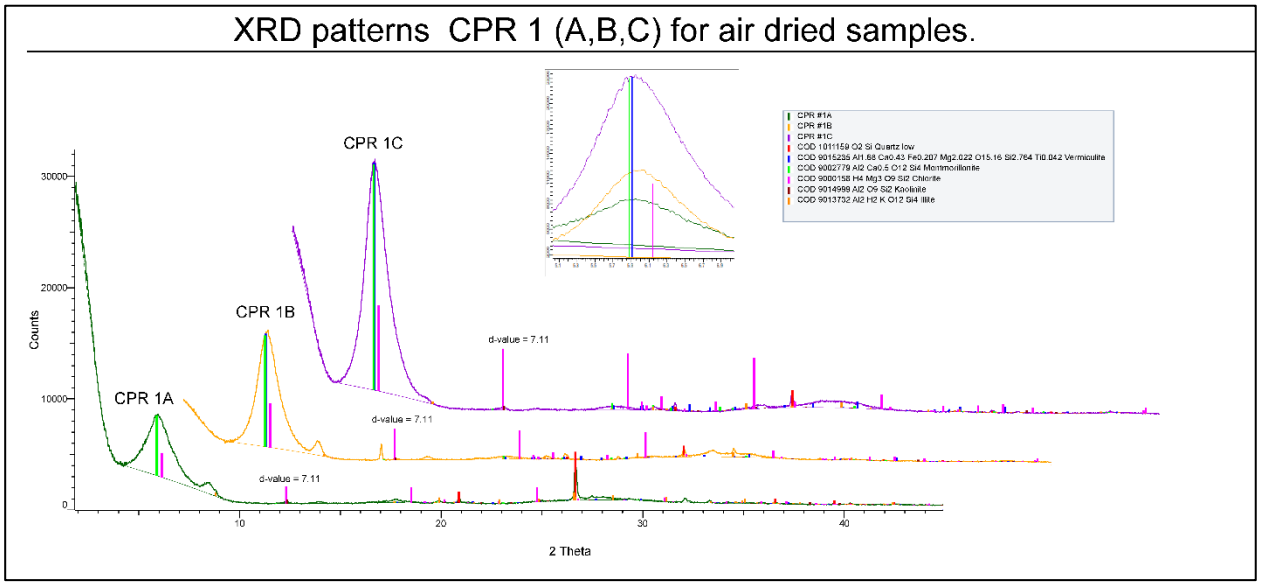

Figure 40. XRD pattern for air dried sample CPR-A, B, and C. Zoomed inset highlights three groups of clay identified under the major peak.

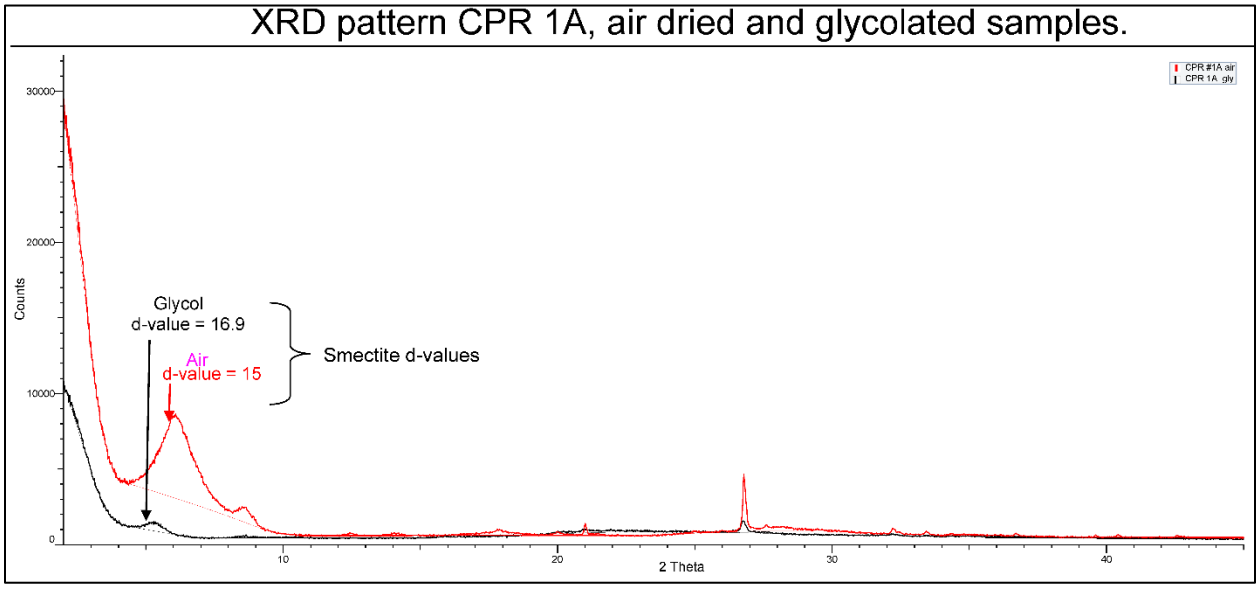

Figure 41. XRD pattern for air-dried and glycolated CPR 1A sample. The shift in smectite d-value (001) indicative of swelling due to the absorption of the Ethylene glycol.

5.6 Eustatic Sea level

Based on the taxonomic results of the present study, the nannofossils suite indicates the RBG clay was deposited within a marine environment of low energy (Pratt and Riding, 1993). These results do not indicate, however, if the water within the depression was being replenished from the oceans or was isolated. The depression in which the clay was identified was noted to be influenced by multiple faults to the northwest and southeast based on the seismic analysis. Such depressions/karst have been identified throughout the country with approximately more than 300,000 ha (3000 km^2) of karst identified within the limestone (Purdy et al., 1975; Miller, 1996). Many of these karsts are drained by more than 1864 mi (150 km) of caves located through the country (Miller, 1996).

This marine influence based on the nannofossils of the RBG indicates an influx of seawater, whereas the age range of the fossils gives a time period for such an influence which can be compared to the accepted eustatic sea-level records (Figure 42). Based on this information sea level fluctuated from a low of approximately 238 ft (72.6 m) to a high of 688.6 ft (209.9 m) during the time interval for deposition of the Red Bank clay (Figure 43) (Miller, 2009).

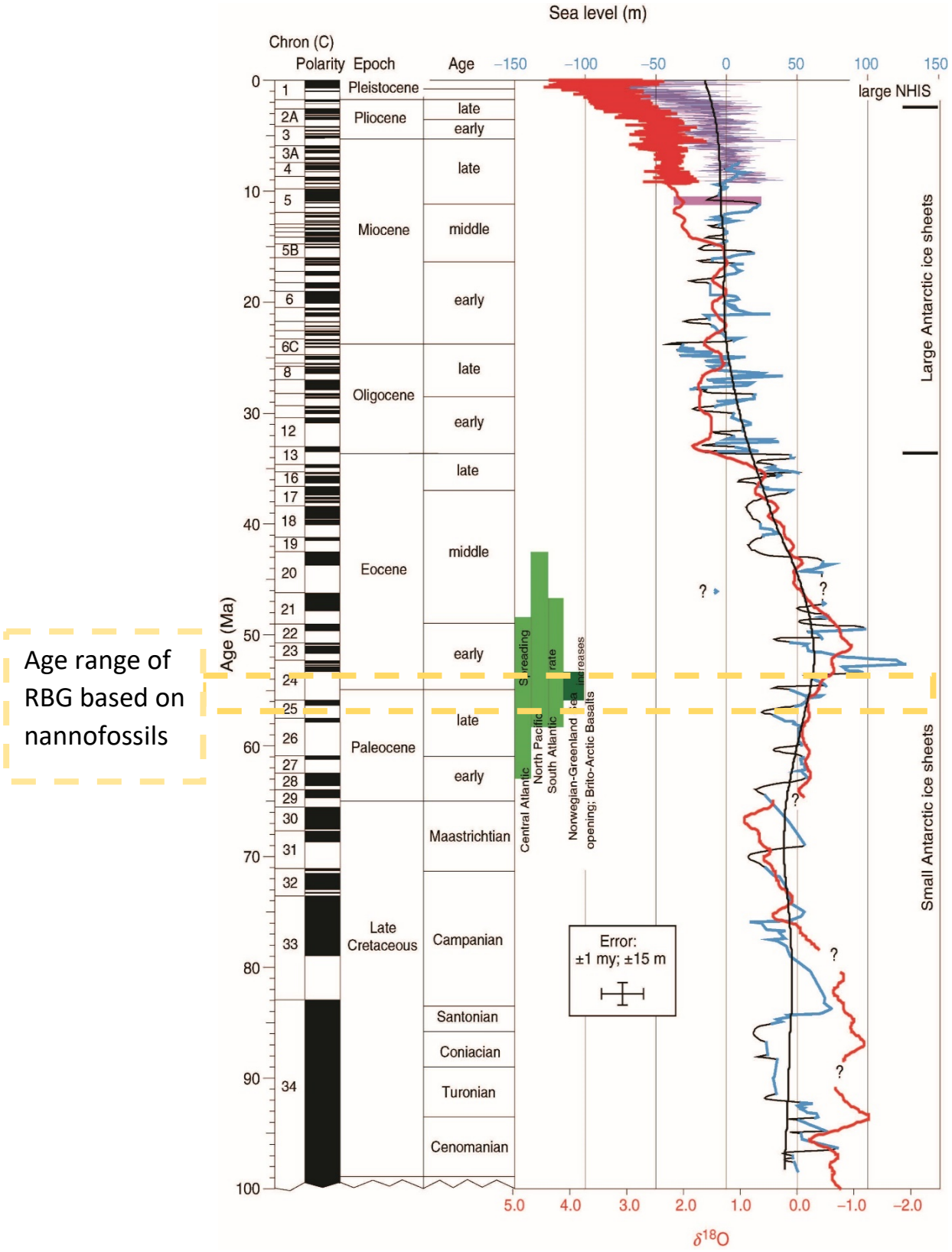

Age range of RBG based on nannofossils

Figure 42. Global sea-level curve based on interpreted backstripping (blue, black), $\delta^{18}O$ (purple), and benthic foraminiferal $\delta^{18}O$ synthesis (red), as determined by (Miller, 2009). *Modified from Miller (2009).*

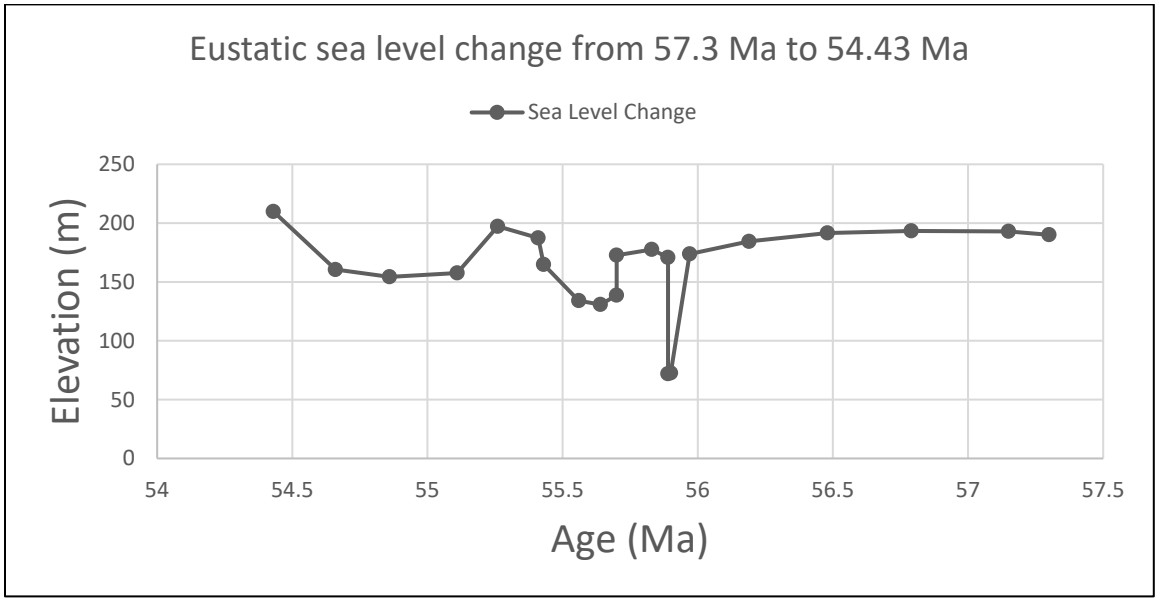

Figure 43. A plot of sea-level curve data during the time of RBG deposition. Data modified from Miller (2016).

This information, combined with the map of Belize highlighting the location of the clay deposit, reveals that the deposit, though relatively thick, was in a shallow marine area concerning sea level (Figure 44).

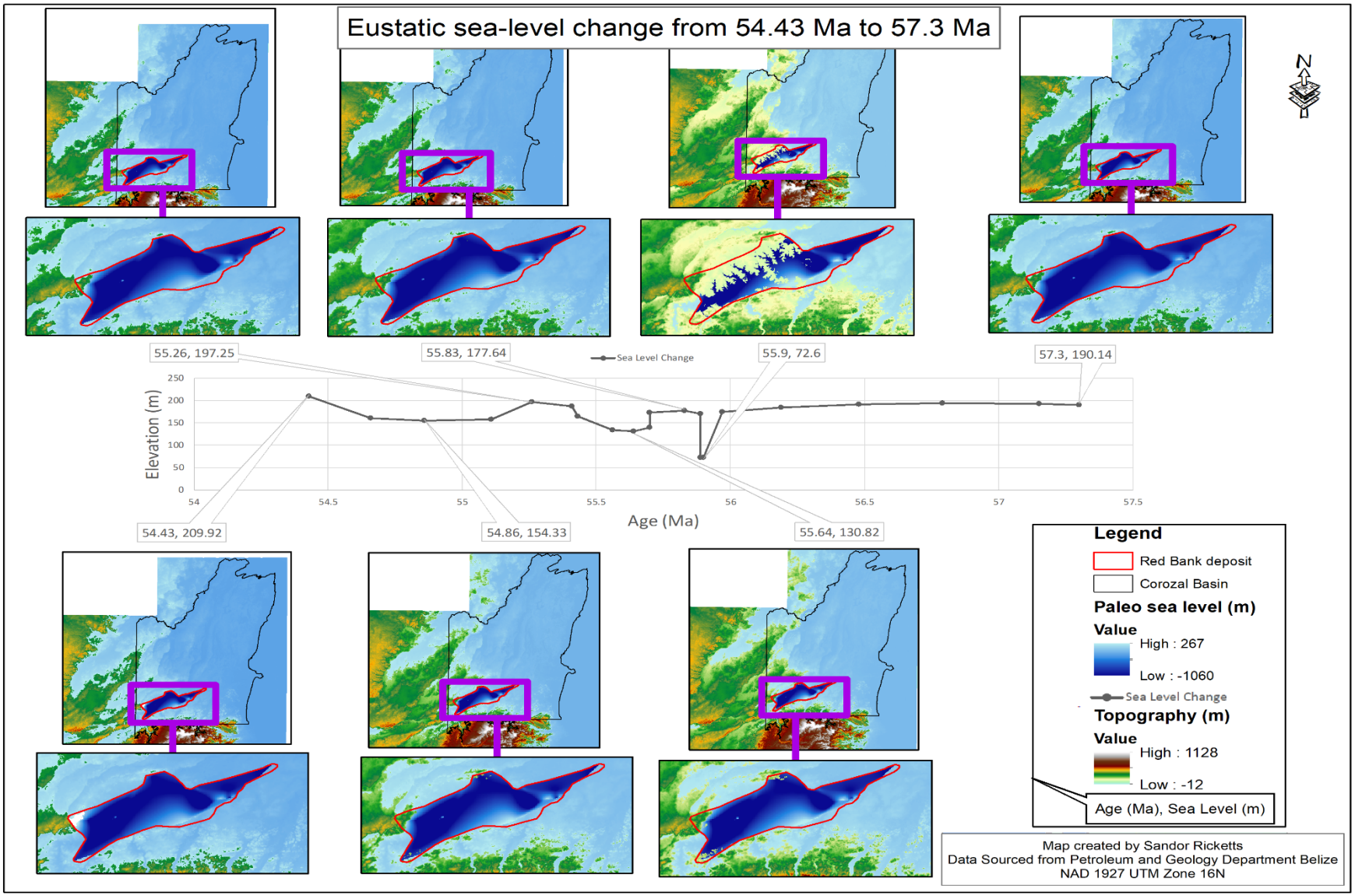

Figure 44. Eustatic sea-level variations during Paleogene, specifically at the time of deposition of RBG clay. Sea-level data is from Miller (2016).

5.7 Correlations

The correlation techniques listed in section 5 were dependent on the availability of data from the GPO. The wells used for each correlation within the study varied as a result. However, to have some control, the wells chosen were all within the thicker portions of the proposed RBG deposit containing clay above 50% by volume as noted from mudlogs (Figure 45). Wells with less clay and interbedded by limestone may be affected by the limestone and this adversely influences the result, therefore these were not used.

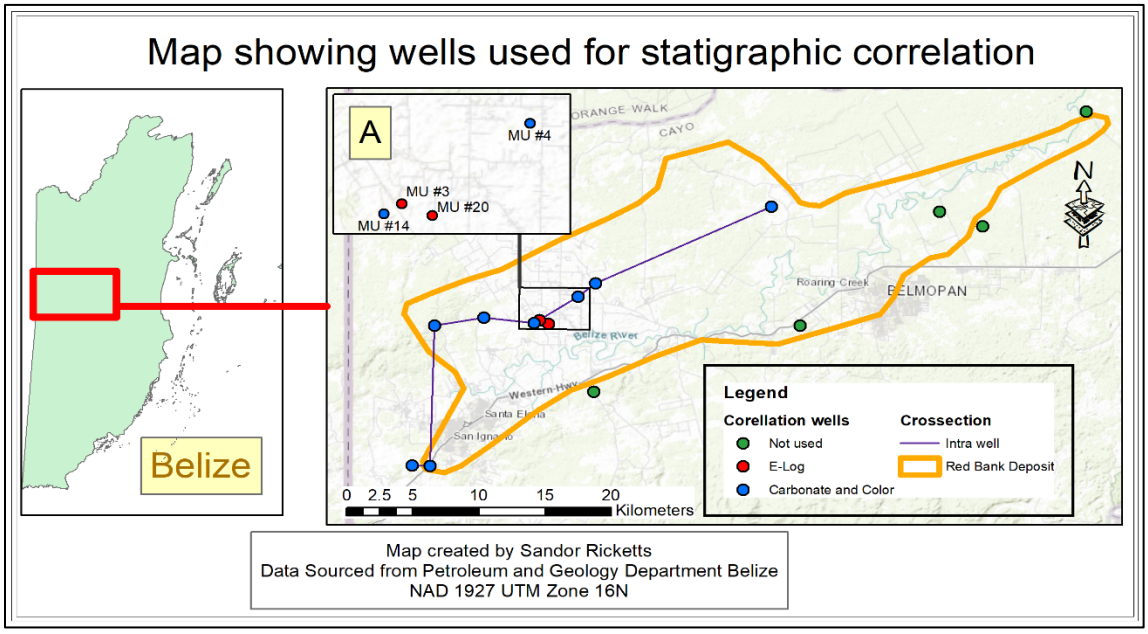

Figure 45. Map indicating location off wells used during stratigraphic correlation. Inset map A indicates the proximity of wells used for e-log analysis to other wells used in the study.

5.7.1 Mud Log

Two aspects of the mudlog were analyzed for correlation of carbonate content of the clay and color of the samples. Though color variations within mudlog description may be relatively subjective, a level of objectivity was achieved by using the Geological Society of America's (GSA)

color (GSA, 1970) for describing the colors of the lithology in each well. The wells used in the analysis were confined to wells with sections containing clay greater than 50% per depth range and within relative proximity to each other to potentially expose similar changes due to environmental conditions. The wells' depths were adjusted to ground level allowing utilization of several of the principles of geology to aid in correlation.

Carbonate content of the clay was identified per depth by searching the log description for keywords including "reaction with dilute hydrochloric acid (HCL)" and "calcic". These depths were then labeled in the table as "calcic" (Figure 47). The clay from the studies indicated a consistent reaction with dilute HCL, therefore identifying appreciable variations was not conclusive.

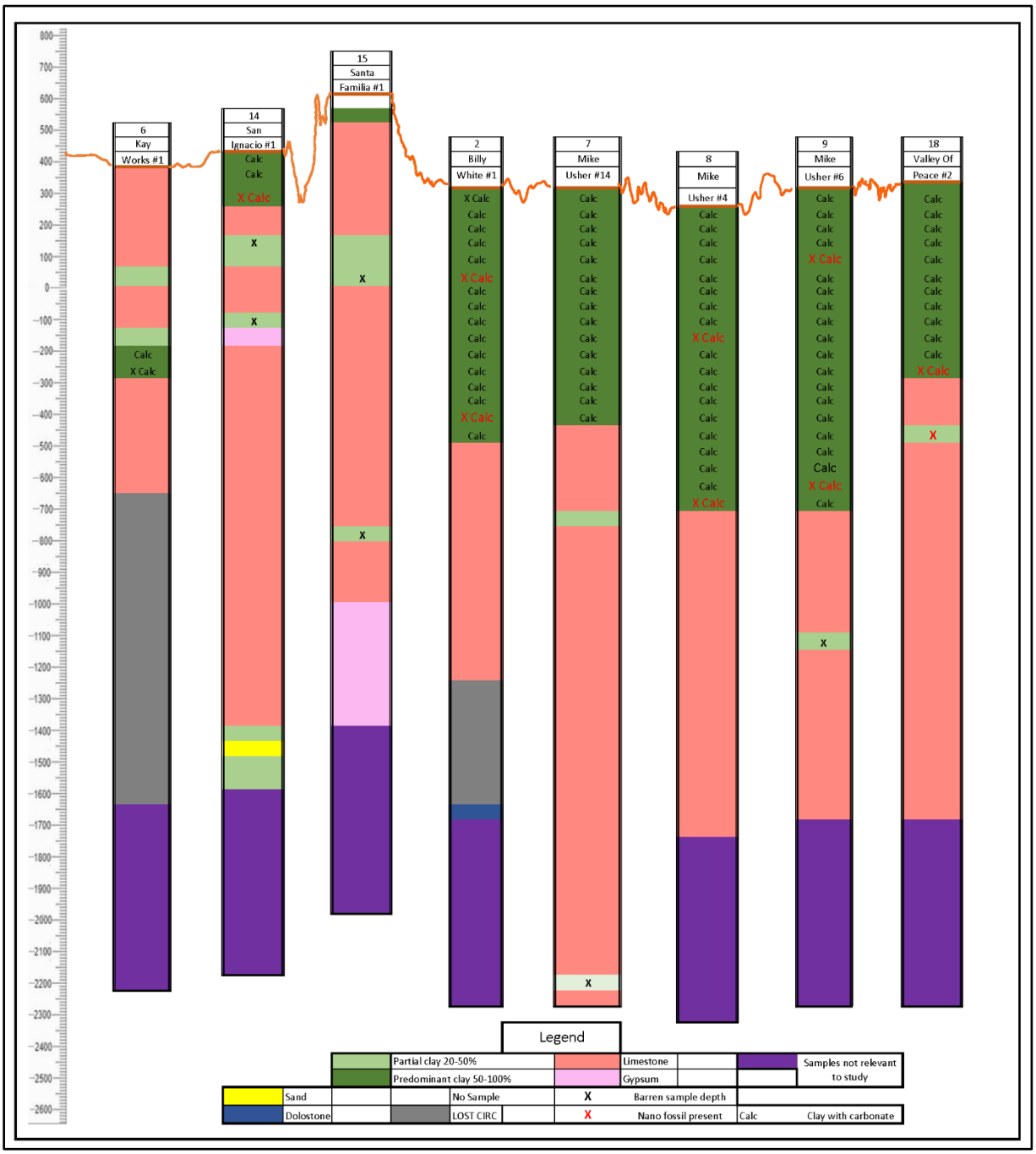

Figure 46. Representation well used for carbonate correlation study adjusted to ground level. Spacing between wells can be ascertained from figure 33. Vertical scale in feet (Horizon Well Logging Inc., 2016).

Sample colors were identified by noting descriptive information on the clay. This was recorded as standardized abbreviations used by the logging company, Horizon Well Logging Inc. (Horizon, 2006). The information was then plotted in well representation plots adjusted to ground level (Figure 48). Correlation-based on color variations was not overwhelmingly definitive when the descriptions were compared for various wells concerning depth. The color data from mudlogs was combined with the location map (Figure 48) to obtain a better perspective of the color variations.

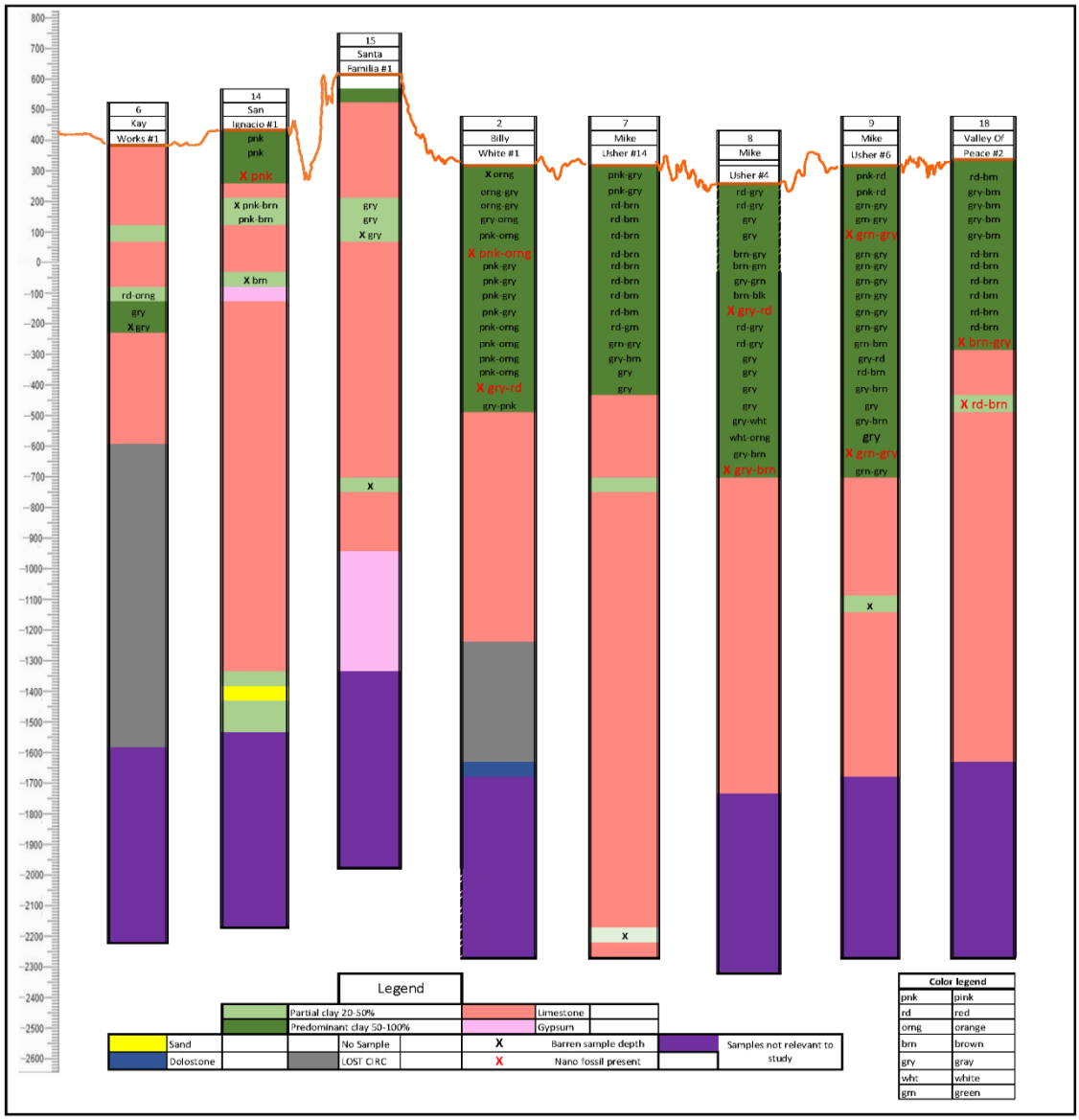

Figure 47. Representation well used for color correlation study adjusted to ground level. Spacing between wells can be ascertained from figure 33. Vertical scale in feet (Horizon Well Logging Inc., 2016).

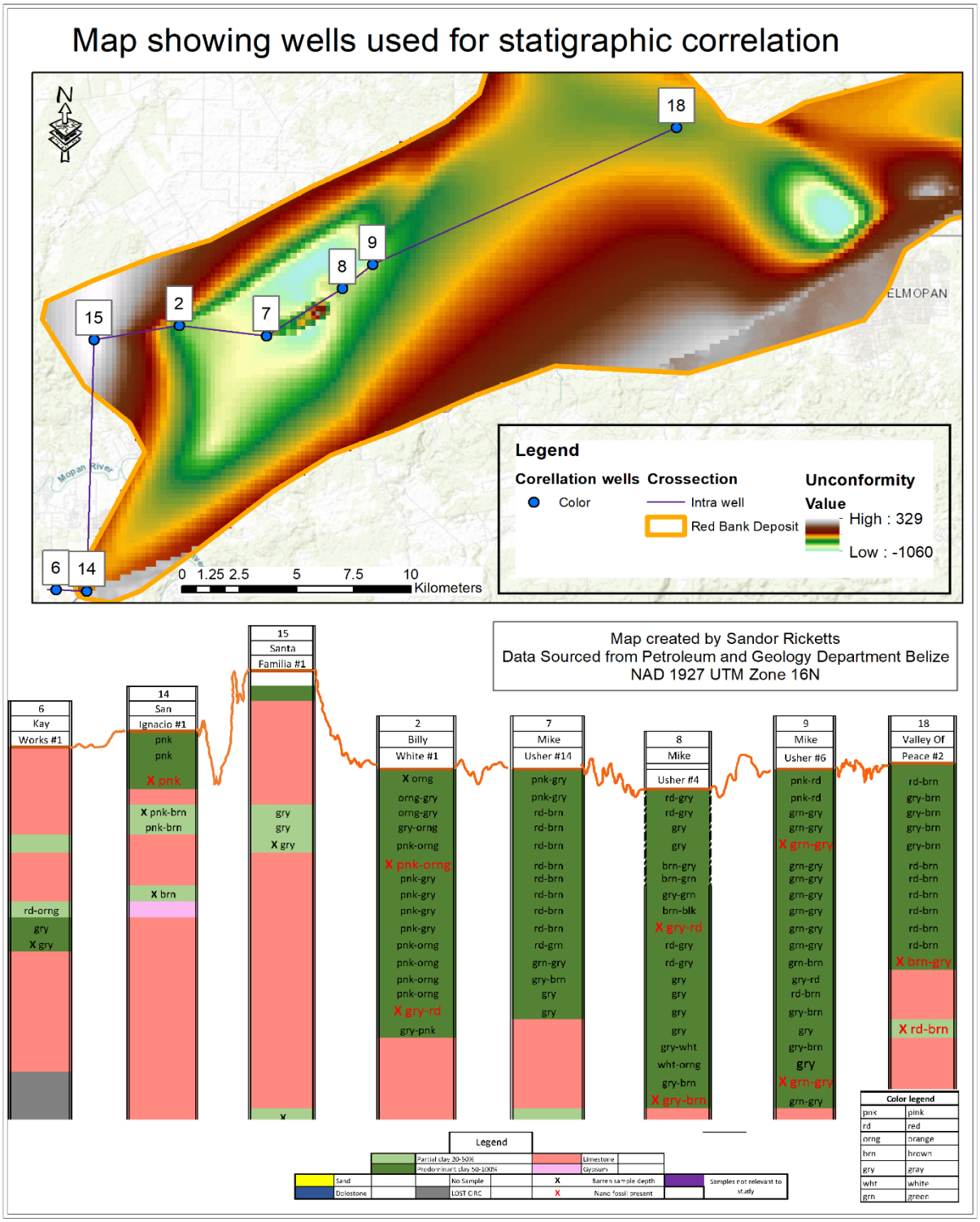

Figure 48. Wells used for color correlation with a map showing the location of the wells. Well data extracted from mudlogs (Horizon Well Logging, Inc., 2016).

As noted on the map, well number 8 and 9 are close to each other, and both wells have variations of gray clay in their lower sections. Gray is also noted in well 7 and a trace amount in the lower portions of well 2. A structural high in the underlying limestone divides the depression, separating well 18 from the others and resulting in multiple facies within the depression, thus causing a different color (red to brown) clay in its lower sections. Except for well 2, the other four wells located in the depression where the RGB is thickest have clay with color variations of red and pink in the upper sections. Wells 15, 14, and 6 are at higher elevations than most, although they also indicate similar colored clay. It should be noted that in well 6, the clay within the limestone exhibits the gray color as noted in the other wells at the same depth.

E-log for only two of the wells exists through the clay section. These two wells were not previously used in other sections of this report; however, they are near to other wells used in this study (Figure 45A). One of the wells with e-log clay data, Mike Usher #20, was used to correlate the mudlog and seismic data to interpret the unconformity between the clay and limestone (Appendix IX), thus allowing for additional correlation within this study.

5.7.2 Biostratigraphic

Age diagnostic nannofossil taxa (Appendix IX) results from section 5.7.2. were found to be situated within two epochs of the Cenozoic (Paleocene and Eocene), equivalent to NP 9 and NP 10 on the Martini calcareous nannofossil scale (Martini, 1971). The data was then plotted on wells correlated with a datum at ground level (Figure 49). This correlation indicated that nannofossils identified, and their respective biozones were consistent across the RBG deposit. This implies that the clay was deposited between approximately 59.2 and 47.8 million years ago,

based on the current version of the International Commission on Stratigraphy's chronostratigraphic chart (Cohen et al., 2020).

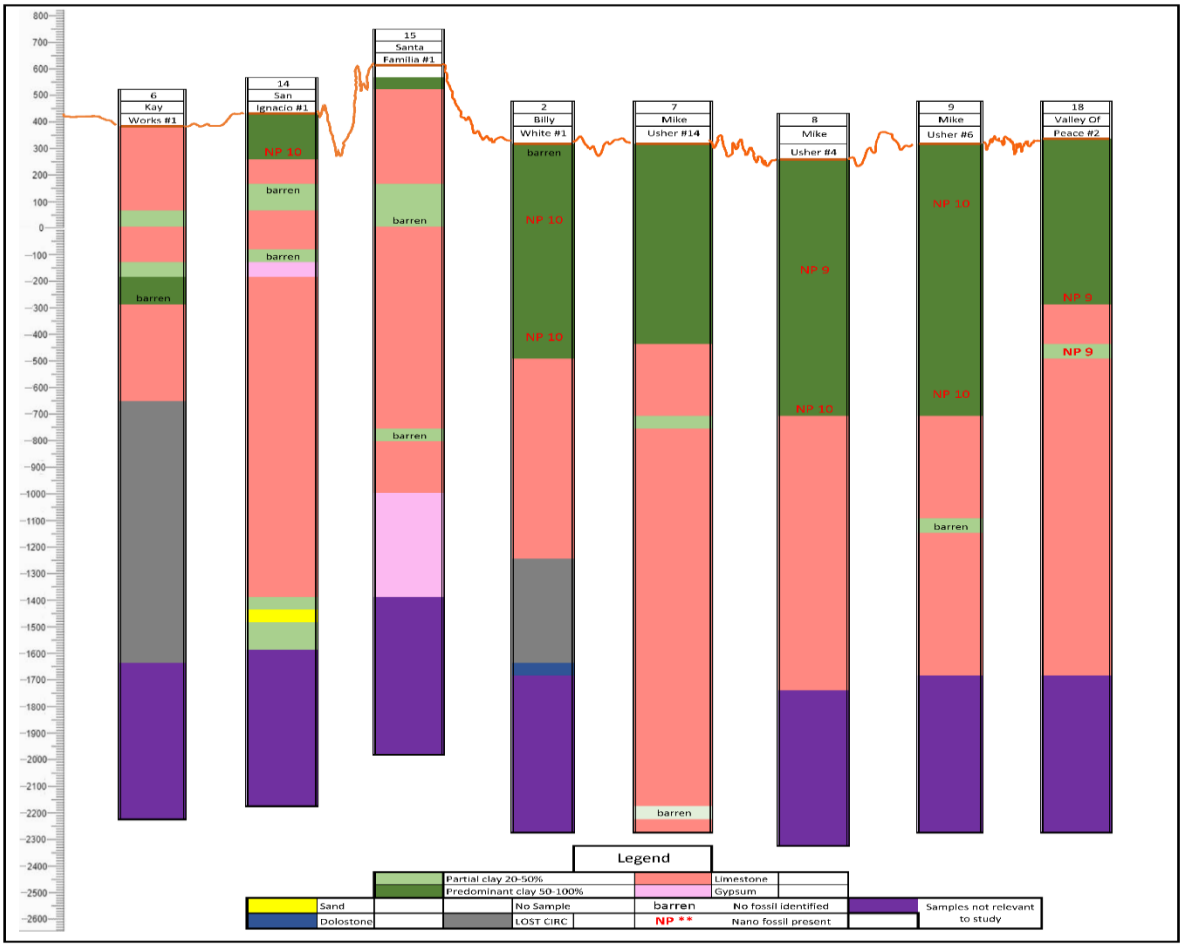

Figure 49. Representation of mudlogs indicating the location of samples used in the biostratigraphic study, along with barren samples. Vertical scale in feet (Horizon Well Logging, Inc., 2016).

A total of 14 calcareous nannofossil taxa were identified, 10 of which were used to assist in the dating of the deposit (Table 10). The occurrence of these taxa was divided into six abundance groups (Table 11), based on the occurrence taxa varied within individual wells and throughout the deposit (Table 5).

*Table 10. List of nannofossils identified from clay samples along with their respective nannofossil zones. Samples and zones identification were done by Paleo Data Inc. (personal communication, 2019), * not used due to extended range.*

Count	Age-Diagnostic Taxa	Martini (1971) zone	Okada & Bukry (1980) zone	Sub-Epoch	Stage
1	*Coccolithus pelagicus*			*	
2	*Cruciplacolithus frequens*	NP10	CP8	Early Eocene	Ypresian
3	*Discoaster multiradiatus*	NP9	CP8	Late Paleocene	Thanetian
4	*Ericsonia formosa*			*	
5	*Ericsonia subpertusa*	NP10	CP8	Early Eocene	Ypresian
6	*Heliolithus cantabriae*	NP9	CP8	Late Paleocene	Thanetian
7	*Prinsius bisulcus*	NP10	CP9	Early Eocene	Ypresian
8	*Prinsius martinii*	NP10	CP9	Early Eocene	Ypresian
9	*Sphenolithus primus*			*	
10	*Toweius callosus*	NP10	CP9	Early Eocene	Ypresian
11	*Toweius eminens*	NP10	CP9	Early Eocene	Ypresian
12	*Toweius pertusus*	NP10	CP9	Early Eocene	Ypresian
13	*Toweius rotundus*			*	
14	*Toweius tovae*	NP9	CP8	Late Paleocene	Thanetian

Table 11. The abundance group used to rate nannofossil occurrence, along with the theoretical rank used for this study.

Ranking	Abundance group
0	Barren
1	Very rare
2	Rare
3	Several to Numerous
4	Low numerous
5	Numerous
6	Numerous to frequent

5.7.3 Petrographic

The petrographic analysis indicated lithological changes throughout the study area. However, the intermingling of clay with all other grains has caused ambiguities in the results. Therefore, for the study emphasis is placed on the framework silicate proportions. For this

analysis, four profile lines of the samples were drawn across the study area (Figure 50), arranged based on elevation (Appendix V).

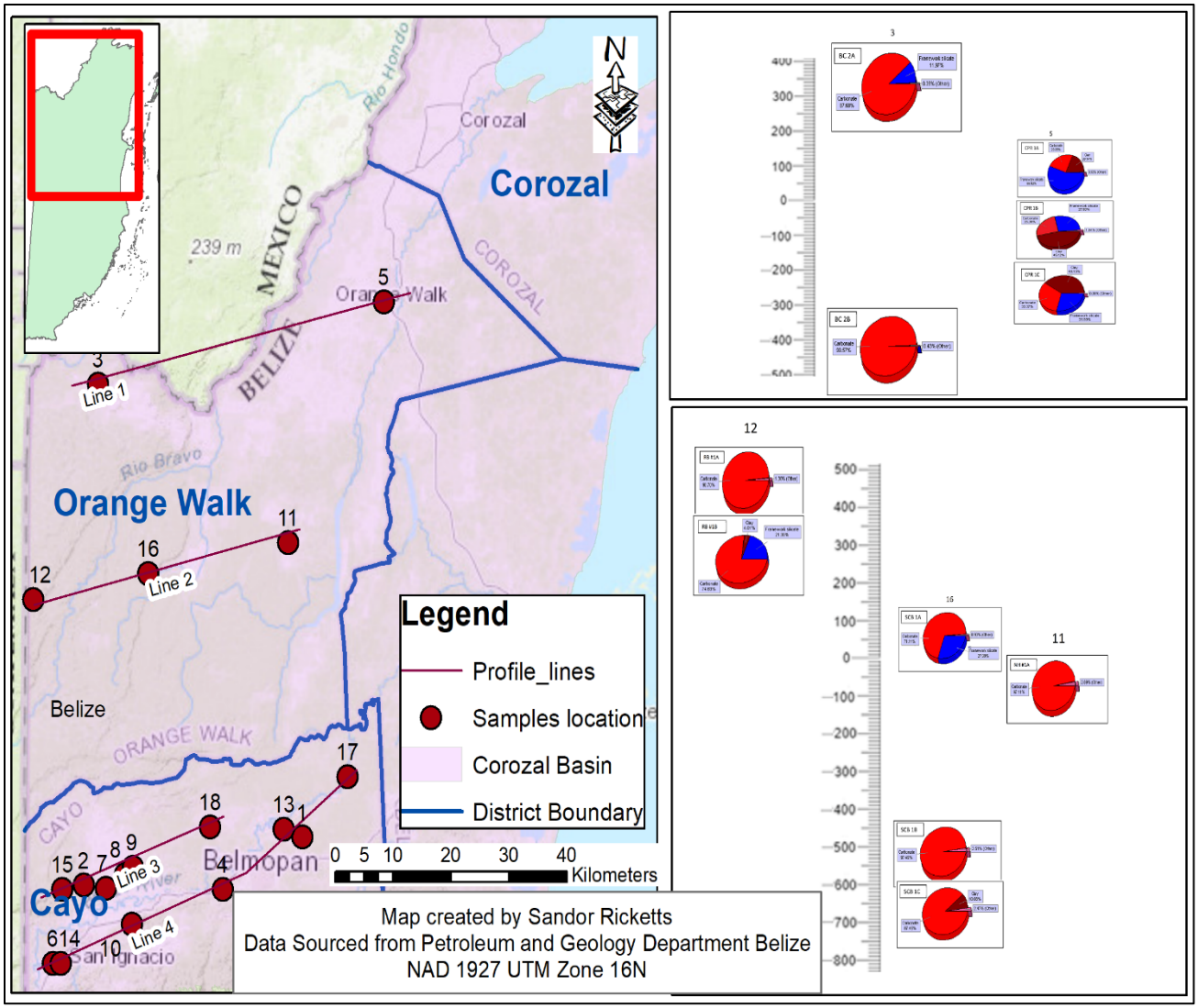

Figure 50. Map showing the location of profiles lines used for framework silicate correlation. Profile lines 1 and 2 are for samples north of the thickest clay deposits. The pie chart represents the percentage proportion, with blue representing framework silicate material. Vertical scale in feet.

The samples on lines one and two show silicates above 300 ft (91.44 m) subsea (Figure 50), while lines three and four (located in thicker clay) (Figure 51, Figure 52) had silicates to a depth of approximately 1800 ft (586.6 m). It should be noted however that samples from CPR were rounded to subrounded and greater than 10 mm.

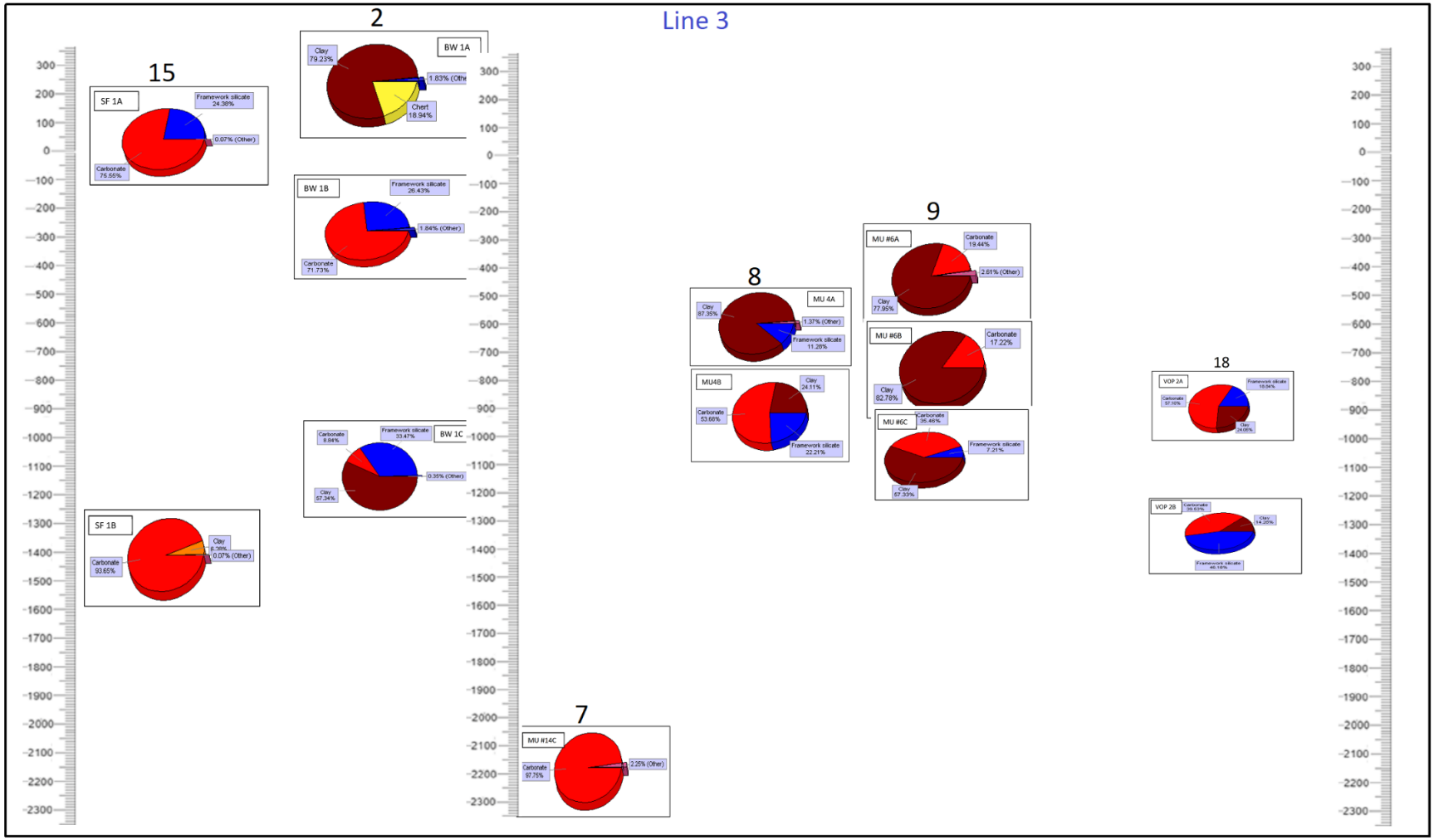

Figure 51. Profile line 3, the northern portion of thick clay deposit. Pie charts representing the proportion percentage with blue representing framework silicate material. Vertical scale in feet.

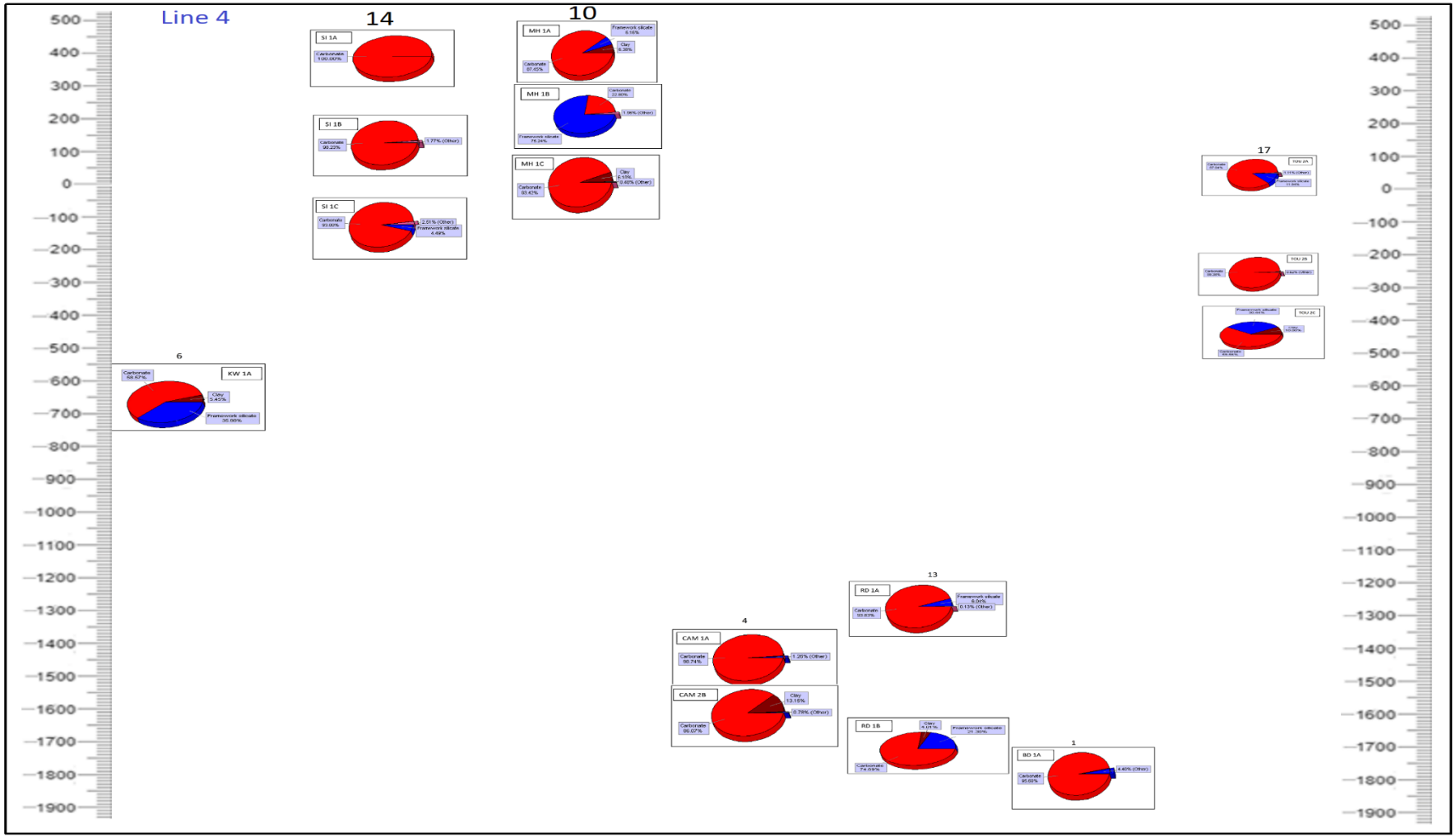

Figure 52. Profile line 3, the southern portion of thick clay deposit. Pie charts representing the proportion percentage with blue representing framework silicate material. Vertical scale in feet.

5.7.4 XRD preparation, sediment distribution

The preparation of samples for the XRD produced two parameters that can be used for correlation, 1) change in carbonate content of the clay, and 2) variation in sand-sized particles (Table 12). The analysis of variation in the sand is a two-fold process as both the quantity and texture (i.e., grain size and sphericity) indicate the distance from the source and energy of the depositional environment.

a. Chan Pine Ridge #1 samples (Figure 53) showed a decrease in both carbonate and sand content with depth. The grain size was the smallest as the upper and lower samples.

Well Number	Well Name	Quantity	Sample number	Carbonate Content change	Sediment quantity change	Sediment size change
5	Chan Pine Ridge #1	3	CPR #1A CPR #1B CPR #1C	Decrease with depth	Decrease with depth	Increase then decrease

Figure 53. Results from XRD sample preparation of CPR #1 samples.

b. Mike Usher #4 samples (Figure 54) showed an increase in carbonate and sediment size with depth. However, the number of sediments was relatively consistent at both depths.

Well Number	Well Name	Quantity	Sample number	Carbonate Content change	Sediment quantity change	Sediment size change
9	Mike Usher # 4	2	MU #4A MU #4B	Increase with depth	No change	Increase with depth

Figure 54. Results from XRD sample preparation of MU #4 samples.

c. San Ignacio #1 samples (Figure 55) showed no consistent patterns for all three criteria with an increase in carbonate content with depth, while the number of sediments showed a decrease then an increase. The size of the sediments was smaller at the upper and lower depth and larger in between.

Well Number	Well Name	Quantity	Sample number	Carbonate Content change	Sediment quantity change	Sediment size change
14	San Ignacio #1	3	SI #1A SI #1B SI #1C	Increase with depth	Decrease then increase	Increase then decrease

Figure 55. Results from XRD sample preparation of SI #1 samples.

d. Toucan #2 samples (Figure 56) also showed no consistent distribution of the three criteria as the carbonate content showed a slight decrease then an increase with depth. The number of sediments increased with depth however, the size change did not parallel this change, as the grain size increased initially then decreased with the deeper sample.

Well Number	Well Name	Quantity	Sample number	Carbonate Content change	Sediment quantity change	Sediment size change
17	Toucan #2	3	Tou #2A Tou #2B Tou #2C	Decrease then increase	Slight decrease with depth	Increase then decrease

Figure 56. Results from XRD sample preparation of Tou #2 samples.

e. Valley of Peace #2 samples (Figure 57) showed a similar change for both carbonate content and sediment quantity with both increasing with depth. The sediment size, however, decreased with depth.

Well Number	Well Name	Quantity	Sample number	Carbonate Content change	Sediment quantity change	Sediment size change
18	Valley of Peace #2	2	VOP #2A VOP #2B	Increase with depth	Increase with depth	Decrease with depth

Figure 57. Results from XRD sample preparation of VOP #2 samples.

Table 12. Table of subsurface samples used for XRD analysis, and changes to the samples during the preparation process. This includes weight changes due to interaction with acid, and residual sediments post decanting of clay.

Well Number	Well Name	Quantity	Sample number	Sample pictures	Extracted clay, on slide	Residual sediments	Percentage Carbonate	Carbonate Content change	Relative Sediment Quantity	Sediment quantity change	Sediment type	Average Sand Grade	Sediment size change
5	Chan Pine Ridge #1	3	CPR #1A				77.50	Decrease with depth	high	Decrease with depth	sand	fine to med	Increase then decrease
			CPR #1B				46.03		medium		sand	fine to coarse	
			CPR #1C	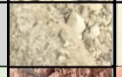	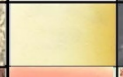		42.65		low		sand	fine to med	
9	Mike Usher # 4	2	MU #4A				36.44	Increase with depth	high	No change	sand to silt	fine to med	Increase with depth
			MU #4B				72.04		high		sand & gypsum	med to coarse	
14	San Ignacio #1	3	SI #1A				15.45	Increase with depth	medium	Decrease then increase	silt to sand	fine to med	Increase then decrease
			SI #1B	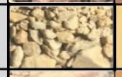			64.79		low		sand to silt	med to coarse	
			SI #1C				71.53		high		silt to sand	fine	
17	Toucan #2	3	Tou #2A		No appreciable clay		91.53	Decrease then increase	low	Slight decrease with depth	sand to silt	fine to med	Increase then decrease
			Tou #2B				59.78		medium		silt to sand	fine to coarse	
			Tou #2C				66.26		medium		silt to sand	fine to med	
18	Valley of Peace #2	2	VOP #2A				34.70	Increase with depth	medium	Increase with depth	silt to sand	fine to coarse	Decrease with depth
			VOP #2B				76.42		high		silt to sand	fine	

XRD results are correlated based on depth and location. Of the groups of clay, illite, montmorillonite, and chlorite were identified in all samples, while other samples also contained kaolinite and/or vermiculite (Figure 58).

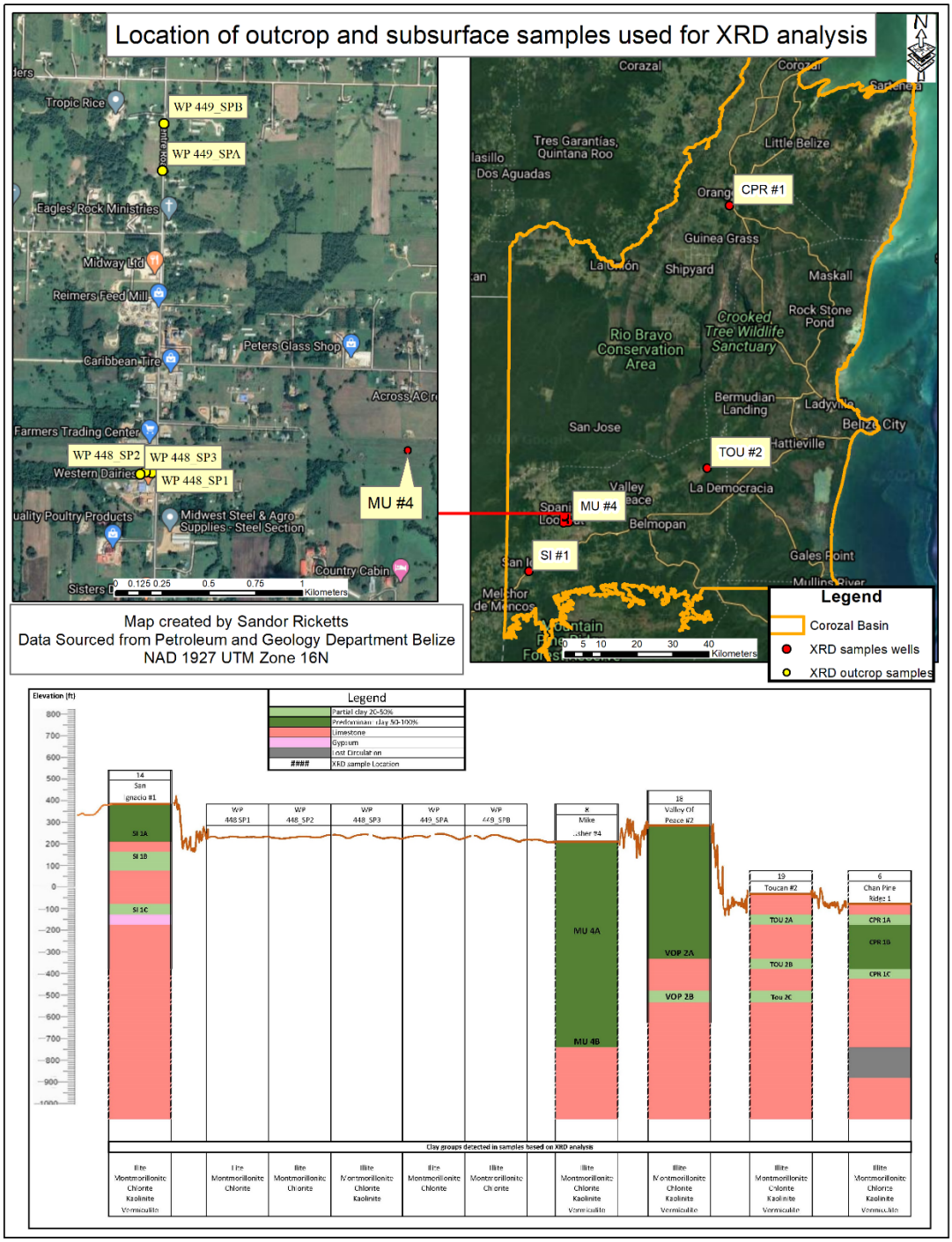

Figure 58. Location of samples used for XRD analysis. The tables below show wells aligned for elevation along with the results of the XRD pattern interpretation. Vertical scale in feet (Horizon Well Logging, Inc., 2016).

5.7.5 Depositional environment

To better understand and explain the process involved in the deposition of the RBG clay, the previous results and correlation were combined to determine how they related to sea-level changes. These are described:

a. The stratigraphic analysis portion of the study is important on various fronts. The fact that the deposit is clay indicates a low-energy environment for deposition. The analysis also determined that the deposit exists in a fault-bounded depression allowing for accommodation space to a depth of approximately 1200 ft (366 m) in some areas.
b. Biostratigraphic data was vital in determining the type of nannofossils present in the clay, allowing for the determination of a marine environment. Categorization of the nannofossils enabled the determination of an approximate age range of the deposit thus enabling a focal time period to investigate eustatic sea-level change, and if the change influenced the deposit.
c. Petrographic analysis of the samples allowed for a measure at a higher resolution of variations between lithology at various depths. Such variations were also gleaned from mudlog data which is of lower resolution. The combination of both resolutions then aided the identification of facies changes.
d. The mineralogical study determined the type of clay allowed for a depositional environment determination for each sample. The combined results then allowed for an overall depositional environment for the deposit.

5.7.6 Sea Level

The results of section 6.7.1 to 6.7.5 above when combined with eustatic sea-level data at the time of deposition indicates a clear relationship between sea-level change and the deposition, distribution, and depositional environment of the RBG (Table 13).

Table 13. Correlation of results with regards to the eustatic sea level.

Well Log Data	Stratigraphic	Biostratigraphic	Eustatic Sea Level (Miller et al., 2005)	Regional sea level (Rosenfeld and Pindell, 2003)	Mineralogical	Petrographic
Clay from the surface to about 1800 ft (548.6 m) deep	Depression due to fault and dissolution of limestone (karst)	Nannofossil biozone age approximately 57 to 54.17 m.y.	Regression of sea level before deposition of clay	Lowering of sea level caused by isolation due to collision of Cuban Arc and Florida/ Bahama Block	Area influenced by river influx	Varying proportion of each lithology with depth and location.
Thicker deposit within limestone enclosed basin	Thick clay within a localized depression	Deposited in a marine environment (shallow or deep). Nannofossil abundance varies with depth	During the proposed age location partially to submerged.	Isolation of waterway influence the flow of seawater.	Carbonate percentages vary with depth. Sphericity, roundness, sorting, and abundance of sand vary with depth and locality.	Presence of gypsum and varying amounts of sand grains.
Thinner deposits in channels in limestone	Karst linked to the cave system	Clay from various wells and locations are in the same age range	Deposited in a marine environment with an intermittent influx of seawater	The potential partial influx of seawater on the eastern section of Yucatan peninsula	All samples composed mainly of the same clay groups	

6 DISCUSSION AND INTERPRETATION

The project aimed to investigate the characteristics of the Red Bank group's clay deposits to determine their age, depositional environment, and the relationship between sea-level change and the deposition of the clay. With this information in hand, we can better resolve how the clay deposit would impact hydrocarbon exploration.

Previous literature and maps on the Corozal basin indicate that the study area is dominated by Cretaceous limestone (Ower, 1927, 1928; Flores, 1952; Purdy et al., 2003; Cornec, 2006). The rapid growth in hydrocarbon exploration since 2006 led to a large data collection in the area, showing that a portion of the Corozal basin is capped by thick deposits of clay. The extent of these deposits has been unknown, until now. Based on the interpretation of well logs it has been determined that a thick clay deposit is in the Spanish Lookout area of the basin. This has been verified from well log and seismic interpretation, and it has been determined that the thickest portions of the deposit are localized within the karstic limestone of the Barton Creek formation. This thick clay area includes various subsurface caverns and channels in the limestone, which help drain the area of rainwater.

This connection between the karst and channels has been determined by analyzing the age of the clay samples and their mineralogy. The nannofossils from both the karst and channels/caves are dated between 57.3 and 54.7 million years, indicating simultaneous deposition. The mineralogy of the clay in the channel also matched that of the thicker deposit. This discovery indicates a possible connection between the karst and channels in the limestone.

Such a connection would reduce the ability of the karst to retain water thereby prohibiting or slowing deposition. Filling of the karst would require blockage of the channels/caves and a constant influx of water and sediments. A steady supply of sediment and water can be attributed to various small tributaries feeding the major river (Belize River) draining the regional valley of the Maya Mountains range, west of the RBG deposit.

It should be noted, however, that based on proximity to the mountain range the deposit is in an area of potentially high energy. However, the sediments identified were below 10mm in grain size. Such small grain size suggests that at the time of the deposition the karst was in a low energy environment.

The nannofossils identified indicate that the sediments were deposited within a marine environment. Eustatic sea-level estimations published by Haq et al. (1987), Miller et al. (2005), and Miller (2009) indicate that the karst is located at a paleo-coastline (Figure 44), accounting for the marine nannofossils. Mudlog descriptions revealed the presence of terrestrial organic matter, suggesting an influx of terrestrial water. The influx of seawater, terrestrial water, and sediments over time could have resulted in deposition within channels and caves eventually blocking them and enabling buildup of clay in the karst. This interpretation addresses the sediment depositional environment and nannofossil but does not address the formation of the karst.

Karst features are formed by the dissolution of limestone in the presence of acidic groundwater, generally fresh rainwater containing dissolved carbon dioxide, thus yielding carbonic acid (Robbins, 2014). This implies that the study area was exposed to the atmosphere during a time of regression of the sea. Based on eustatic records we see that before the

deposition of the RBG, there was a period of regression that allowed for karst formation (Figure 59). The exposure of limestone to rainwater tends to be

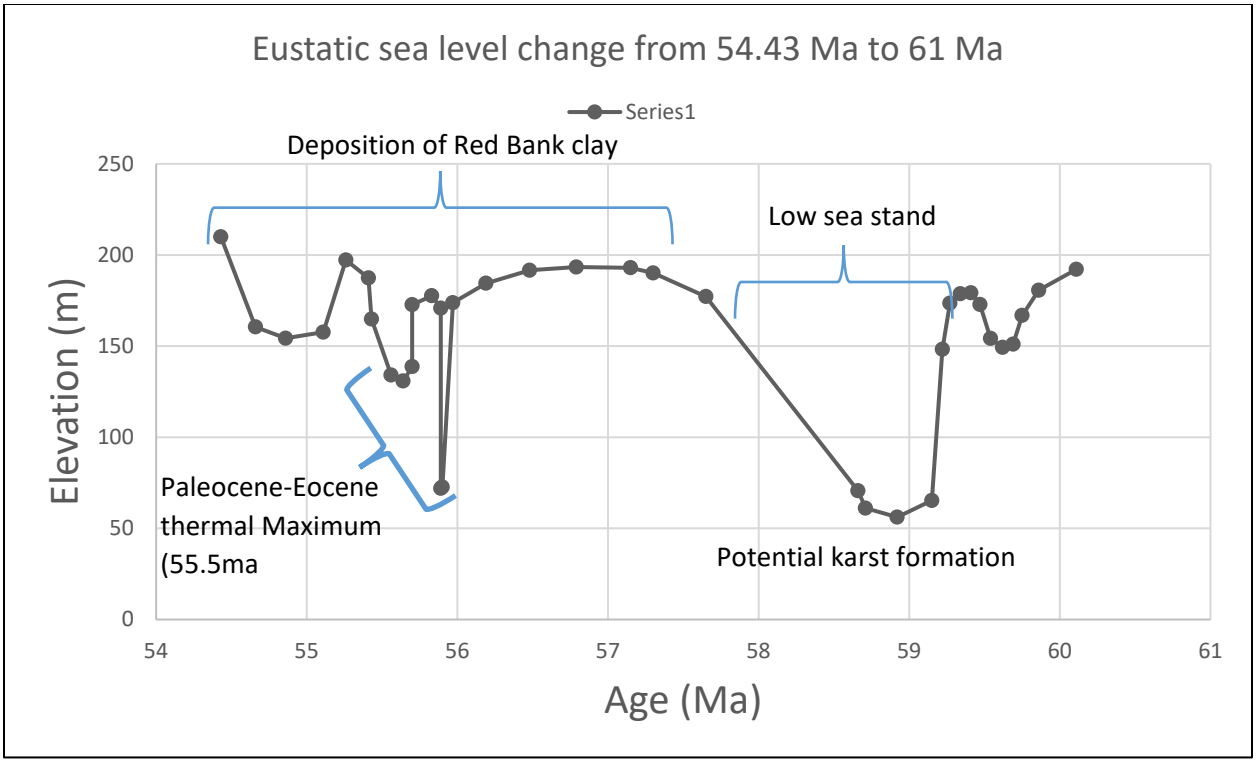

Figure 59. Sea-level curve data, lighting the time period during RBG deposition and period of regression of sea level allowing for karst formation.

aided by other factors such as cracks and fractures in the limestone and atmospheric changes (Robbins, 2014). The stratigraphic analysis using seismic data revealed several faults in the area which could have fractured the limestone allowing for the rapid dissolution of the limestone (Xu et al., 2017). This fracturing increased the infiltration of rainwater and water from the Belize River potentially increasing the dissolution of the limestone accelerating the karstification process during a period of regression (Figure 60). This increase in the dissolution rate of the limestone would result in a relatively rapid formation of karst/depression (Bauer-Gottwein et al., 2011) creating accommodation space for clay deposition.

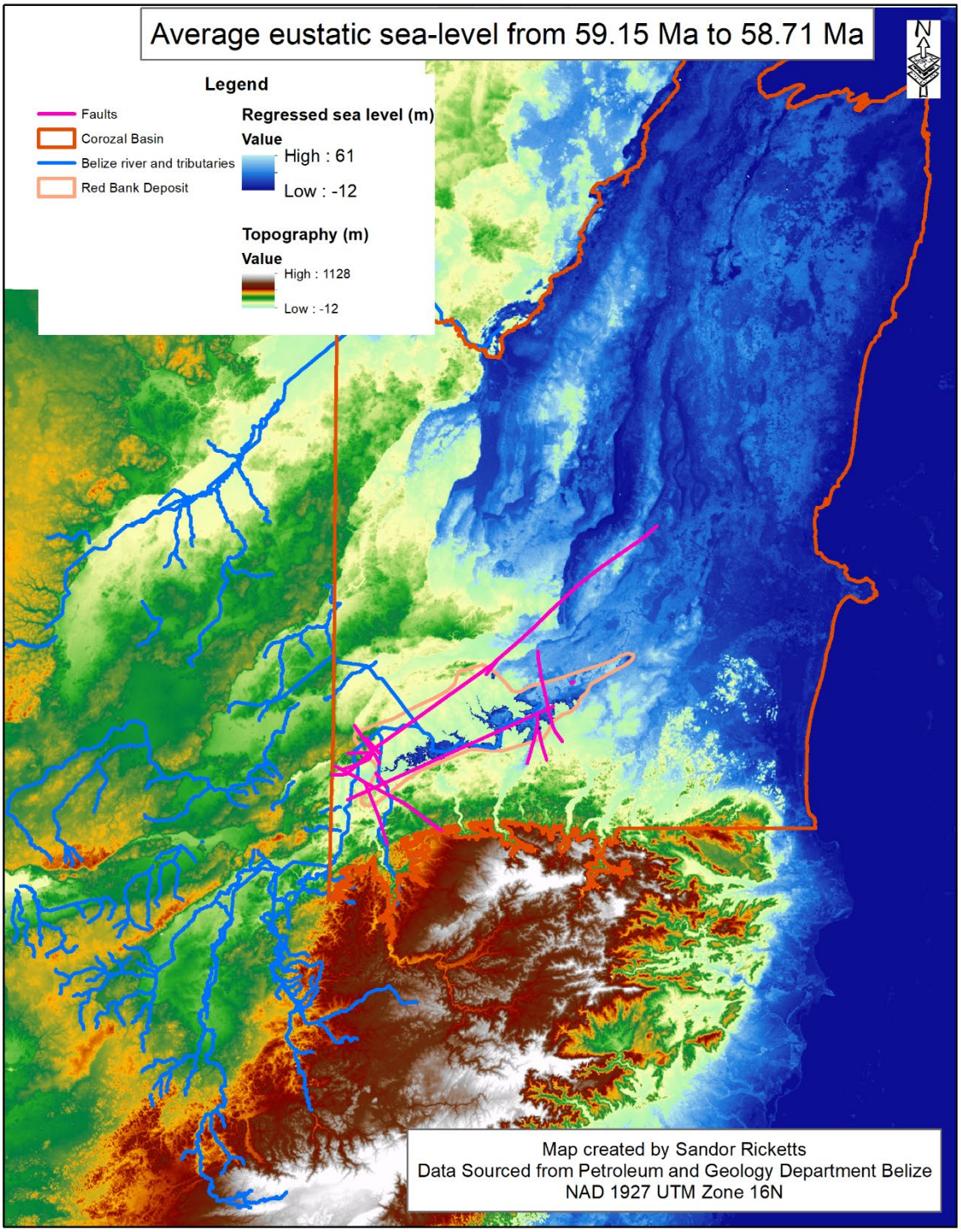

Figure 60. Regression of sea level allowing for karst formation before deposition of the RBG clay.

Work by Rosenfeld and Pindell (2003) has introduced a hypothesis of isolation of the Gulf of Mexico and the Yucatan Peninsula region during Paleogene. Such regional isolation could have resulted in a drawdown of the local sea level, perhaps leaving the study area exposed and

allowing for the development of karst. This drawdown suggested by Rosenfeld and Pindell (2003) would not have attributed to the formation of the karst in which the clay was deposited since the clay's origin share the same age range as the isolation. The nature of the nannofossils found in the clay also indicates that the area was inundated by seawater, which would have been absent during the isolation and drawdown suggested by Rosenfeld and Pindell (2003). The drawdown suggested does however coincide closely with the Paleocene-Eocene thermal maximum (PETM), which is thought to have occurred approximately 55.5 million years ago (Maslin et al., 2010). The occurrence of the PETM during the deposition of clay would have contributed to the development of evaporitic gypsum beds noted on the mudlog and interpreted from e-logs (Figure 61).

Such variations among sea level and other factors, such as fluctuations between marine and terrestrial influence would impact the mineralogy of the clay. As noted from the XRD analysis several major groups/species of clay were identified (Table 14), along with other associated mineral identified using the DIFFRAC.EVA software v4.2 (Table 15). Minerals such as smectite, palygorskite, and dolomite have been identified in deep-marine Cretaceous sediments in drill cores from the north and south Atlantic (Thiry, 1993). In that instance, smectite formation in those areas was attributed to alteration of silicate minerals at the water/sediment interface during periods of extended sea-level rise (Thiry, 1993), whereas, the occurrence of palygorskite is described as an indicator of an Mg-rich hypersaline warm environment (Thiry, 1993). A wider variety of minerals were identified during the analysis which may include mixed-layer clays because most sedimentary rock contains varieties of mixed-layer clay species (Scott, 1975).

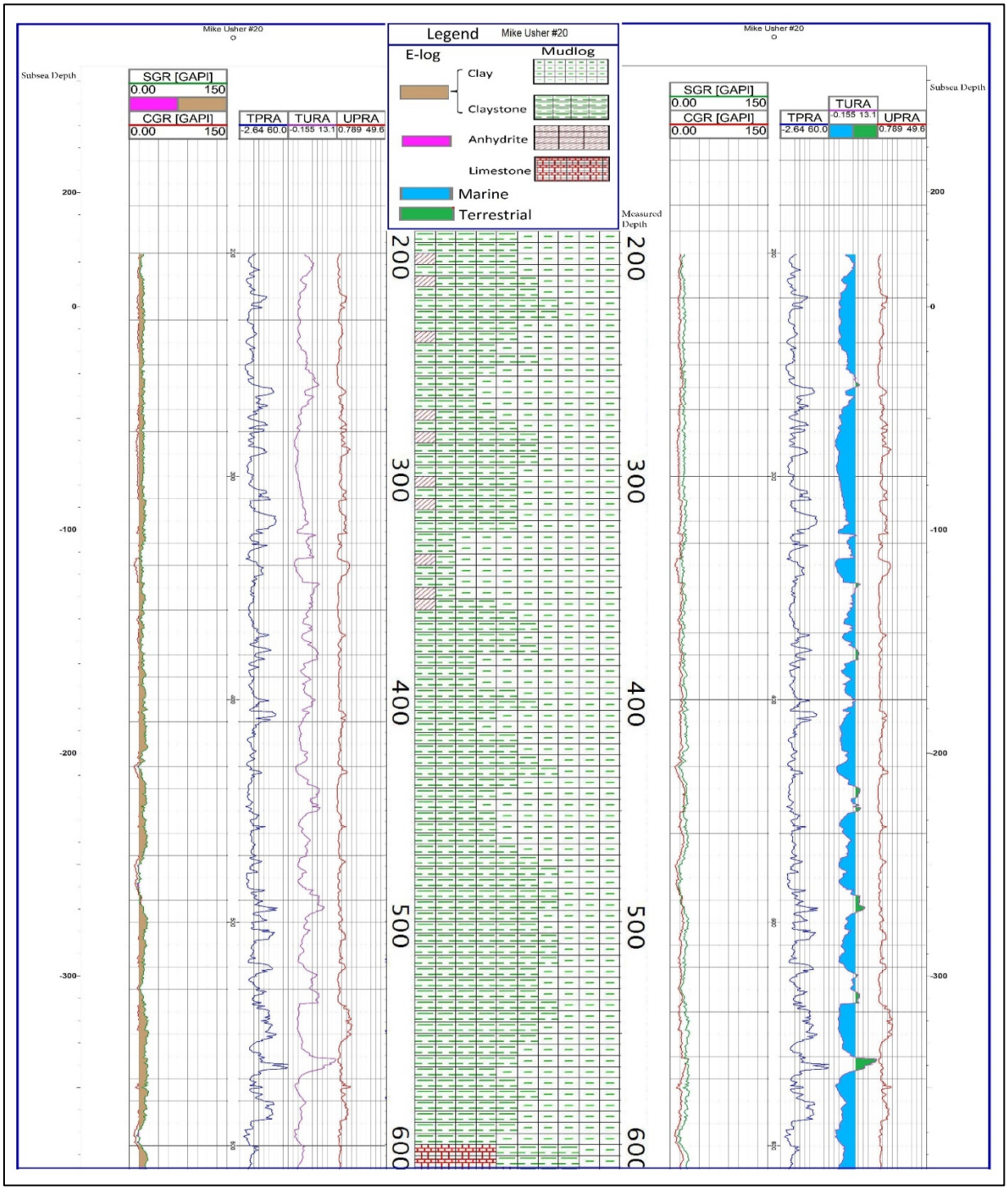

Figure 61. Combination of e-logs interpretation and lithology logs to identify gypsum along with regression and transgression facies changes. E-log on the left used to interpret gypsum (pink) clay (brown. E-log on the right used to interpret marine (blue) and terrestrial (green) influence. The lithology log in the middle shows variation between clay and claystone, variation may be attributed to variation in clay groups, increased clay results from increased hydration during the drilling process. Vertical scale in feet.

Table 14. Main mineral groups identified with XRD analysis. Tables created with data from Douglas (1993) and Barthelmy (2014).

Mineral	Group/species	information
Illite	Mica	Weathered product of feldspar and felsic silicates. Also, the authigenic alteration of K-spar or recrystallization of smectites in marine sediments.
Montmorillonite/ Smectite	Smectite	Originates from the weathering of mafic silicates, stable in arid semi-arid, or temperate climates. Absorbs large amounts of water.
Chlorite	Chlorite	Chlorites exist in soils as primary minerals that weather to form vermiculite and smectite. Also found in some metamorphic rocks.
Kaolinite	Kaolinite	Secondary mineral derived from the weathering of alumino-silicate minerals
Vermiculite	Mica	Appears to have been formed by weathering or hydrothermal alteration of iron-bearing phlogopite an annite

Table 15. Additional minerals identified with DIFFAC.EVA software. tables generated with data from DIFFRAC.EVA software and information from Thiry, (1993) and Barthelmy, (2014).

Mineral	Group	Description
Alunite	Alunite	Rock-forming mineral where acid, often ore-bearing, solutions have altered orthoclase feldspar-rich rocks.
Beraunite	Dana	A component of bog iron ores; a cement in clays, sands, and bone material; an alteration product of triphylite in granite pegmatites.
Billietite	Becquerelite	Occurs as an uncommon product of uraninite.
Chamosite	Chlorite	Metamorphosed iron deposits.
Clinochlore	Chlorite	Contact, hydrothermal, and regional metamorphism of mafic minerals
Manganiandrosite	Epidote	Forms a series with piemontite. Found in a manganese-rich silicate-carbonate rock.
Palygorskite	Palygorskite-sepiolite	Diagnostic of Mg-rich warm hypersaline environment
Tobelite	Mica	Hydrothermal alteration of biotite andesite dike or in a hydrothermally altered rhyolite tuff.

Variations in the clay resulted in multiple seismic reflectors (Figure 30, andFigure 31) some of which were misinterpreted as formation changes, resulting in inaccurate well prognosis and planning. Whereas the existence of such a thick clay deposit was not expected because previous literature did not indicate its presence, the thickness of clay deposits above Cretaceous limestone in northern Belize was not compensated for in seismic interpretations. Such a misinterpretation resulted in well planning that was shorter than the actual time required to drill the well, driving up the operational cost. Other properties of the clay including how readily sections expanded on rehydration also added delays to the exploration process. This rehydrated clay both affected the drilling fluid and the wellbore diameter adding to the delays. Prior knowledge of such a thick clay deposit, and their lateral dimensions, could have reduced these delays as there are many methods available in the hydrocarbon exploration process for counteracting the multiple effects of clay.

7 CONCLUSIONS

Mudlog data interpretation determined that the thickness of the clay varied based on its depositional location. The thickest clay deposit identified in the study was in an elongate karst-rich feature having an unconformable contact with the underlying Upper Cretaceous limestone (Figure 62). Thinner clay deposits have unconformable contacts within the limestone section. Both clay deposits were found to have the same nannofossils and same mineralogy, indicating the same sediment source and depositional time. These findings indicate that the karst was drained by a multiple cave system. Karst systems such as this one, have been identified

throughout the Caribbean and Gulf region including Belize (Miller, 1996; Bauer-Gottwein et al., 2011). Based on the age of the clay the karst development would have occurred sometime prior during a period of regression in sea level. Analysis of the sea-level records indicates that such a regression took place 58.71 to 59.15 Ma. ago, allowing exposure to atmospheric and meteoric water, facilitating dissolution of the faulted (verified from seismic) limestone, and formation of the karst and channel system.

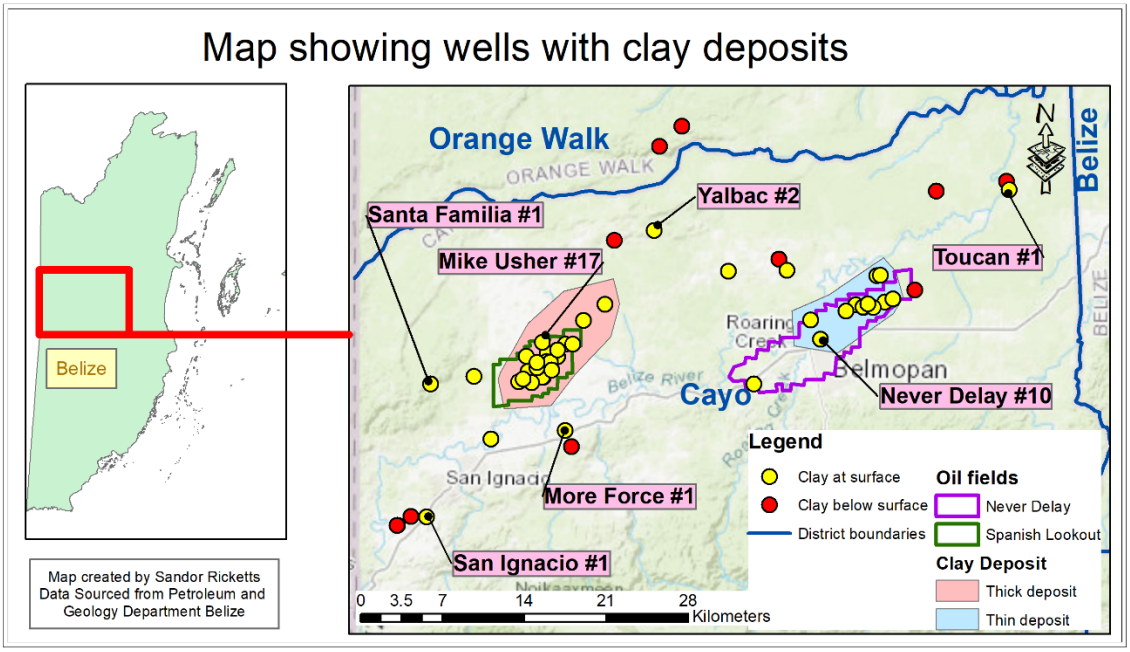

Figure 62. Surficial clay deposits in the study area identified from mudlog analysis.

This cave system was replenished with water and sediments from both a marine and terrestrial source as indicated by e-log interpretation and the presence of marine fossils. The terrestrial influence was corroborated by petrographic analysis and XRD sample preparation, during which fluctuating quantities of fine to coarse quartz grains were identified. The XRD analysis also indicated that components of the clay were generated by the weathering of

metamorphic rocks further emphasizing a terrestrial influx of sediments. This dual influx of water and sediments allowed for sedimentation in the subterranean channels and infilling of the karst. Such mixing would only occur at the mouth of a river that may have occupied that area. However, the location of the deposit is approximately 22.7 miles (36.5 km) inland from the current coastline.

Using sea-level records, it was determined that during the period of deposition the coastline was further west of its current position, approximately where the Red Bank clay deposit is located. This meant that with deposition, at the coastline, of clay and fine sand occurred in a low-energy environment.

This low-energy environment and low relief of the area with a constant influx of freshwater fits an environment for formation on an estuary, in which the deposition of the clay was influenced and affected by regression and transgression of the sea, with a potentially lesser influence by the sea level draw-down in the Gulf of Mexico region during the Paleocene to Eocene transition.

8 REFERENCES CITED

Agnini, C., S. Monechi, and I. Raffi, 2017, Calcareous nannofossil biostratigraphy: historical background and application in Cenozoic chronostratigraphy: Lethaia, v. 50, no. 3, p. 447–463.

Aitken, J. A., and R. R. Stewart, 2002, A geological / geoscience overview of the hydrocarbon exploration potential of Belize, Central America: America, CREWES research report v. 14, no. 2002.

Al-Ani, T., and O. Sarapaa, 2008, Clays and Clay Mineralogy: Industrial and Engineering Chemistry Research, v. 31, p. 1–91.

Barthelmy, D., 2014, Mineralogy Database: <http://www.webmineral.com/> (accessed June 17, 2020).

Bauer-Gottwein, P., B. R. N. Gondwe, G. Charvet, L. E. Marín, M. Rebolledo-Vieyra, and G. Merediz-Alonso, 2011, Review: The Yucatán Peninsula karst aquifer, Mexico: Hydrogeology Journal, v. 19, p. 507–524.

Cohen, K. ., S. C. Finney, P. L. Gibbard, and J.-X. Fan, 2020, The ICS International Chronostratigraphic Chart 2020/01. International Commission on Stratigraphy, IUGS: p. 199–204: <http://www.stratigraphy.org/ICSchart/ChronostratChart2020-01.pdf>.

Cornec, J. H., 2006, Geology map of Belize with bathymetry (1-750,000): Geology and Petroleum Office, Belmopan, Belize.

Douglas, L. A., 1993, Introduction to Clay Minerals. 1992: Soil Science, v. 156, p. 289.

Fisher, J. D., and D. T. King, Jr., 2015, Stratigraphy of the Toledo Formation, Belize Basin, Southern Belize: GCAGS Transactions, v. 65, p. 107–123.

Flores, G., 1952, Summary report of the preliminary geological studies of the area north of 17° North Latitude, British Honduras: Geology and Petroleum Office, Belmopan, Belize, 71 p.

Gill, K. K., D. T. King, Jr., H. Zou, and F. Smith, 2018, Sedimentary Facies Analysis and Strontium-Isotope Stratigraphy of the Hillbank and Yalbac Formation, Corozal Basin, Belize: Gulf Coast

Association of Geological Societies Transactions, v. 68, p. 229–254.

GSA (Geological Society of America), 1970, Rock color chart: Boulder, Colorado, Geological Society of America.

Haq, B. U., J. Hardenbol, and P. R. Vail, 1987, Chronology of fluctuating sea levels since the Triassic: Science, v. 235, no. 4793, p. 1156–1167.

Horizon Well Logging, Inc., 2006, Lexicon of Descriptive Terms For Wellsite Geology with Standard Abbreviations: 1–12 p.

Horizon Well Logging, Inc., 2016, Mudlogs.

Kansas Geological Survey, 2017, KGS--Geological Log Analysis--The Gamma-Ray Log: <http://www.kgs.ku.edu/Publications/Bulletins/LA/03_gamma.html> (accessed June 13, 2020).

Lewis, K. (2000). *Colonial education: A history of education in Belize*. Paper presented at the Annual Meeting of the American Educational Research Association. New Orleans, LA. (April 24–28, 2000).

King, Jr., D. T., J. Cornec, L. Petruny, D. Milham, B. Holland, S. Ricketts, N. R. Myers, R. D. Weber, and R. George, 2018, Sedimentary Characteristics and Geological History of the Cenozoic Red Bank Group, Nothern Belize: Gulf Coast Association of Geological Societies Transactions, V. 68, p. 269–284.

King, Jr., D. T., and L. Petruny, 2012, Northern Belize's onshore petroleum stratigraphy, structures, and oil seeps: Gulf Coast Association of Geological Societies Transactions, v. 62, p. 227–242.

King, Jr., D. T., L. W. Petruny, K. O. Pope, and Anonymous, 2003, Shallow-marine facies of the Orange Walk Group, Miocene-Pliocene, northern Belize (Central America); Gulf Coast Association of Geological Societies Transactions, v. 53, p. 384–397.

King, Jr., D. T., K. O. Pope, and L. W. Petruny, 2004, Stratigraphy of Belize, North of the 17th Parallel: Gulf Coast Association of Geological Societies Transactions, v. 54, p. 289–304.

Larsen, D., D. J. Ashe, and J. Gustavson, 2015, Mineralogy and petrology of the Paleocene

Clayton and Porters Creek Formations, Missouri, USA: Influence of Cretaceous-Paleogene impact debris and diagenesis: Geological Society of America, Special Paper 515, p. 103–123.

Lary, E., B. Cymes, M. Burke, and M. Krekeler, 2018, An unusual clay-rich karst fill in the southeastern Yucatan reveals unrecognized geologic complexities and potential resources in the region: Geological Society of America Abstracts with Program V.50, paper number 35-3.

Mann, P., 1999, Caribbean sedimentary basins: classification and tectonic setting from Jurassic to present, *in* Sedimentary Basins of the World: p. 3–31.

Martini, E., 1971, Standard Tertiary, and Quaternary Calcareous Nannoplankton Zonation, *in* Proceedings of the 2nd Planktonic Conference: p. 739–785.

Maslin, M., M. Owen, R. Betts, S. Day, T. D. Jones, and A. Ridgwell, 2010, Gas hydrates: Past and future geohazard. Philosophical Transactions of the Royal Society A: Mathematical, Physical and Engineering Sciences, v. 368, p. 2369–2393.

Miller, T. E., 1996, Geologic and hydrologic controls on karst and cave development in Belize: Journal of Cave and Karst Studies, v. 58, p. 100–120.

Miller, K. G., 2016, Index of /ftp.ncdc.noaa.gov/pub/data/paleo/contributions_by_author/miller2005/: <https://1.climate.daknob.net/ftp.ncdc.noaa.gov/pub/data/paleo/contributions_by_author/miller2005/> (accessed June 8, 2020).

Miller K.G. (2009) Sea Level Change, Last 250 Million Years. In: Gornitz V. (eds) Encyclopedia of Paleoclimatology and Ancient Environments. Encyclopedia of Earth Sciences Series. Springer, Dordrecht, p. 649–651.

Miller, K. G., M. A. Kominz, J. V. Browning, J. D. Wright, G. S. Mountain, M. E. Katz, P. J. Sugarman, B. S. Cramer, N. Christie-Blick, and S. F. Pekar, 2005, The phanerozoic record of global sea-level change: Science, v. 310, p. 1293–1298.

Moore, D. M., and R. C. Reynolds, 1997, X-ray diffraction and the identification and analysis of clay minerals: X-ray diffraction and the identification and analysis of clay minerals, Second edition, p. 84–103.

Muhs, D. R., J. F. Wehmiller, K. R. Simmons, and L. L. York, 2003, Quaternary sea-level history of the United States: Development in Quaternary Science, 1, p. 147–183.

NACSN (North American Commission on Stratigraphic Nomenclature), 2005, North American Stratigraphic Code: American Association of Petroleum Geologists Bulletin, v. 89, p. 1547–1591.

Okada, H., and D. Bukry, 1980, Supplementary modification and introduction of code numbers to the low-latitude coccolith biostratigraphic zonation: Marine Micropaleontology, v. 5, p. 321–325.

Ower, L. H., 1927, Features of British Honduras: The Geographical Journal, v. 70, p. 372.

Ower, L. H., 1928, Geology of British Honduras: The Journal of Geology, v. 36, p. 494–509.

Poppe, L. J., V. F. Paskevich, J. C. Hathaway, and D. S. Blackwood, 2001, A Laboratory Manual For X-Ray Powder Diffraction: US Geological Survey Open-File Report, v. 1.041, p. 1–88.

Pratt, B. R., and R. Riding, 1993, Calcareous Algae and Stromatolites: PALAIOS, p 21-51.

Purdy, E. G., E. Gischler, and A. J. Lomando, 2003, The Belize margin revisited. 2. Origin of Holocene antecedent topography: International Journal of Earth Sciences, v. 92, p. 552–572.

Purdy, E. G„ Pusey, W. C., and Wantland, K. F., 1975, Continental shelf of Belize- Regional shelf attributes, *in* Wantland, K. F., and Pusey, W. C., eds., Belize shelf-carbonate sediments, clastic sediments, and ecology: Am. Assoc. Petroleum Geologists Studies in Geology, v. 2, p. 1-40.

Rica, C., R. Weyl, and H. Williams, 2007, Stratigraphy and geologic history: Chapter 13 16–18 p.

Robbins, P., 2014, Karst Topography: Encyclopedia of Environment and Society (Vols. 1-5) Thousand Oaks, CA: Sage

Rosenfeld, J., 2016, Paleocene-Eocene Drawdown and Refill of the Gulf of Mexico *: Search and Discover Article v. 30455.

Rosenfeld, J., and J. Pindell, 2003, Early Paleogene isolation of the Gulf of Mexico from the world's oceans. Implications for hydrocarbon exploration and eustasy, in C. Bartolini, R. T. Buffler, and J. Blickwede, eds., The Circum-Gulf of Mexico and the Caribbean: Hydrocarbon habitats, basin formation, and plate tectonics: AAPG Memoir 79, p. 89– 103.

Rosenfeld, J., and J. Pindell, 2002, US Gulf's early isolation from ocean hypothesis for steep base-level fall: Offshore Magazine, International Edition, v. 62, no. 1.

Salvador, A., ed., 1994, International stratigraphic guide: A guide to stratigraphic classification, terminology, and procedure: Geological Society of America, Boulder, Colorado, 214 p.

Scott MR, 1975, Distribution of clay minerals on Belize Shelf. In: Wantland KF, Pusey WC (eds) Belize shelf-carbonates sediments, clastic sediments, and ecology. AAPG Stud Geol 2:97–130

Thiry, M., 1993, Clay Mineral Distribution Related to Rift Activity, Sea-Level Changes, and Paleoceanography in the Cretaceous of the Atlantic Ocean: Clay Minerals, v. 28, p. 61–84.

Varol, O., 1989, Eocene calcareous nannofossils from Sile, (northwest Turkey). Revista Española de Micropaleontologia: 21 (2) 273–320 p.

Williams G., Fensome R., Miller M., Bujak J. (2018) Microfossils: Palynology. In: Sorkhabi R. (eds) Encyclopedia of Petroleum Geoscience. Encyclopedia of Earth Sciences Series. Springer, Cham p. 2–16.

Xu, X., Q. Chen, C. Chu, G. Li, C. Liu, and Z. Shi, 2017, Tectonic evolution and paleokarstification of carbonate rocks in the Paleozoic Tarim Basin: Carbonates and Evaporites, v. 32, no. 4, p 487- 496

9 APPENDICES

Appendix I, Map compiled using Owers' 1927 notes.

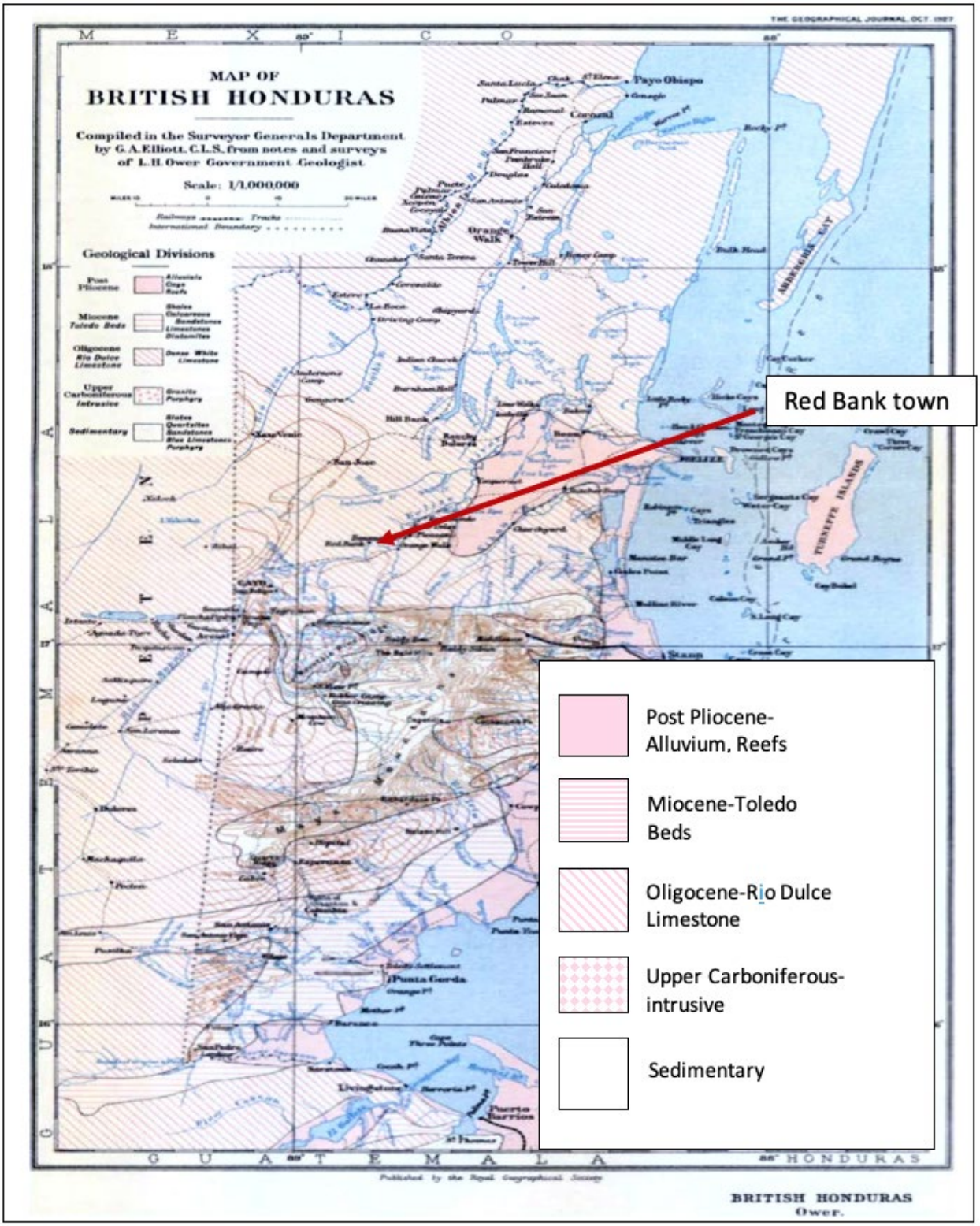

Appendix II, Fossils identified in Flores' 1952 study.

FOSSILS OF MIO-PLEISTOCENE AGE

	F-14	F-16	F-38	F-39	F-42		F-278	C-91
Amphistegina sp.		X	X	X				X
Angulogerina sp.					X			
Bolivina sp.					X			
Bryozoa			X	X				X
Cibicides sp.		X			X			
Discorbis sp.					X			
Elphidium sp.	X		X	X	X		X	X
Mollusca fragments		X	X				X	X
Nonionella sp.		X			X		X	
Pecten		X		X				
Rotalia beccarii	X	X	X	X	X		X	X
Textidaria sp.					X			

FOSSILS OF MIDDLE EOCENE AGE

	F-45	C-134	C-136		C-142	C-146
Amphistegina cf. ***A.*** *lopeztrigoi*			X			
Bolivina sp.					X	
Coskinolina fioridana	X	X	?		X	X
Discocyclina sp.			X			
Dictyoconus cookei		X				
Dictyoconus cf. ***D.*** *americanus*	X		X			
Globigerina sp.						
Globorotalia sp.					X	?
Helicostegina			?			
Lituonella fioridana						X
Miliolids	X	X			X	X

FOSSILS OF PALEOCENE-LOWER EOCENE AGE

	F-48	F-109	F-117	F-119	F-123	F-154	F196	F-202	Y-20	Y-25	C-47	C-76
Discocyclina sp.									X			
Globigerina sp.	X											
Globorotalia sp.	X											
Flexagonocyclina cattdri												?
Lockhartia	X									X		X
Miliolids	X		X	X		X	X	X	X	X	X	
Miscellanea cf. M. nassauensis?										X		X
Miscellanea cf. M. bermttdezi									X	X		
Pellatspirella cf. P. nassattensis			X							X	X	
Raadshoovenia guatemalensis(?)										X		
Rhapydionina limbata				X	X	X	X	X				
Rhapydionina sp.	X							X				
Rotalia aff. *R. trochidiformis*		X	X	X	X			X		X	X	
Rotalia sp.						X	X					X
Taberina cubana		X								X	X	
Taberina sp.												?
Valvttlina sp.	X	X	X		X	X	X	X		X	X	X

FOSSILS OF UPPER CRETACEOUS AGE

	F-107	F=174	F-235	F-258	F-263	Y-33	C-42
Dicyclina sp.	X			X			X
Locklzartia				X			
Miliolids sp.	X		X	X	X		X
Nummoloculina sp.						X	
Rotalids sp.	X	?					
Rudistid fragments		X	X		X	X	
V alvulina sp.	X						X

Appendix III, Localities of fossils used in Flores' 1952 study

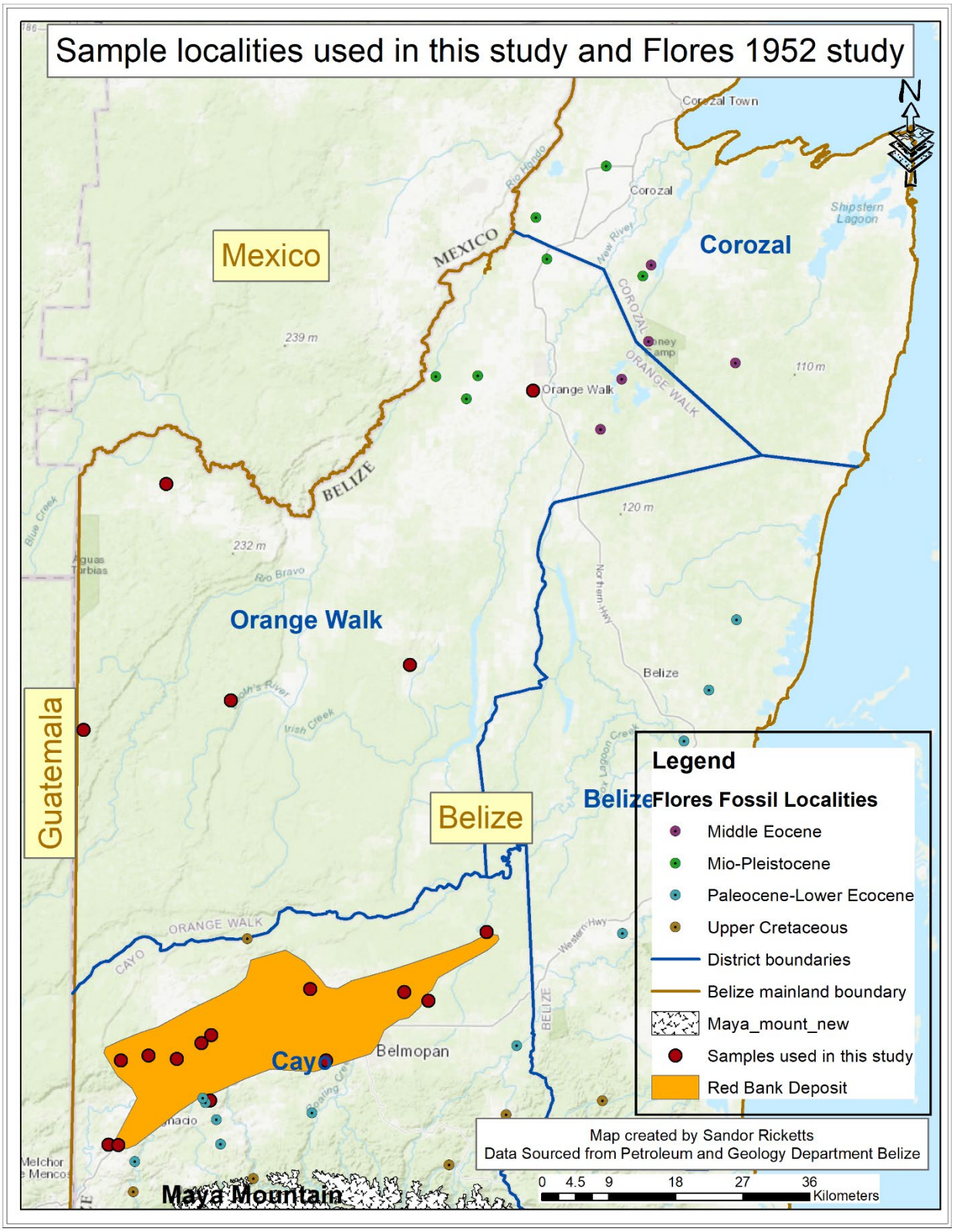

Appendix IV, Geologic map of Belize produced by J. Cornec (2006).

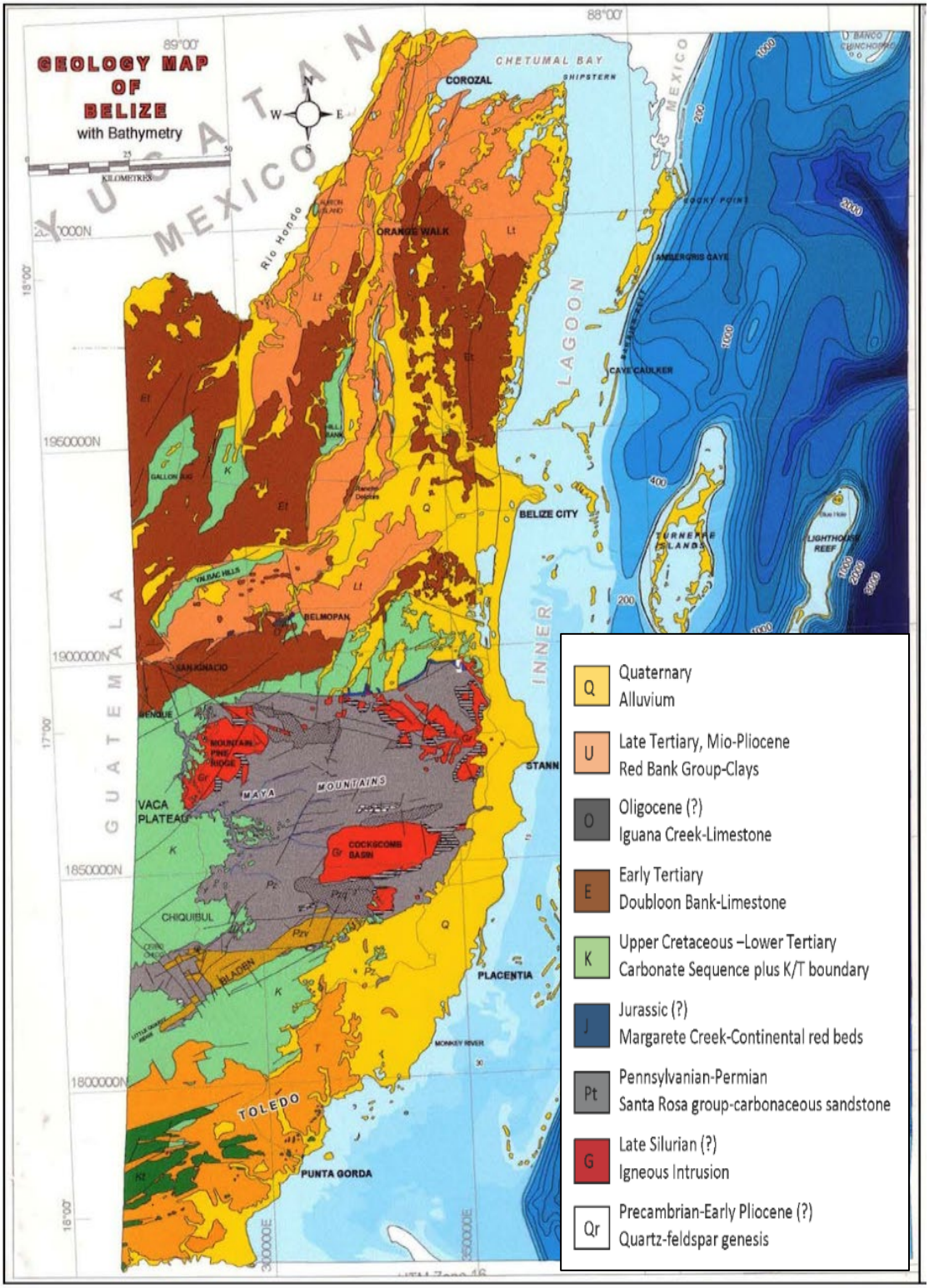

Appendix V, Petrographic analysis of samples.

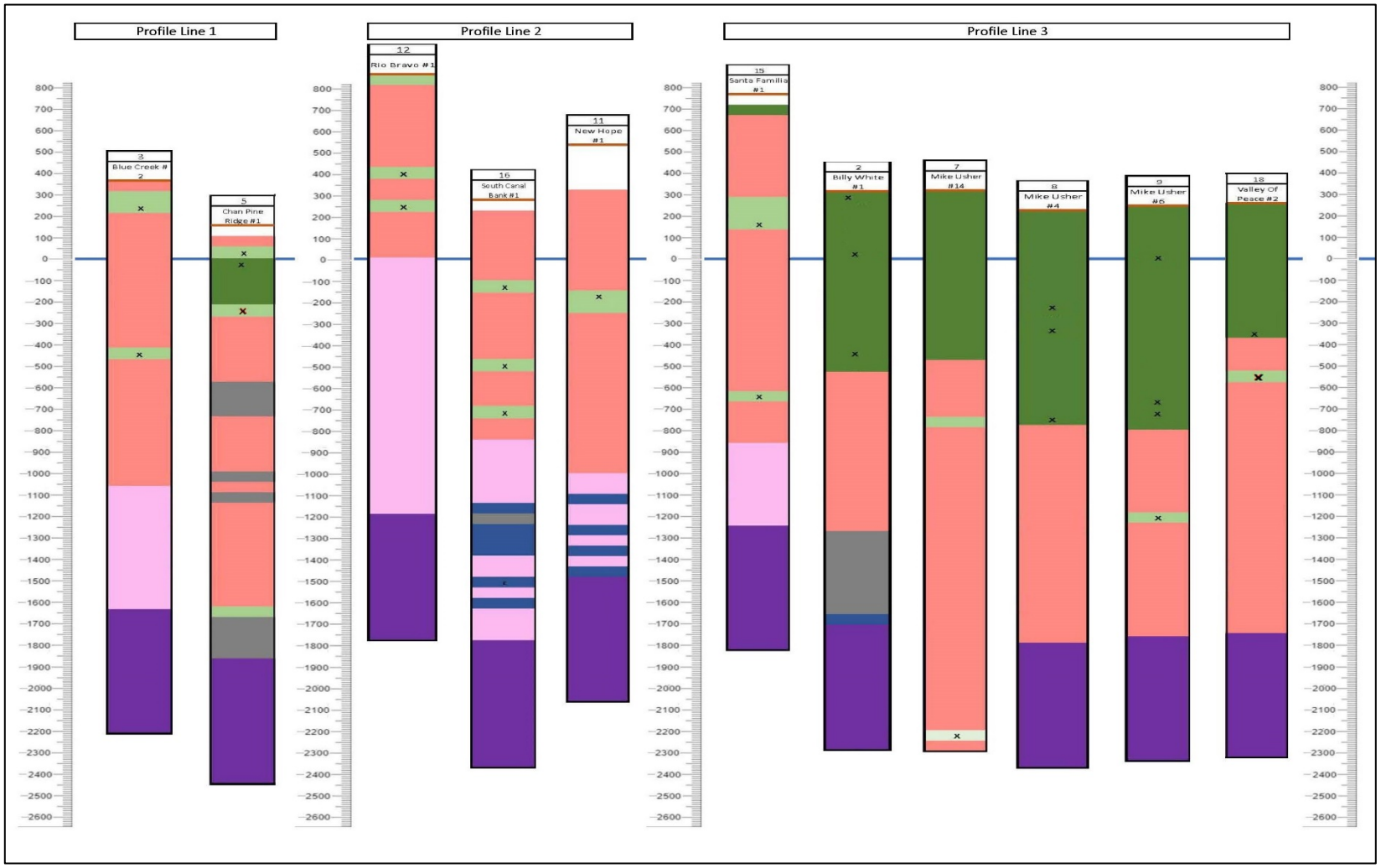

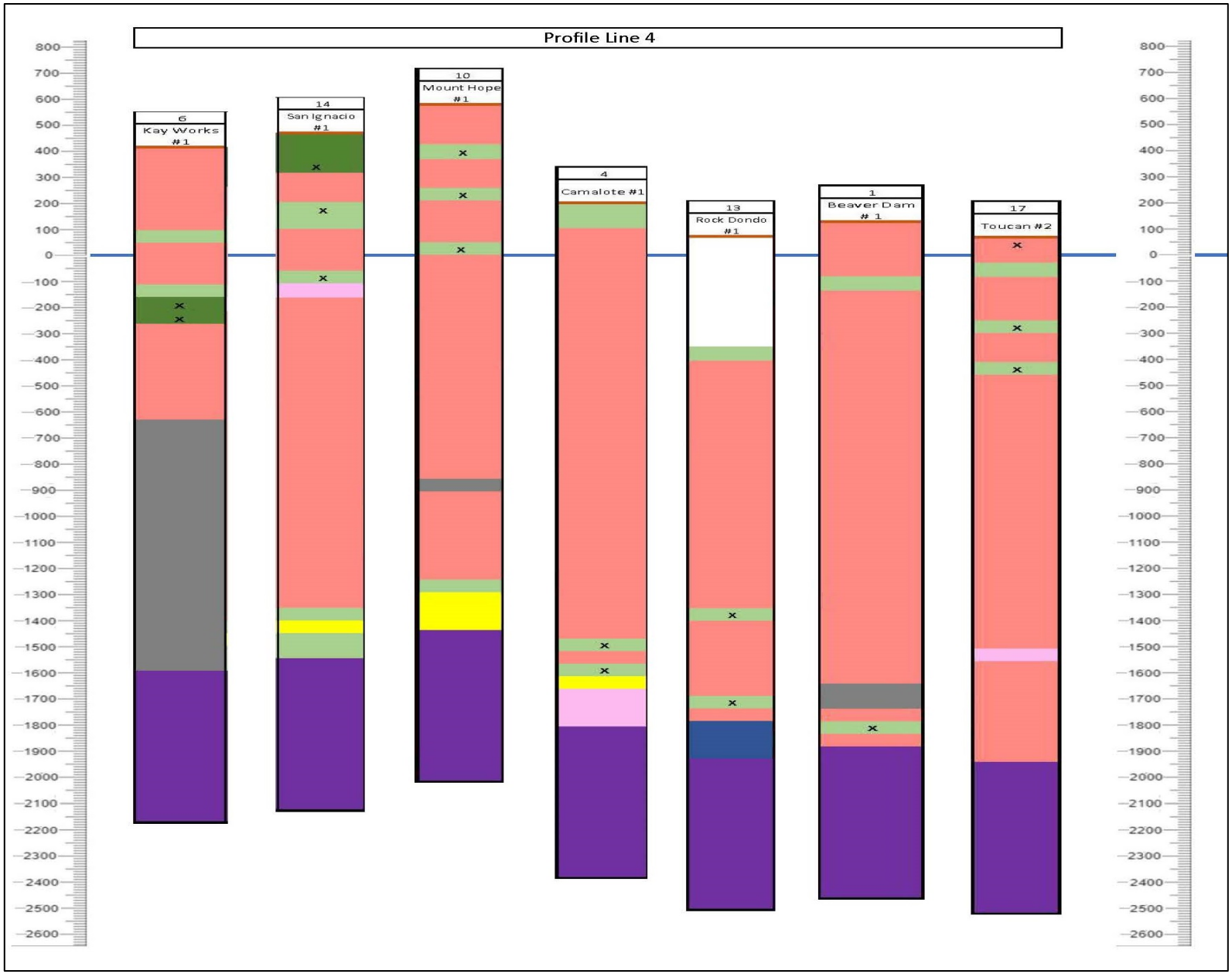
Profile Line 4
6
Kay Works
#1
14
San Ignacio
#1
10
Mount Hope
#1
4
Camalote #1
13
Rock Dondo
#1
1
Beaver Dam
1
17
Toucan #2
800
700
600
500
400
300
200
100
0
-100
-200
-300
-400
-500
-600
-700
-800
-900
-1000
-1100
-1200
-1300
-1400
-1500
-1600
-1700
-1800
-1900
-2000
-2100
-2200
-2300
-2400
-2500
-2600

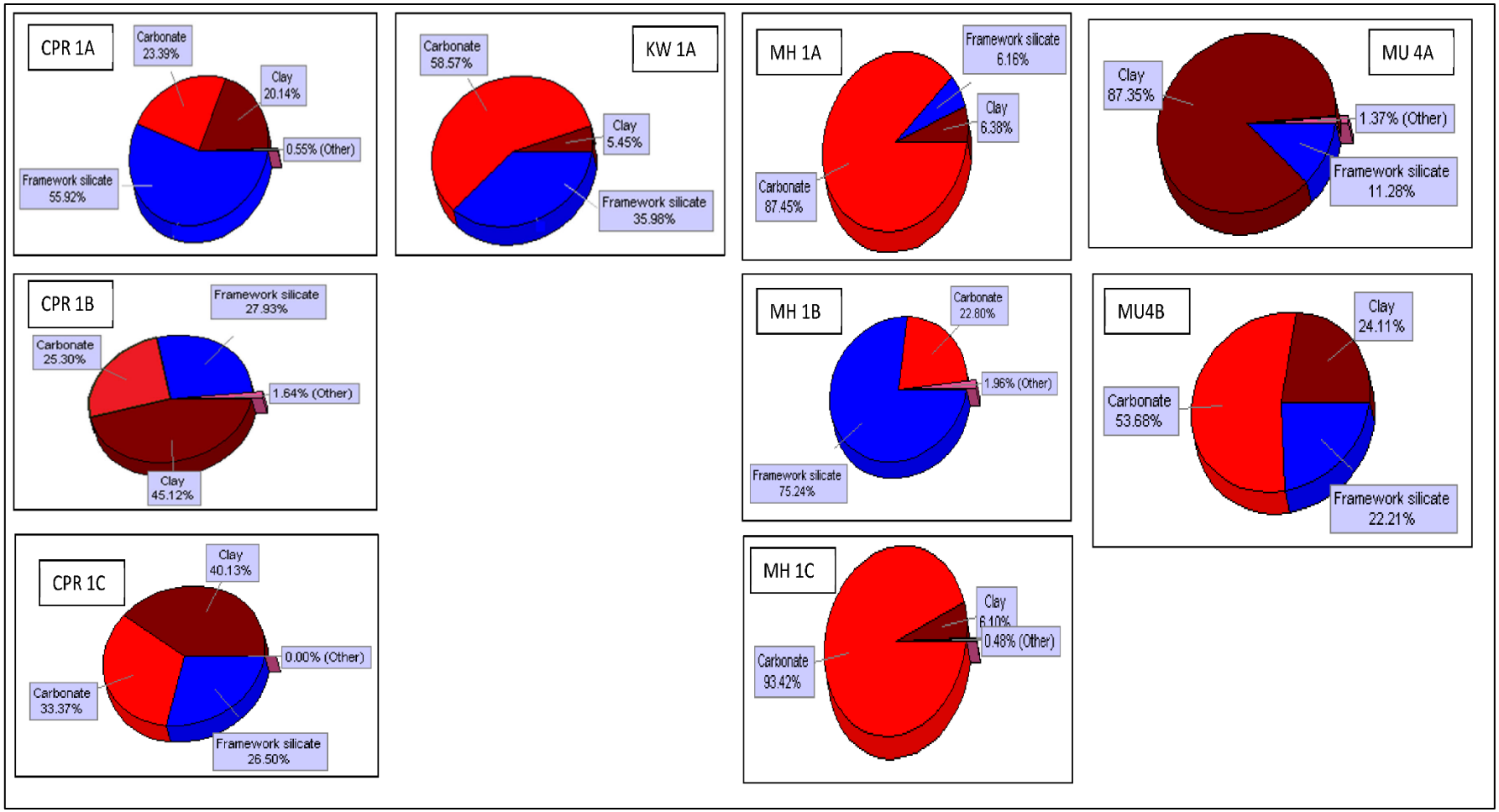
CPR 1A
Carbonate 23.39%
Clay 20.14%
0.55% (Other)
Framework silicate 55.92%
KW 1A
Carbonate 58.57%
Clay 5.45%
Framework silicate 35.98%
MH 1A
Framework silicate 6.16%
Clay 6.38%
Carbonate 87.45%
MU 4A
Clay 87.35%
1.37% (Other)
Framework silicate 11.28%
CPR 1B
Framework silicate 27.93%
Carbonate 25.30%
1.64% (Other)
Clay 45.12%
MH 1B
Carbonate 22.80%
1.96% (Other)
Framework silicate 75.24%
MU4B
Clay 24.11%
Carbonate 53.68%
Framework silicate 22.21%
CPR 1C
Clay 40.13%
0.00% (Other)
Carbonate 33.37%
Framework silicate 26.50%
MH 1C
Clay 6.10%
0.48% (Other)
Carbonate 93.42%

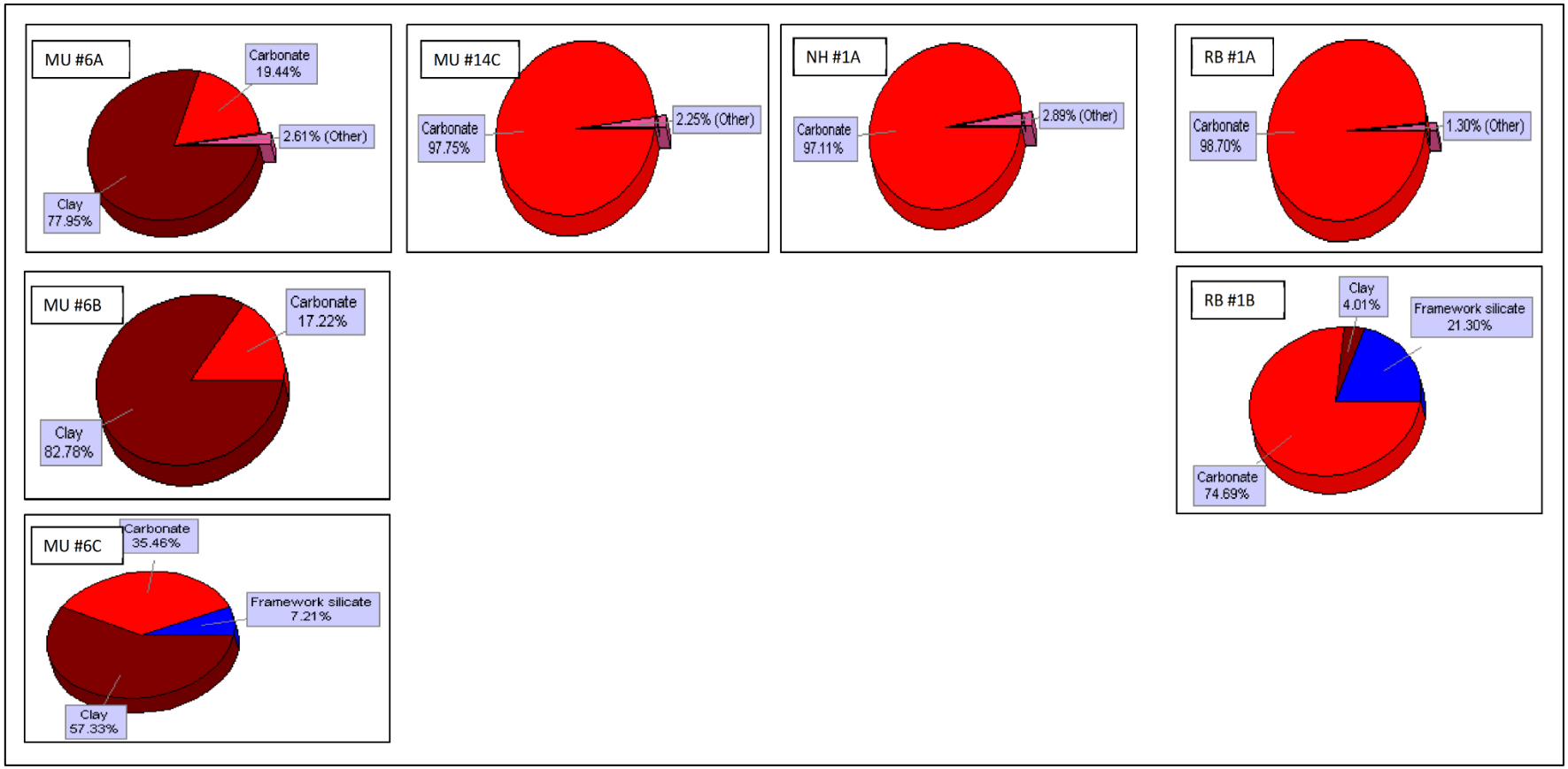
MU #6A
Carbonate 19.44%
2.61% (Other)
Clay 77.95%
MU #14C
Carbonate 97.75%
2.25% (Other)
NH #1A
Carbonate 97.11%
2.89% (Other)
RB #1A
Carbonate 98.70%
1.30% (Other)
MU #6B
Carbonate 17.22%
Clay 82.78%
RB #1B
Clay 4.01%
Framework silicate 21.30%
Carbonate 74.69%
MU #6C
Carbonate 35.46%
Framework silicate 7.21%
Clay 57.33%

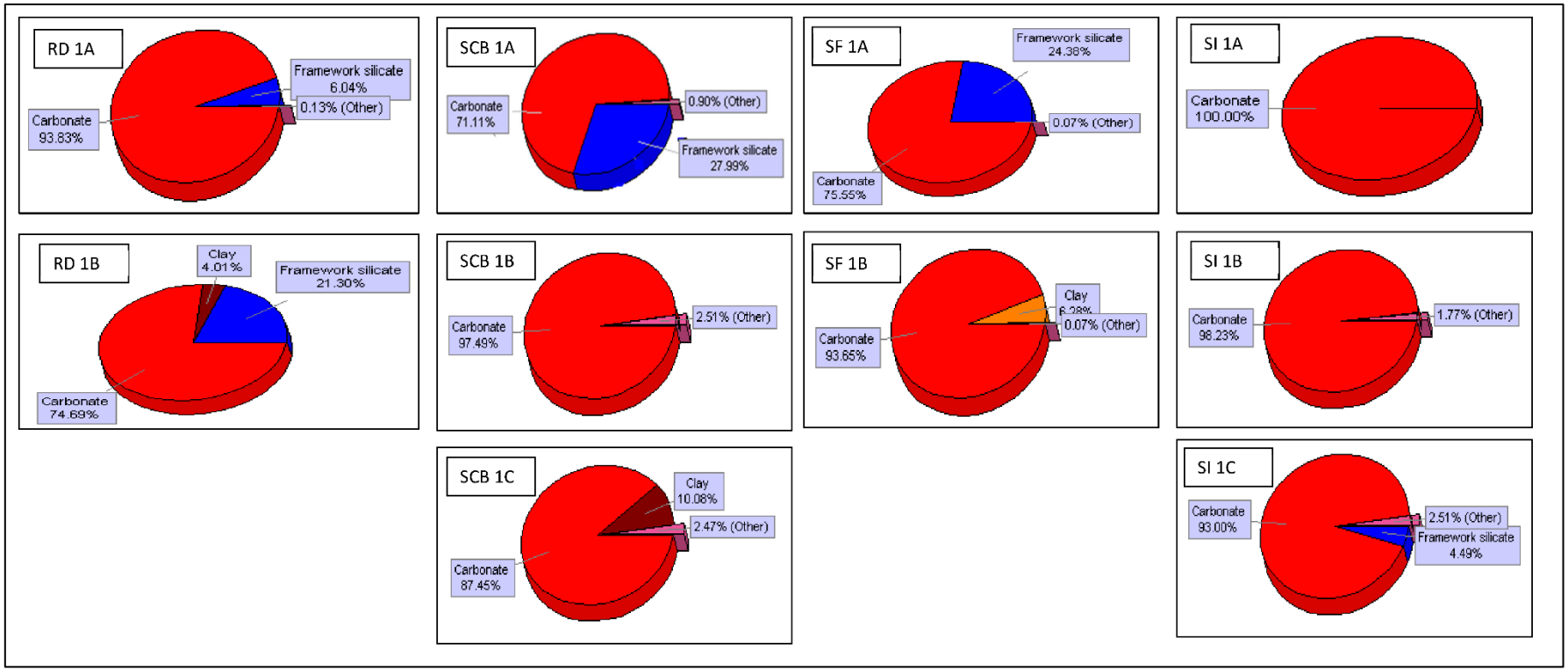
RD 1A
Framework silicate 6.04%
0.13% (Other)
Carbonate 93.83%
SCB 1A
Carbonate 71.11%
0.90% (Other)
Framework silicate 27.99%
SF 1A
Framework silicate 24.38%
0.07% (Other)
Carbonate 75.55%
SI 1A
Carbonate 100.00%
RD 1B
Clay 4.01%
Framework silicate 21.30%
Carbonate 74.69%
SCB 1B
Carbonate 97.49%
2.51% (Other)
SF 1B
Clay 6.28%
0.07% (Other)
Carbonate 93.65%
SI 1B
Carbonate 98.23%
1.77% (Other)
SCB 1C
Clay 10.08%
2.47% (Other)
Carbonate 87.45%
SI 1C
Carbonate 93.00%
2.51% (Other)
Framework silicate 4.49%

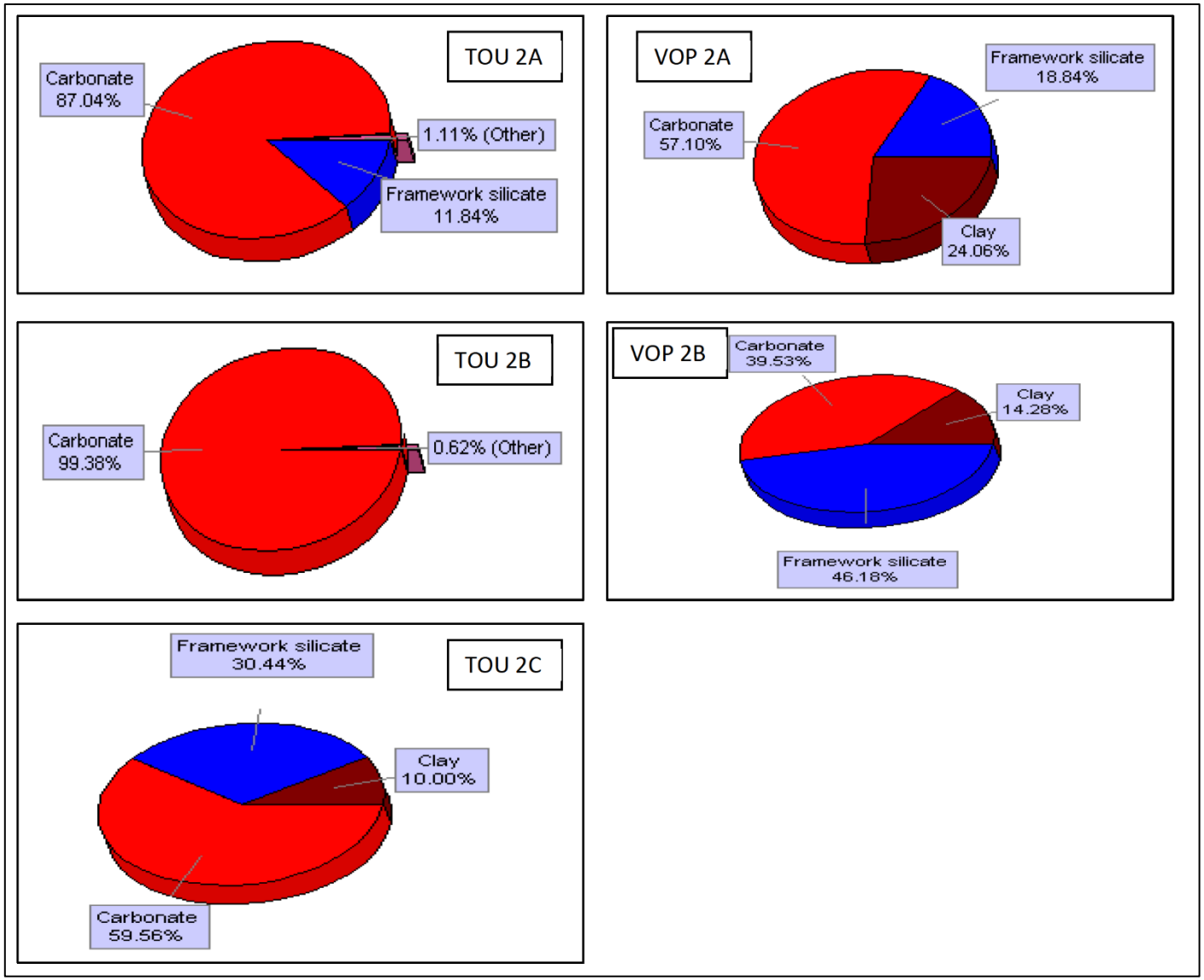
TOU 2A
Carbonate
87.04%
1.11% (Other)
Framework silicate
11.84%
VOP 2A
Framework silicate
18.84%
Carbonate
57.10%
Clay
24.06%
TOU 2B
Carbonate
99.38%
0.62% (Other)
VOP 2B
Carbonate
39.53%
Clay
14.28%
Framework silicate
46.18%
TOU 2C
Framework silicate
30.44%
Clay
10.00%
Carbonate
59.56%

Appendix VI, Location map and selected outcrop pictures (from King et al., 2018)

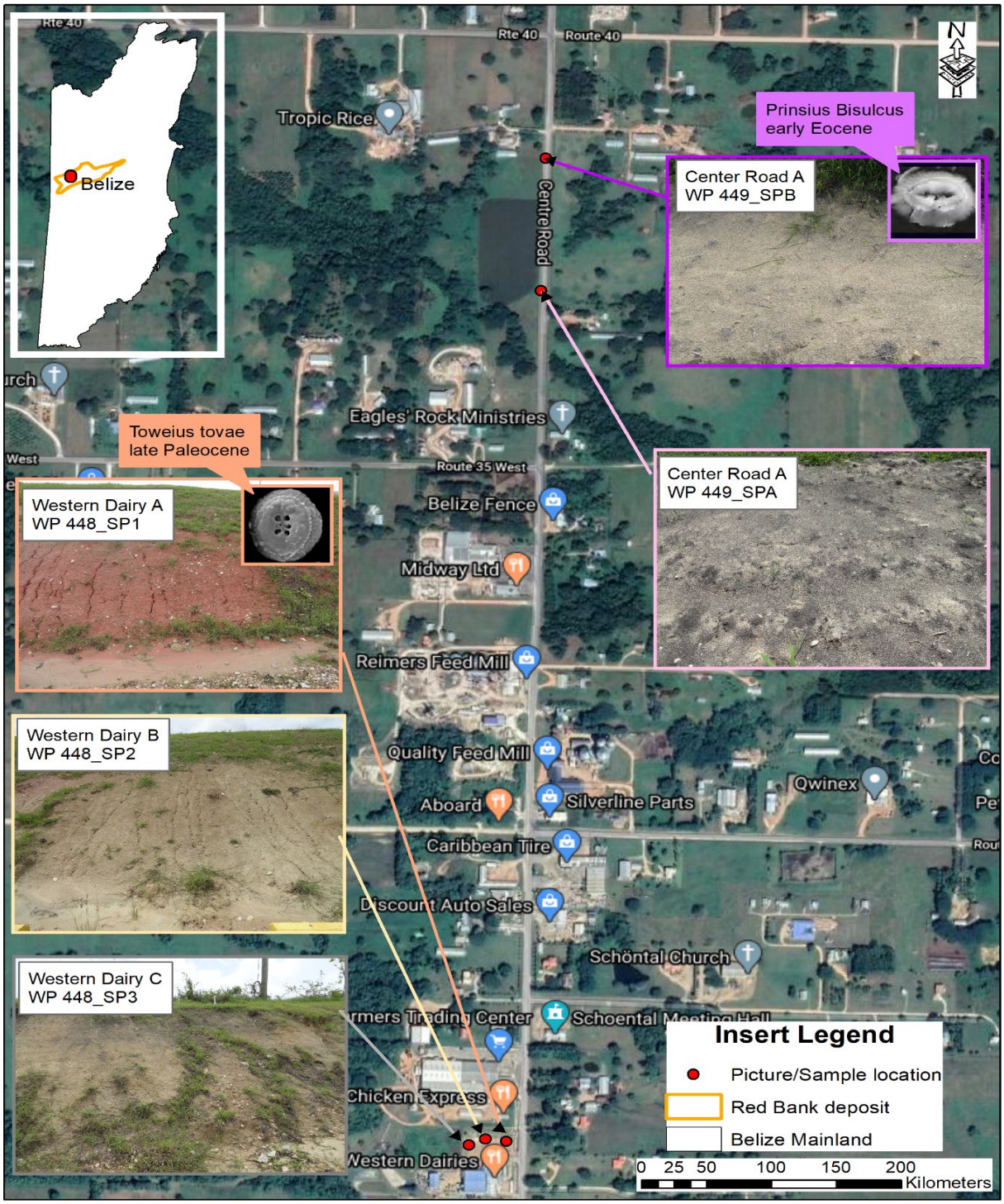

Appendix VII, results of nannofossil analysis, indicating samples with nannofossils.

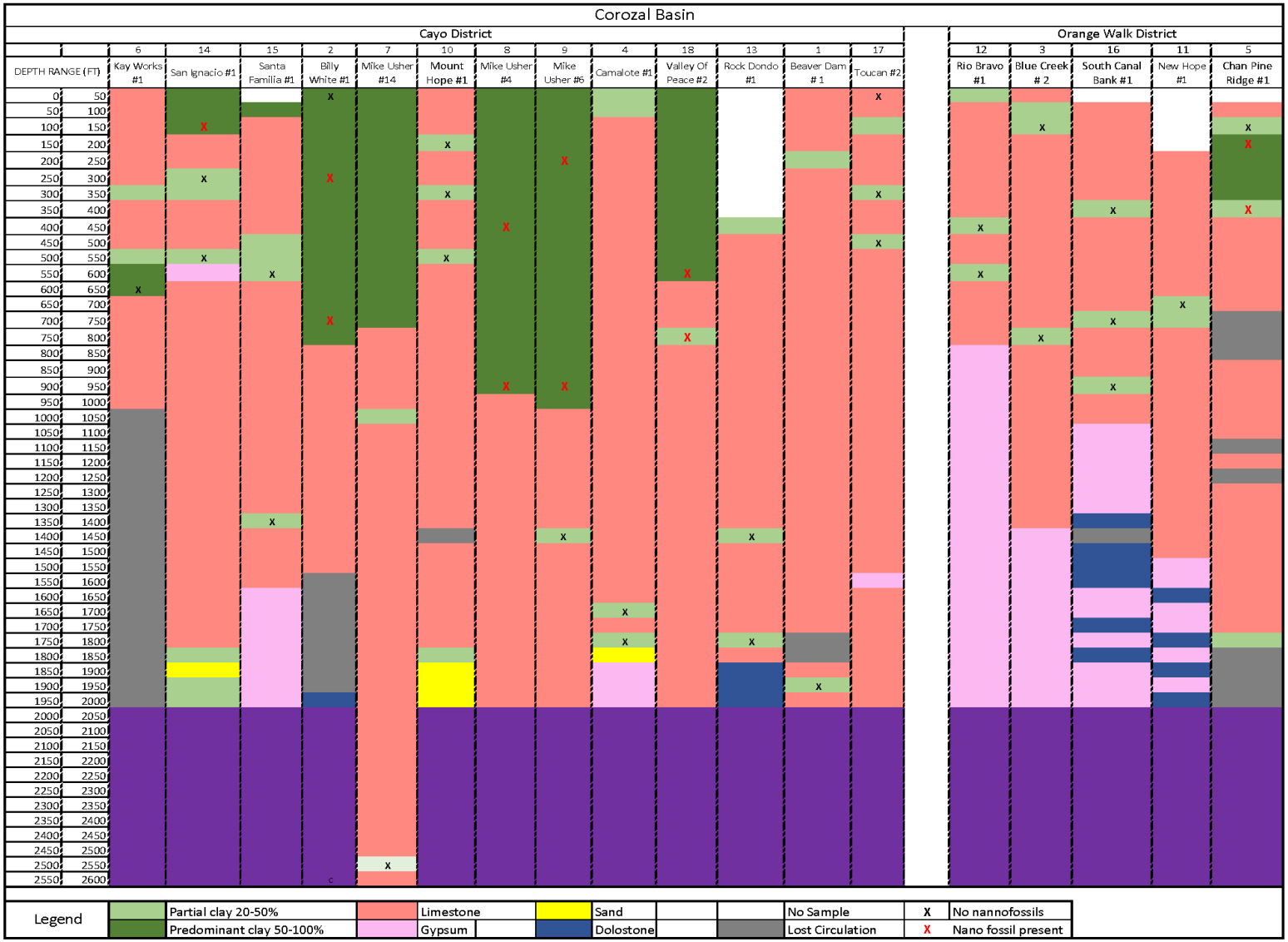

Appendix VIII, Nannofossil range chart for samples from Paleo Data, Inc. Oldest age-diagnostic taxa are indicated by red text, and range of occurrence by red lines.

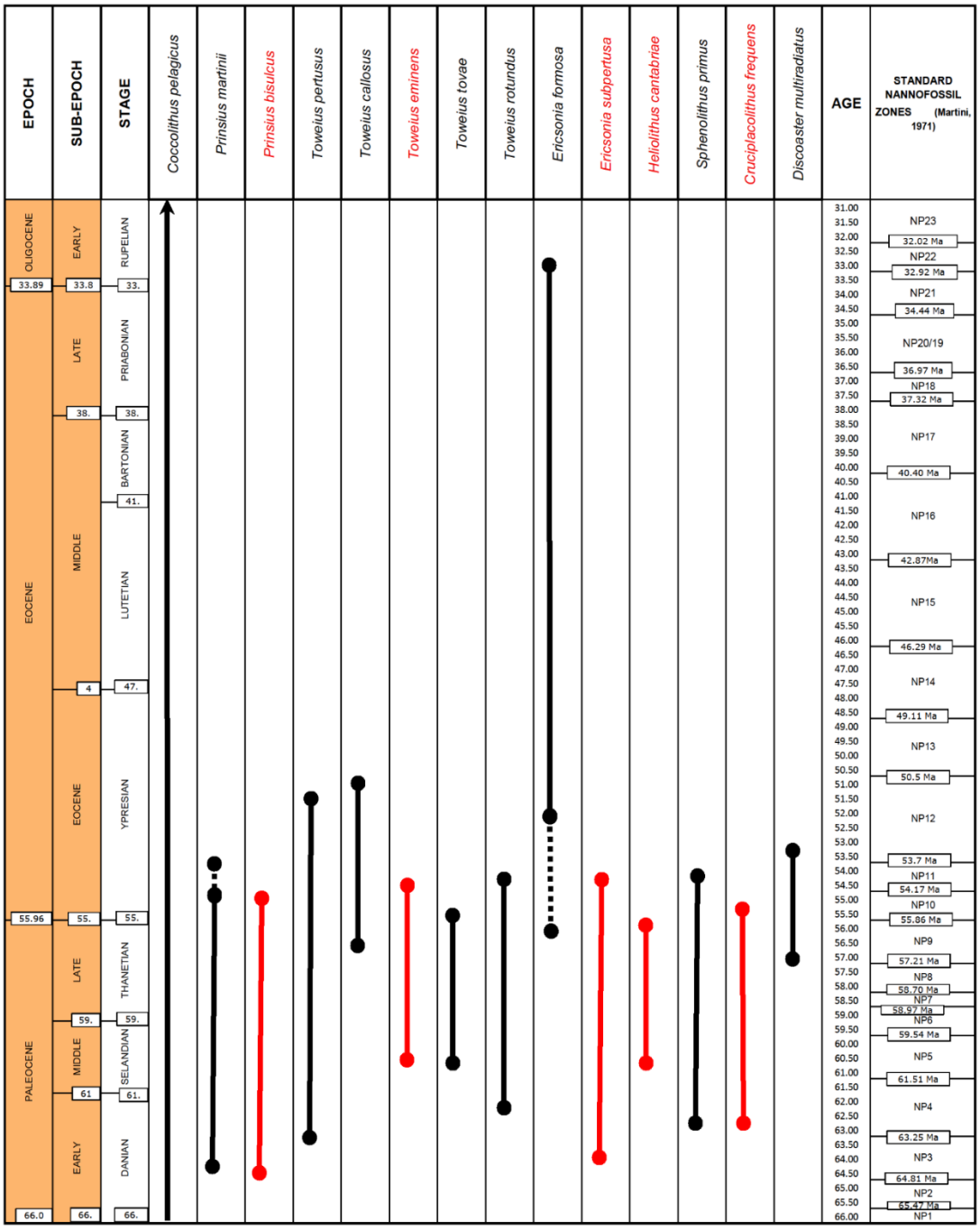

Appendix IX, Seismic line with the Mike Usher #20 well used as a tie-in to determine unconformity with the underlying limestone.

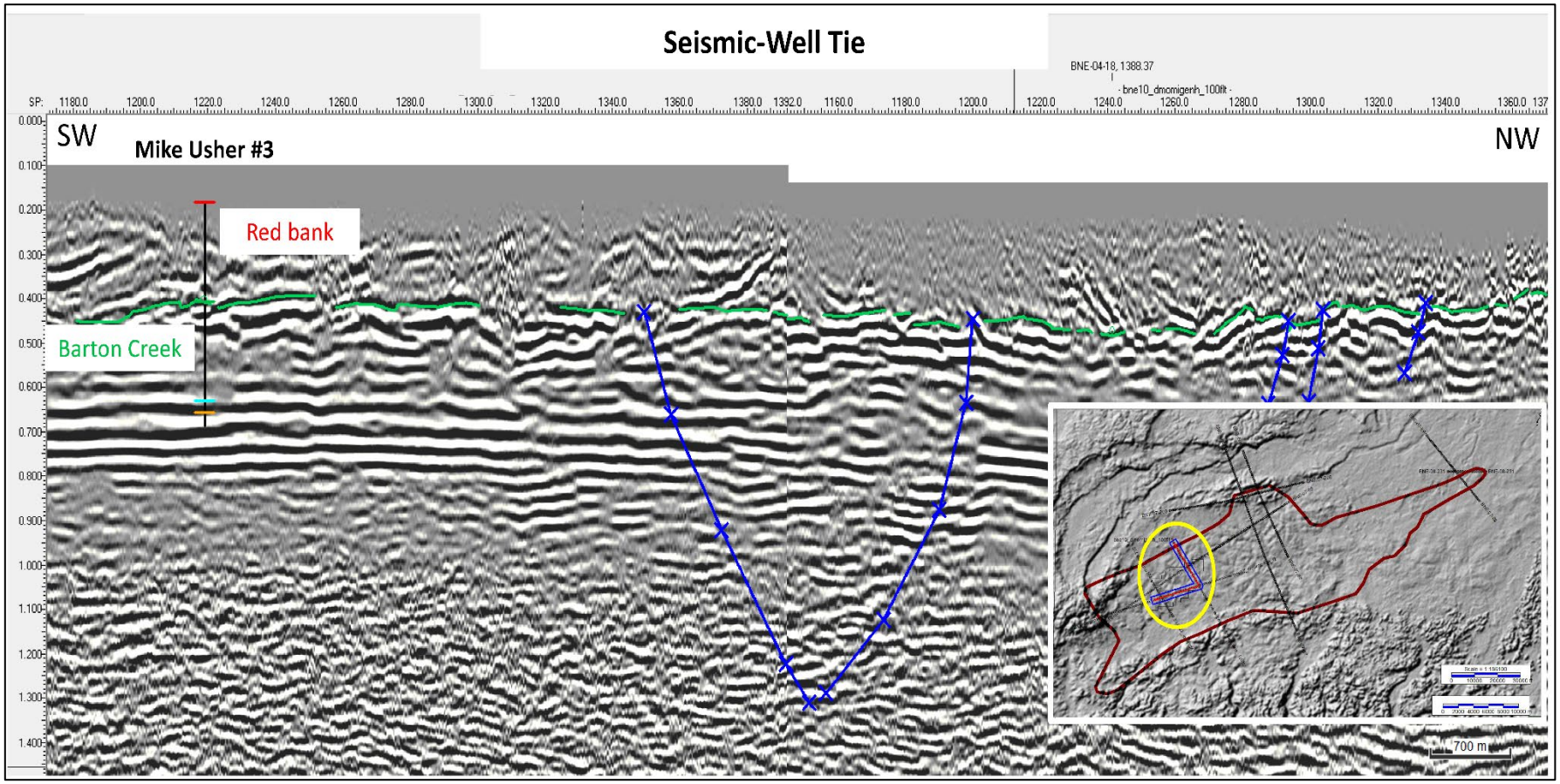

Appendix X, XRD of selected outcrop samples; prepared by Dan Larsen, U. Memphis. Localities (WP) are from King et al. (2018).

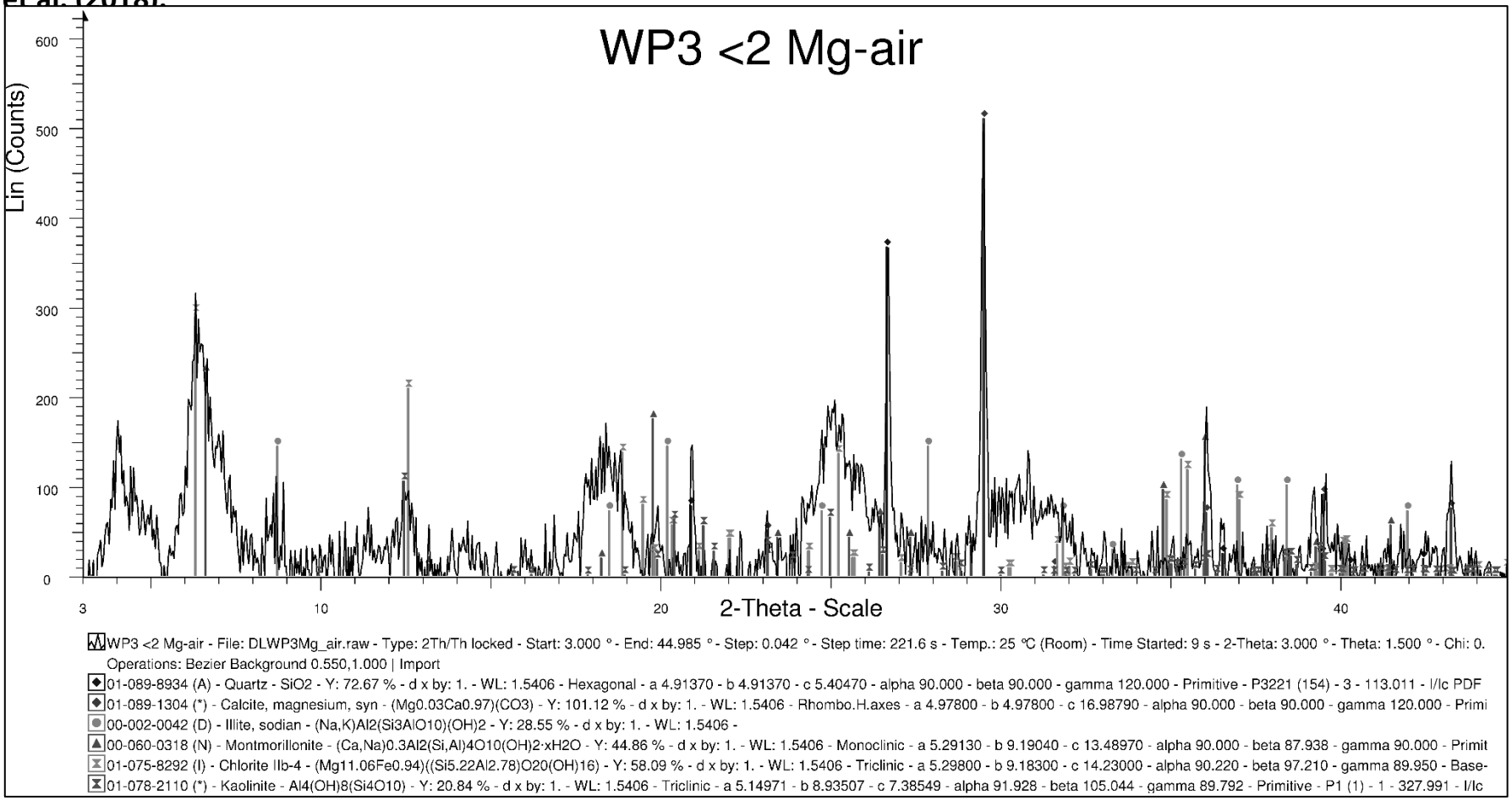

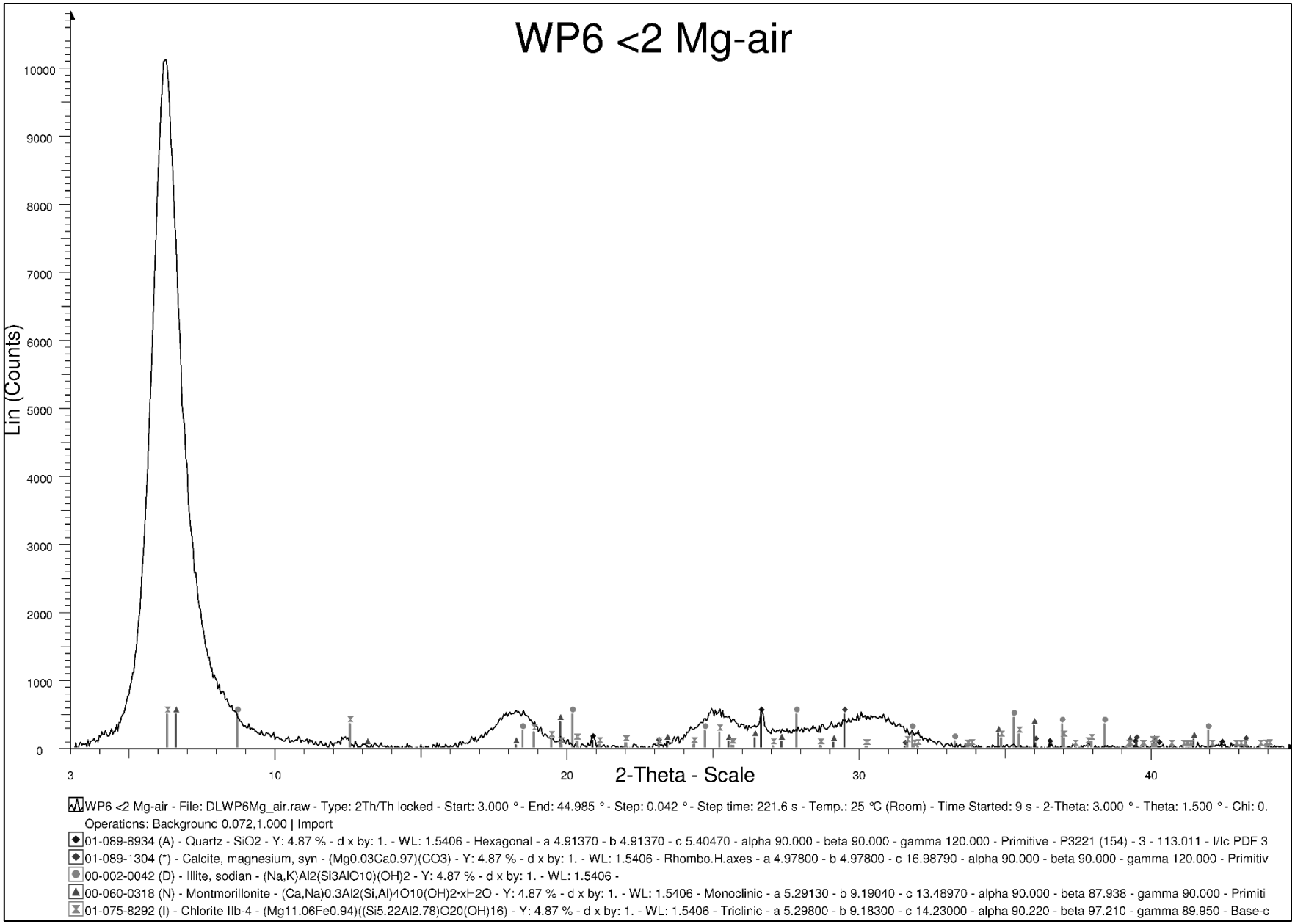
WP6 <2 Mg-air
Lin (Counts)
10000
9000
8000
7000
6000
5000
4000
3000
2000
1000
0
3
10
20
30
40
2-Theta - Scale
WP6 <2 Mg-air - File: DLWP6Mg_air.raw - Type: 2Th/Th locked - Start: 3.000 ° - End: 44.985 ° - Step: 0.042 ° - Step time: 221.6 s - Temp.: 25 °C (Room) - Time Started: 9 s - 2-Theta: 3.000 ° - Theta: 1.500 ° - Chi: 0.
Operations: Background 0.072,1.000 | Import
01-089-8934 (A) - Quartz - SiO2 - Y: 4.87 % - d x by: 1. - WL: 1.5406 - Hexagonal - a 4.91370 - b 4.91370 - c 5.40470 - alpha 90.000 - beta 90.000 - gamma 120.000 - Primitive - P3221 (154) - 3 - 113.011 - I/Ic PDF 3
01-089-1304 (*) - Calcite, magnesium, syn - (Mg0.03Ca0.97)(CO3) - Y: 4.87 % - d x by: 1. - WL: 1.5406 - Rhombo.H.axes - a 4.97800 - b 4.97800 - c 16.98790 - alpha 90.000 - beta 90.000 - gamma 120.000 - Primitiv
00-002-0042 (D) - Illite, sodian - (Na,K)Al2(Si3AlO10)(OH)2 - Y: 4.87 % - d x by: 1. - WL: 1.5406 -
00-060-0318 (N) - Montmorillonite - (Ca,Na)0.3Al2(Si,Al)4O10(OH)2•xH2O - Y: 4.87 % - d x by: 1. - WL: 1.5406 - Monoclinic - a 5.29130 - b 9.19040 - c 13.48970 - alpha 90.000 - beta 87.938 - gamma 90.000 - Primiti
01-075-8292 (I) - Chlorite IIb-4 - (Mg11.06Fe0.94)((Si5.22Al2.78)O20(OH)16) - Y: 4.87 % - d x by: 1. - WL: 1.5406 - Triclinic - a 5.29800 - b 9.18300 - c 14.23000 - alpha 90.220 - beta 97.210 - gamma 89.950 - Base-c

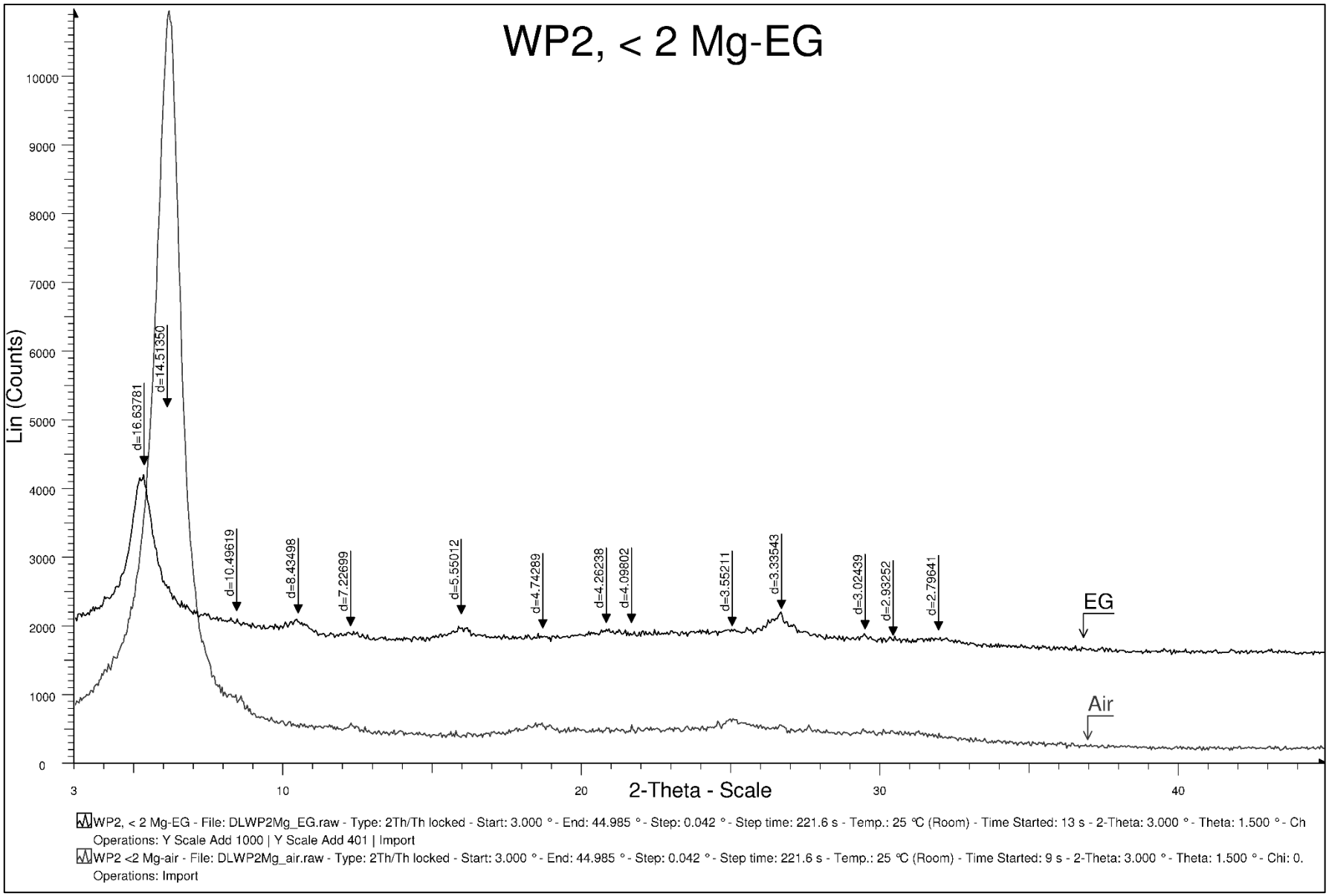
WP2, < 2 Mg-EG
Lin (Counts)
2-Theta - Scale
d=16.63781
d=14.51350
d=10.49619
d=8.43498
d=7.22699
d=5.55012
d=4.74289
d=4.26238
d=4.09802
d=3.55211
d=3.33543
d=3.02439
d=2.93252
d=2.79641
EG
Air
WP2, < 2 Mg-EG - File: DLWP2Mg_EG.raw - Type: 2Th/Th locked - Start: 3.000 ° - End: 44.985 ° - Step: 0.042 ° - Step time: 221.6 s - Temp.: 25 °C (Room) - Time Started: 13 s - 2-Theta: 3.000 ° - Theta: 1.500 ° - Ch
Operations: Y Scale Add 1000 | Y Scale Add 401 | Import
WP2 <2 Mg-air - File: DLWP2Mg_air.raw - Type: 2Th/Th locked - Start: 3.000 ° - End: 44.985 ° - Step: 0.042 ° - Step time: 221.6 s - Temp.: 25 °C (Room) - Time Started: 9 s - 2-Theta: 3.000 ° - Theta: 1.500 ° - Chi: 0.
Operations: Import

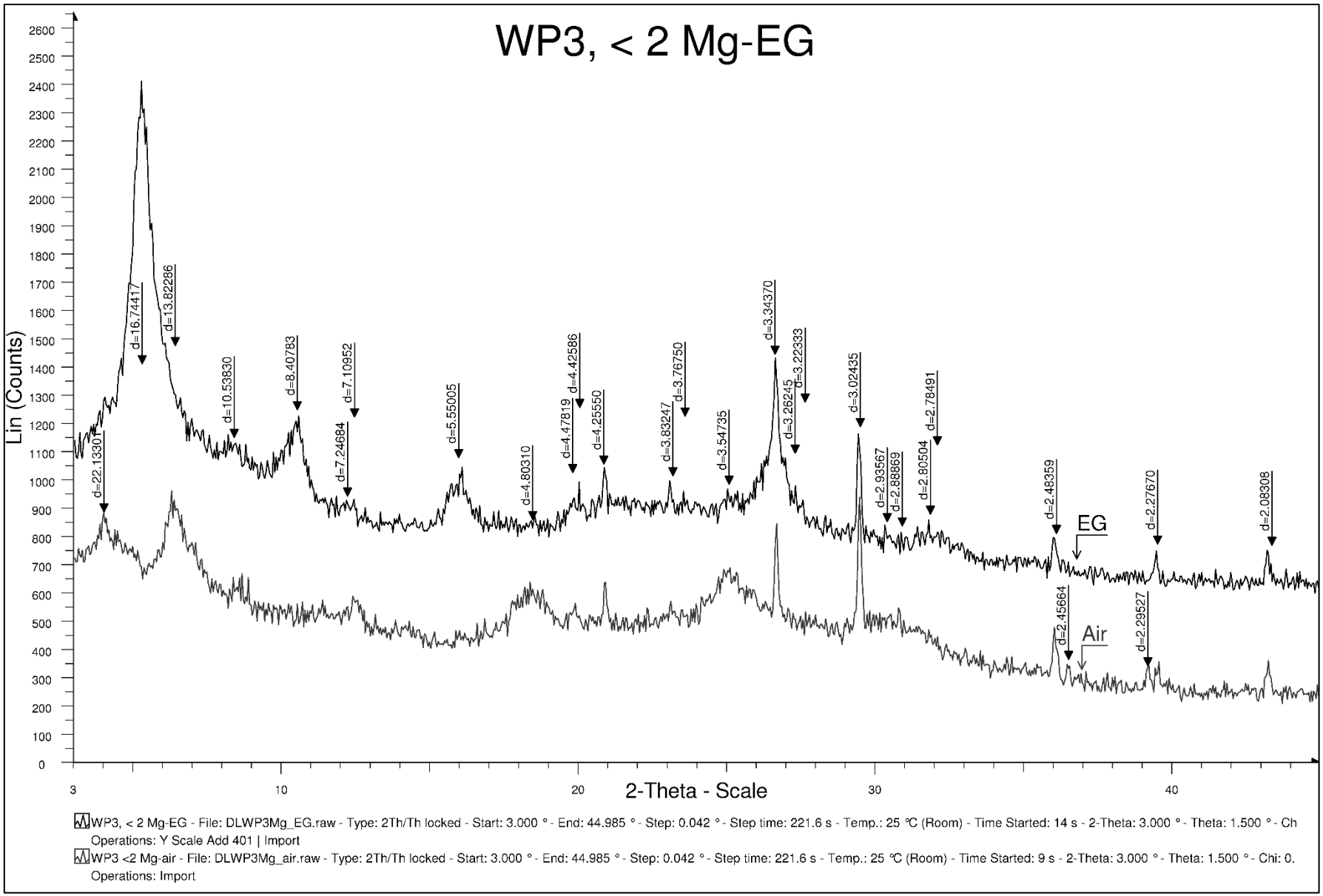
WP3, < 2 Mg-EG
Lin (Counts)
2-Theta - Scale
d=16.74417
d=13.82286
d=10.53830
d=8.40783
d=7.10952
d=7.24684
d=5.55005
d=4.80310
d=4.47819
d=4.42586
d=4.25550
d=3.83247
d=3.76750
d=3.54735
d=3.34370
d=3.26245
d=3.22333
d=3.02435
d=2.93567
d=2.88869
d=2.80504
d=2.78491
d=2.48359
d=2.45664
d=2.29527
d=2.27670
d=2.08308
d=22.13301
EG
Air
WP3, < 2 Mg-EG - File: DLWP3Mg_EG.raw - Type: 2Th/Th locked - Start: 3.000 ° - End: 44.985 ° - Step: 0.042 ° - Step time: 221.6 s - Temp.: 25 °C (Room) - Time Started: 14 s - 2-Theta: 3.000 ° - Theta: 1.500 ° - Ch
Operations: Y Scale Add 401 | Import
WP3 <2 Mg-air - File: DLWP3Mg_air.raw - Type: 2Th/Th locked - Start: 3.000 ° - End: 44.985 ° - Step: 0.042 ° - Step time: 221.6 s - Temp.: 25 °C (Room) - Time Started: 9 s - 2-Theta: 3.000 ° - Theta: 1.500 ° - Chi: 0.
Operations: Import

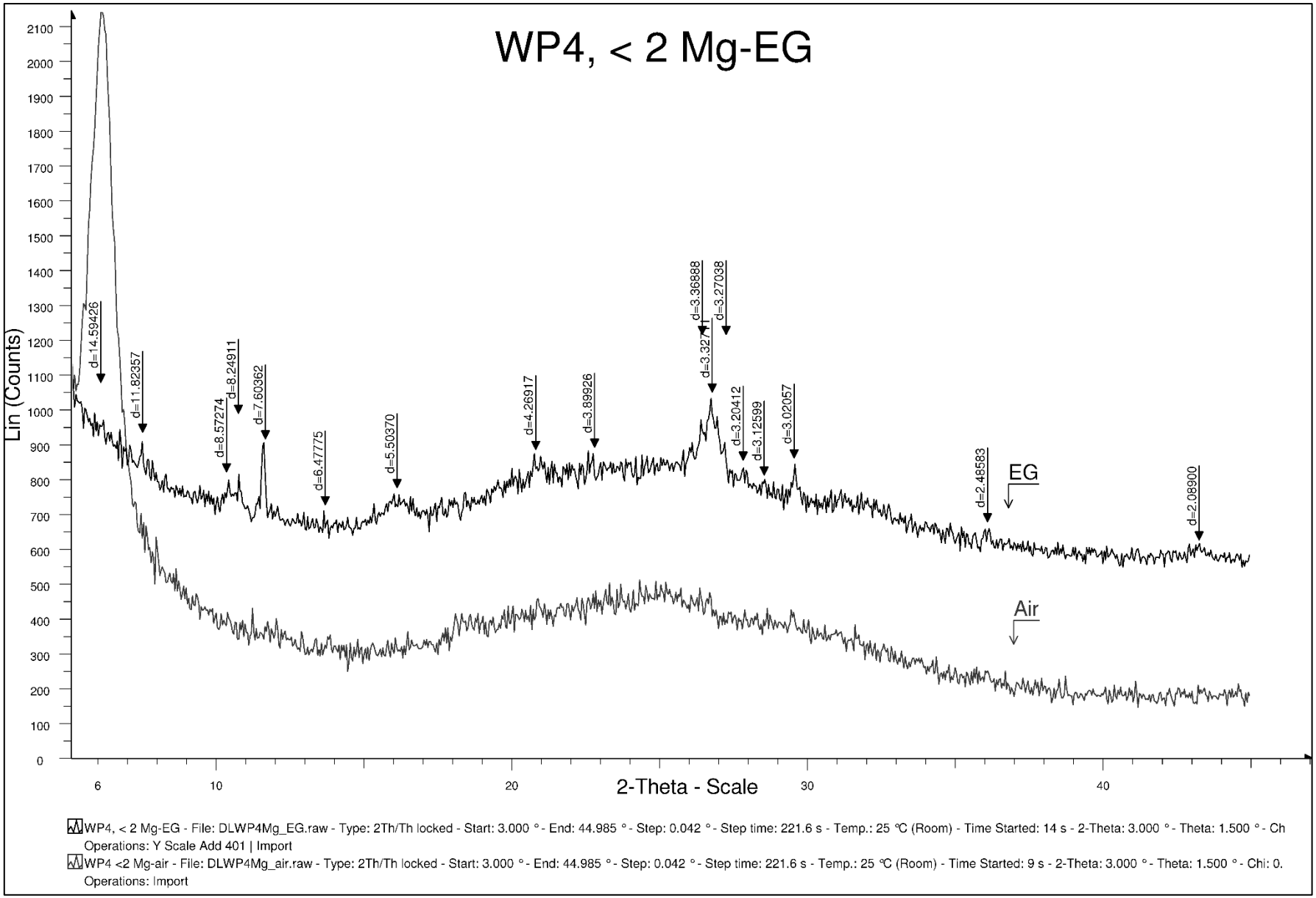
WP4, < 2 Mg-EG
Lin (Counts)
2-Theta - Scale
d=14.59426
d=11.82357
d=8.57274
d=8.24911
d=7.60362
d=6.47775
d=5.50370
d=4.26917
d=3.89926
d=3.36888
d=3.32711
d=3.27038
d=3.20412
d=3.12599
d=3.02057
d=2.48583
d=2.08900
EG
Air
WP4, < 2 Mg-EG - File: DLWP4Mg_EG.raw - Type: 2Th/Th locked - Start: 3.000 ° - End: 44.985 ° - Step: 0.042 ° - Step time: 221.6 s - Temp.: 25 °C (Room) - Time Started: 14 s - 2-Theta: 3.000 ° - Theta: 1.500 ° - Ch
Operations: Y Scale Add 401 | Import
WP4 <2 Mg-air - File: DLWP4Mg_air.raw - Type: 2Th/Th locked - Start: 3.000 ° - End: 44.985 ° - Step: 0.042 ° - Step time: 221.6 s - Temp.: 25 °C (Room) - Time Started: 9 s - 2-Theta: 3.000 ° - Theta: 1.500 ° - Chi: 0.
Operations: Import

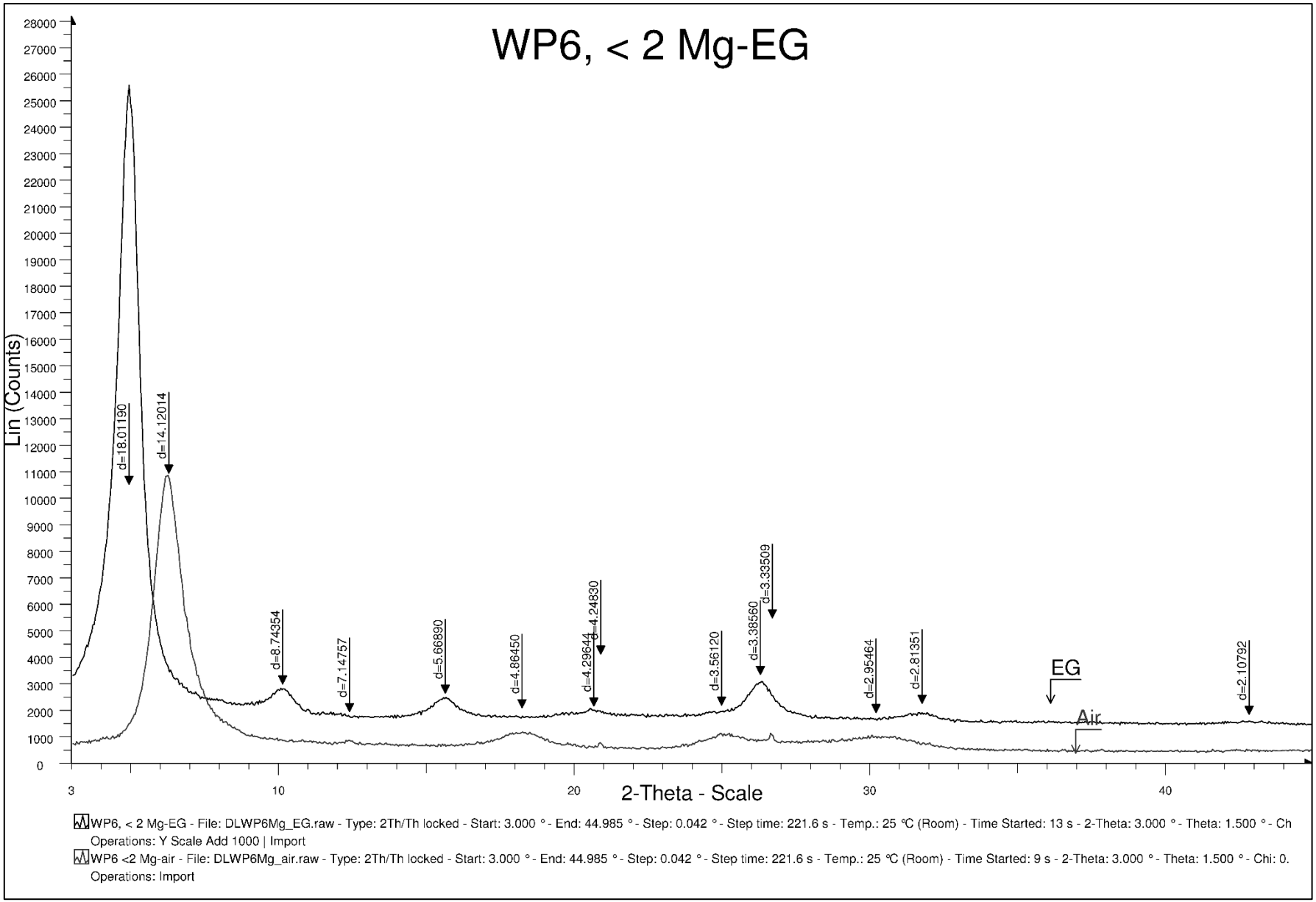
WP6, < 2 Mg-EG
Lin (Counts)
2-Theta - Scale
d=18.01190
d=14.12014
d=8.74354
d=7.14757
d=5.66890
d=4.86450
d=4.29644
d=4.24830
d=3.56120
d=3.38560
d=3.33509
d=2.95464
d=2.81351
d=2.10792
EG
Air
WP6, < 2 Mg-EG - File: DLWP6Mg_EG.raw - Type: 2Th/Th locked - Start: 3.000 ° - End: 44.985 ° - Step: 0.042 ° - Step time: 221.6 s - Temp.: 25 °C (Room) - Time Started: 13 s - 2-Theta: 3.000 ° - Theta: 1.500 ° - Ch
Operations: Y Scale Add 1000 | Import
WP6 <2 Mg-air - File: DLWP6Mg_air.raw - Type: 2Th/Th locked - Start: 3.000 ° - End: 44.985 ° - Step: 0.042 ° - Step time: 221.6 s - Temp.: 25 °C (Room) - Time Started: 9 s - 2-Theta: 3.000 ° - Theta: 1.500 ° - Chi: 0.
Operations: Import

Appendix XI, XRD patterns for Red Bank subsurface samples.

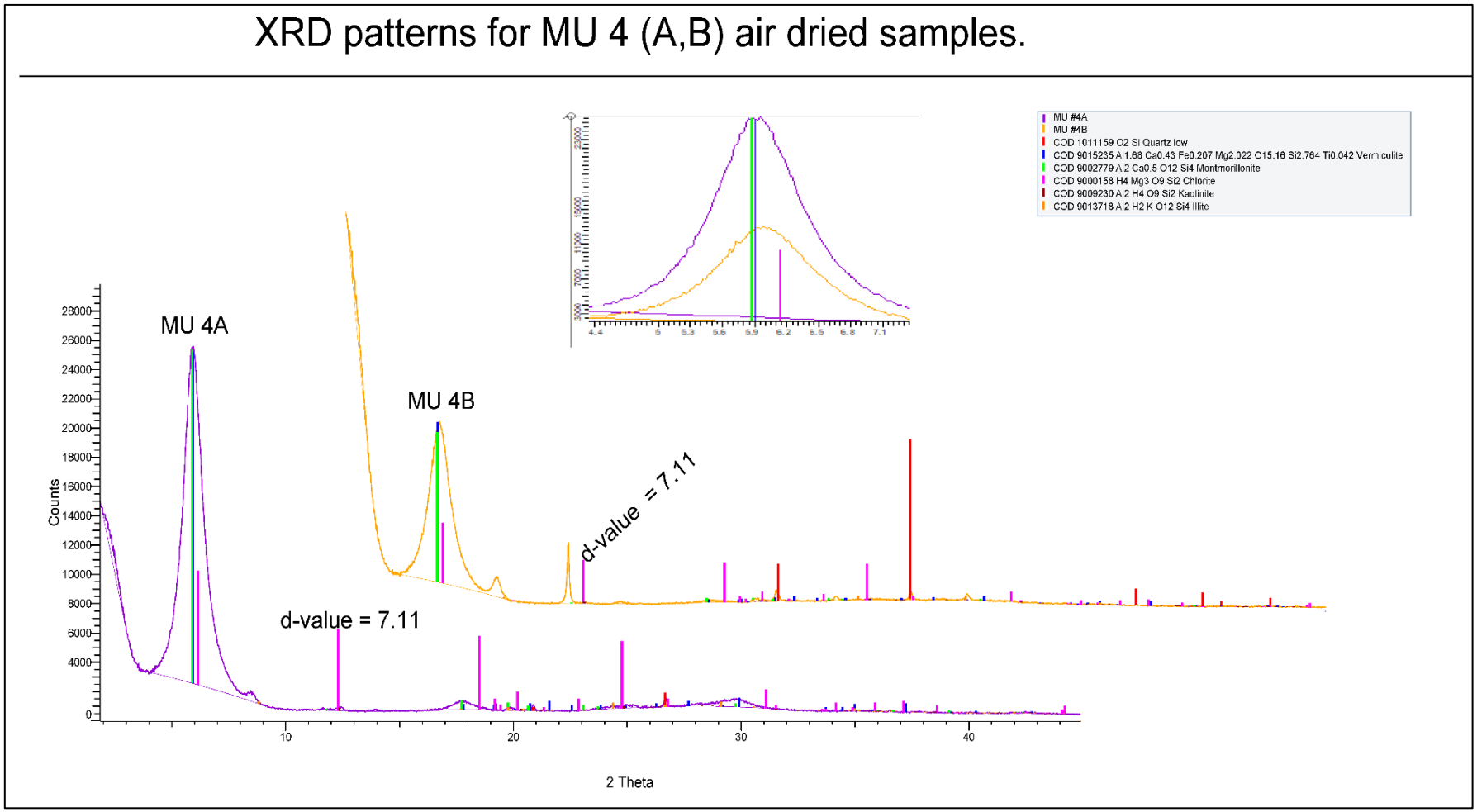

XRD patterns for SI 1 (A,B,C) air dried samples.

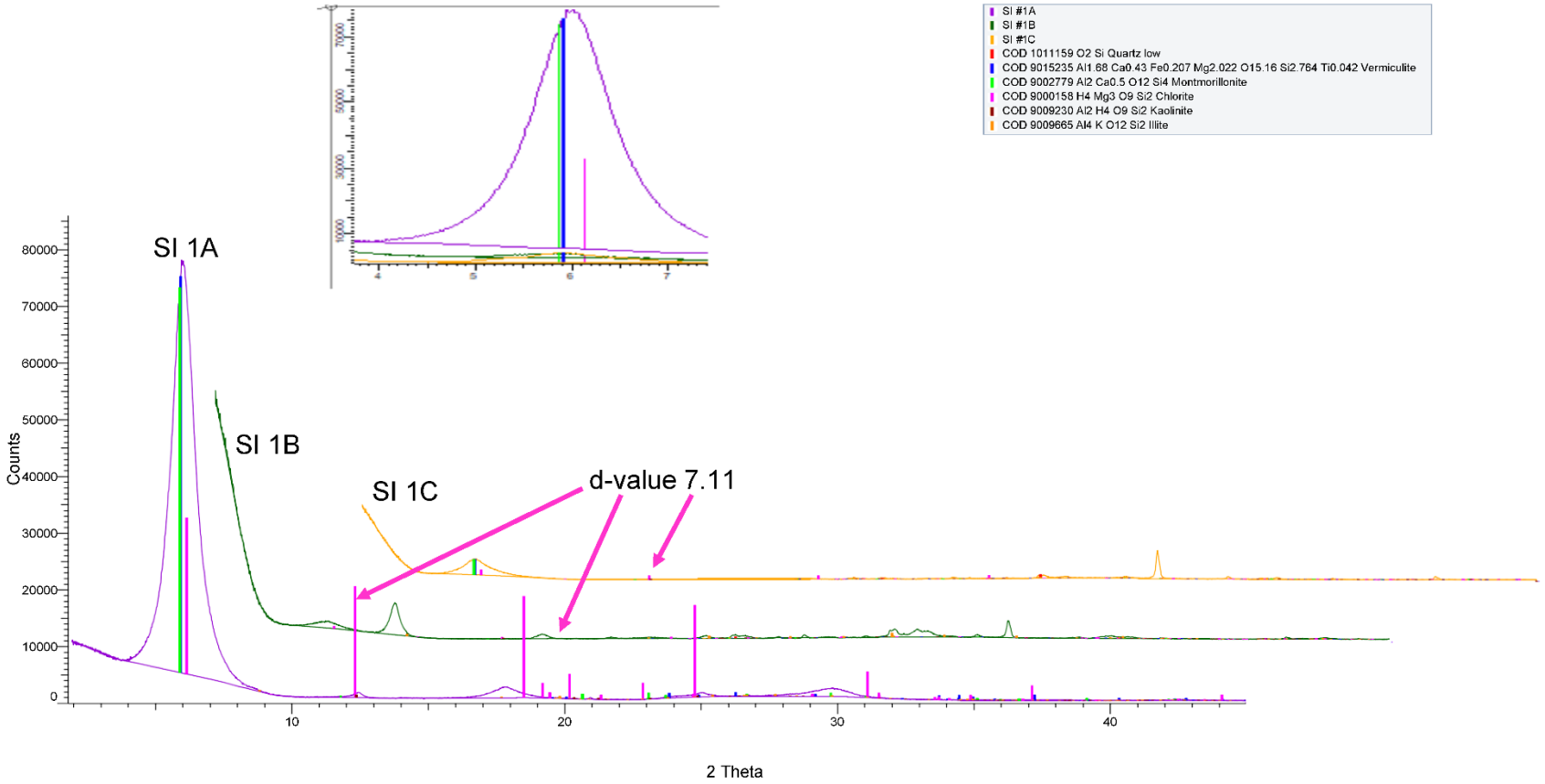

XRD patterns for Tou 2 (B,C) for air dried samples.

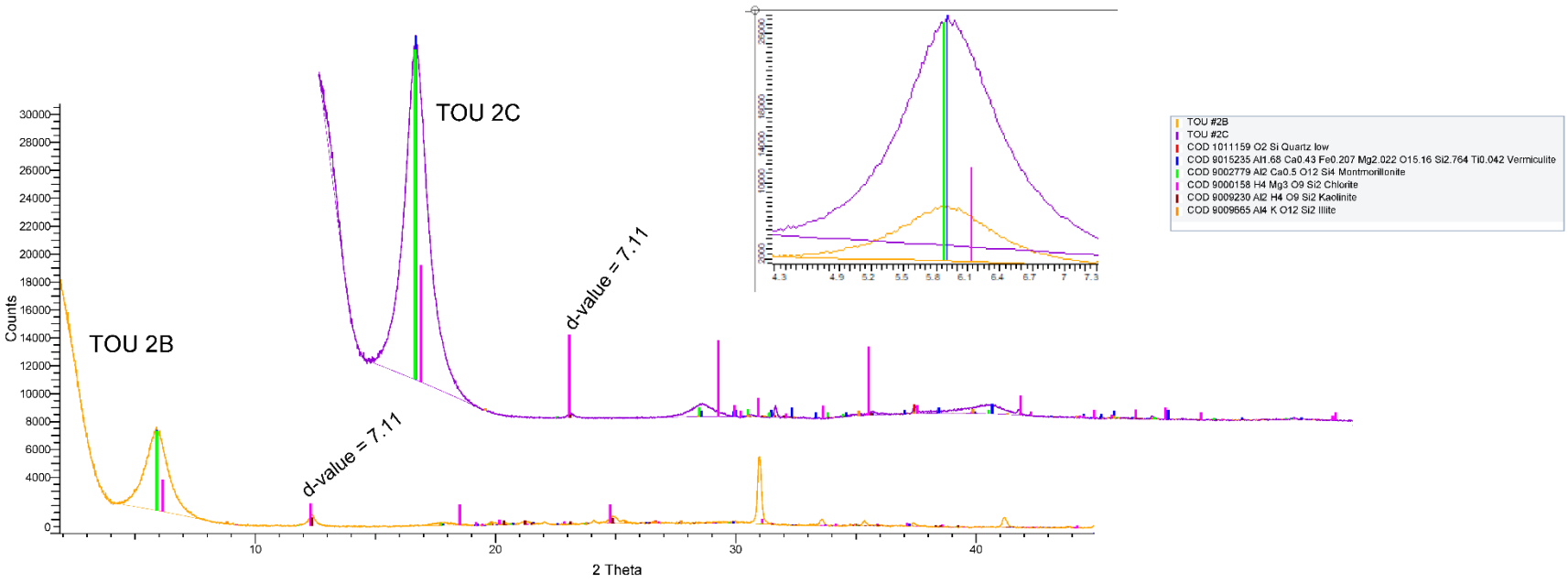

XRD patterns for VOP 2 (A,B) air dried samples.

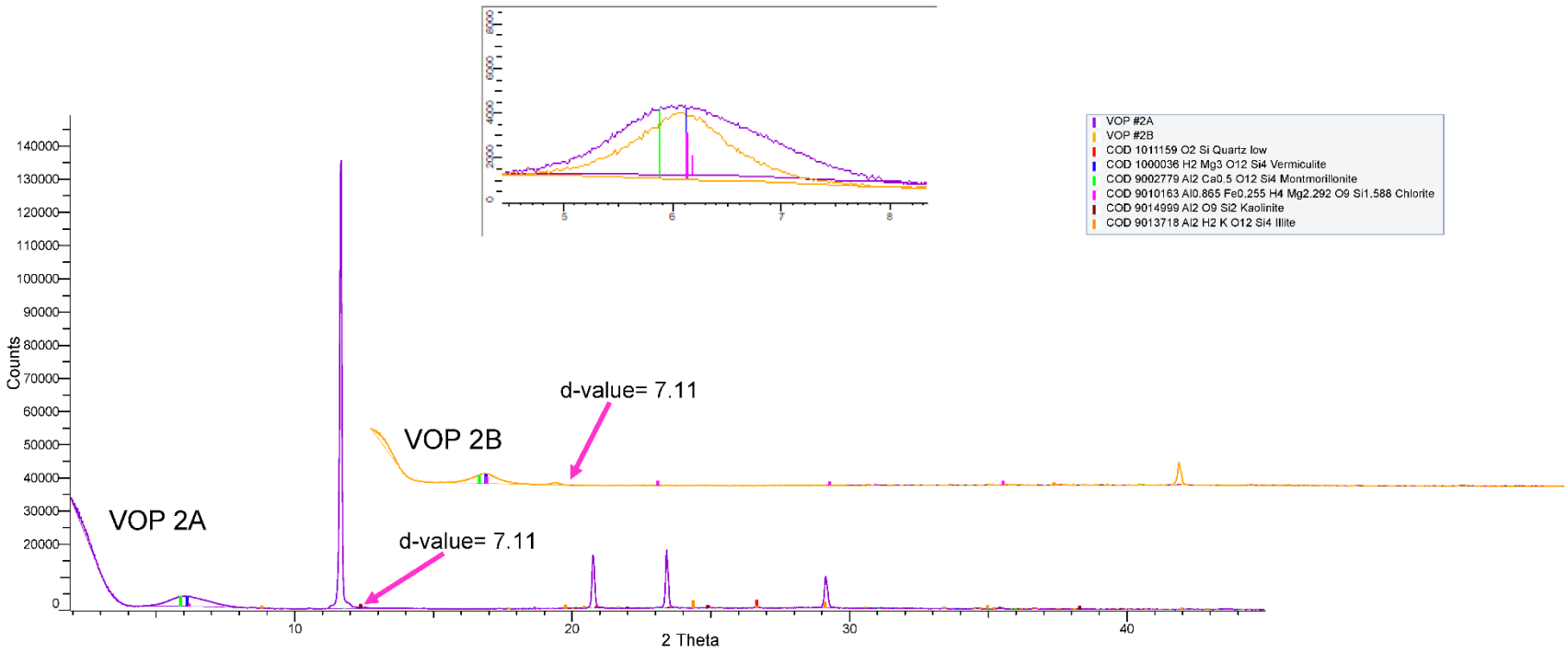

XRD pattern for CPR 1B, air dried and glycolated samples.

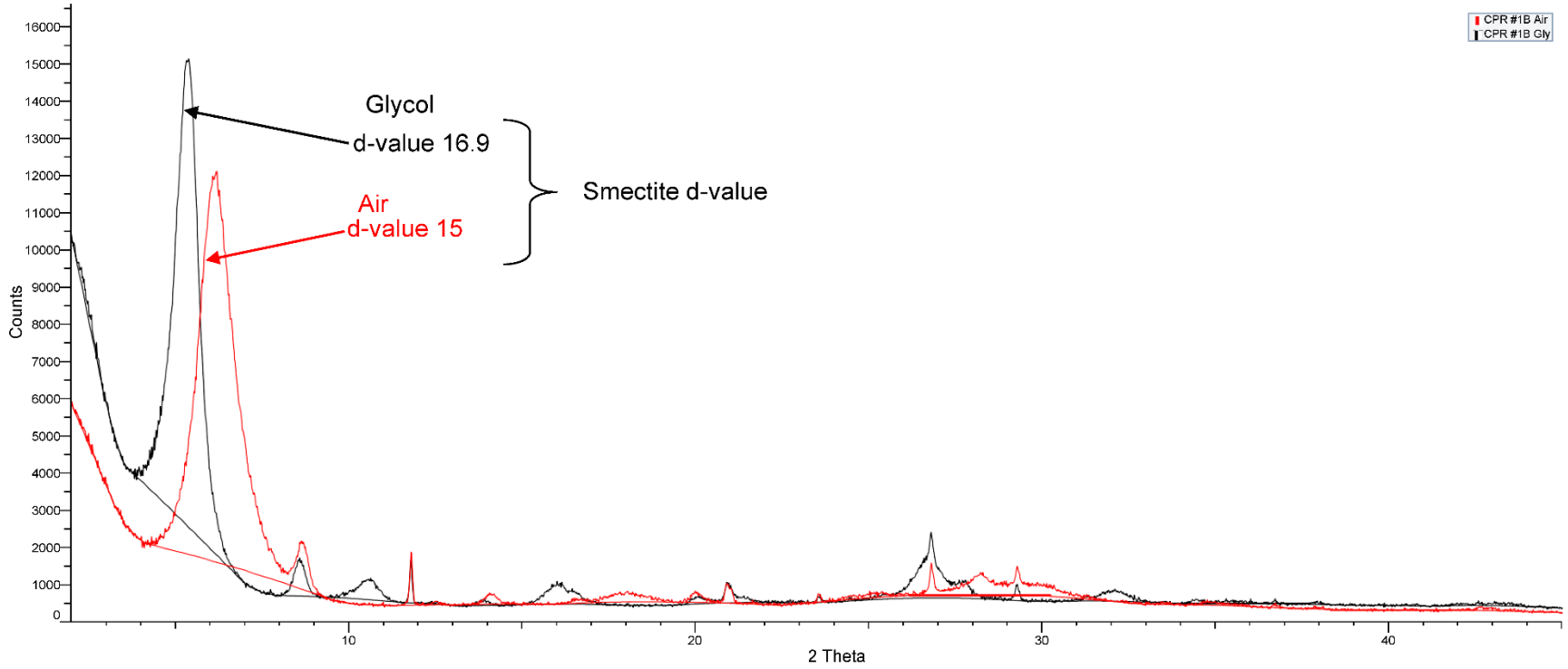

XRD pattern for CPR 1C, air dried and glycolated samples.

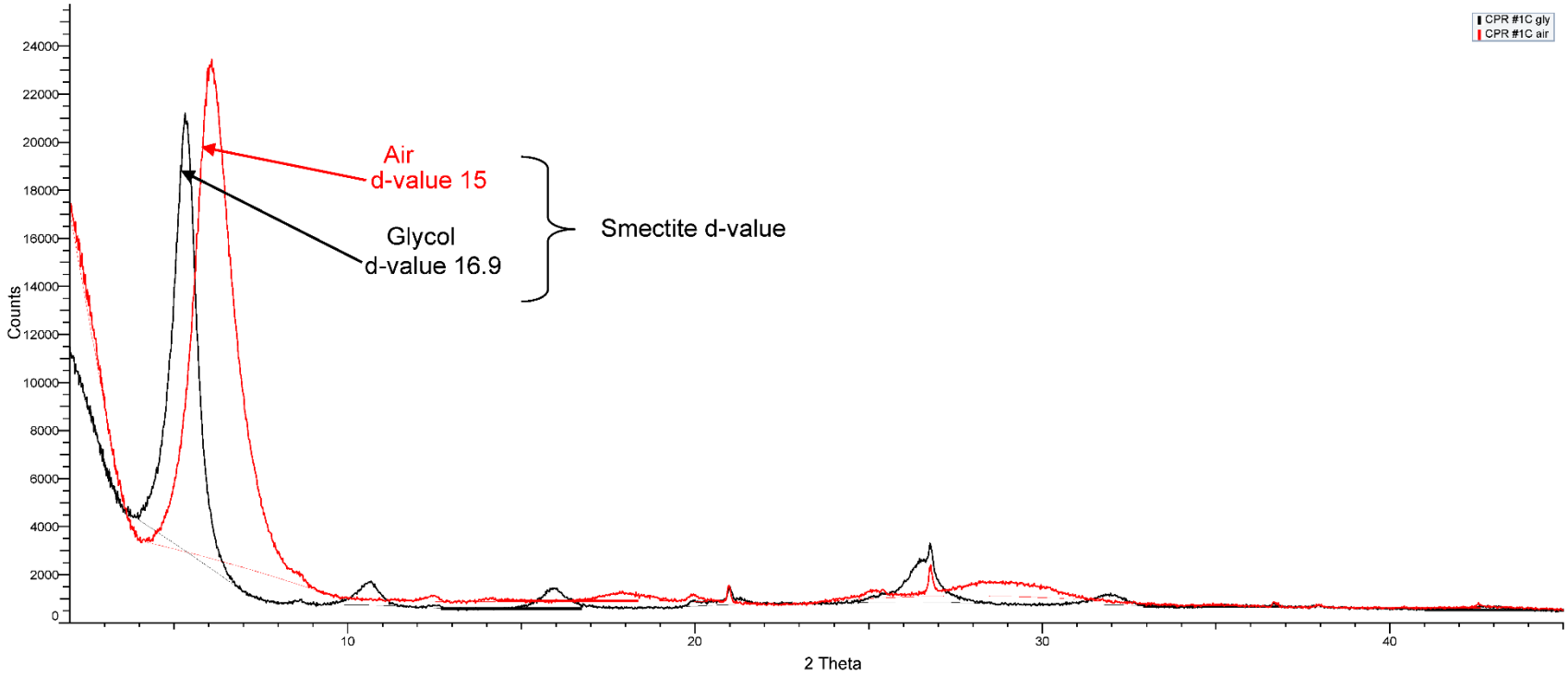

XRD pattern for MU 4B, air dried and glycolated samples.

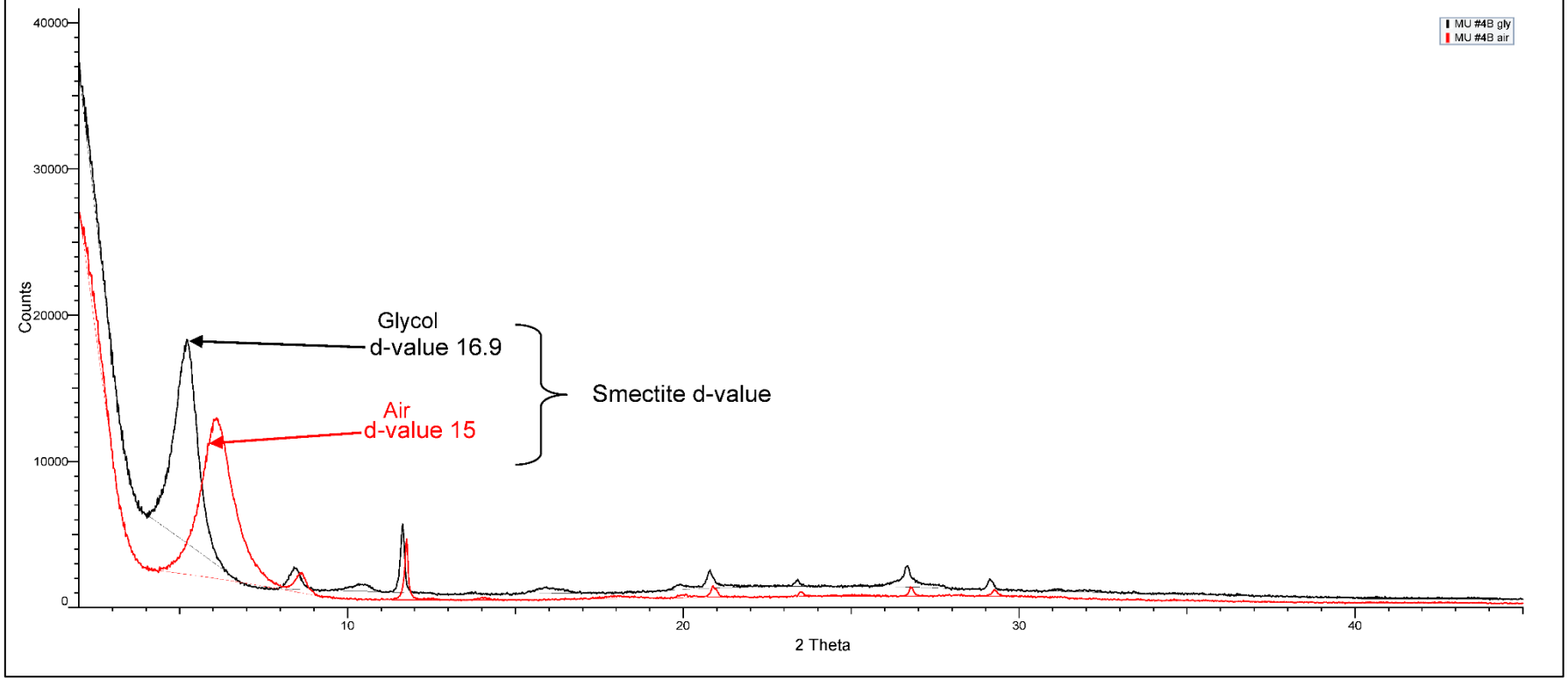

XRD pattern for SI 1A, air dried and glycolated samples.

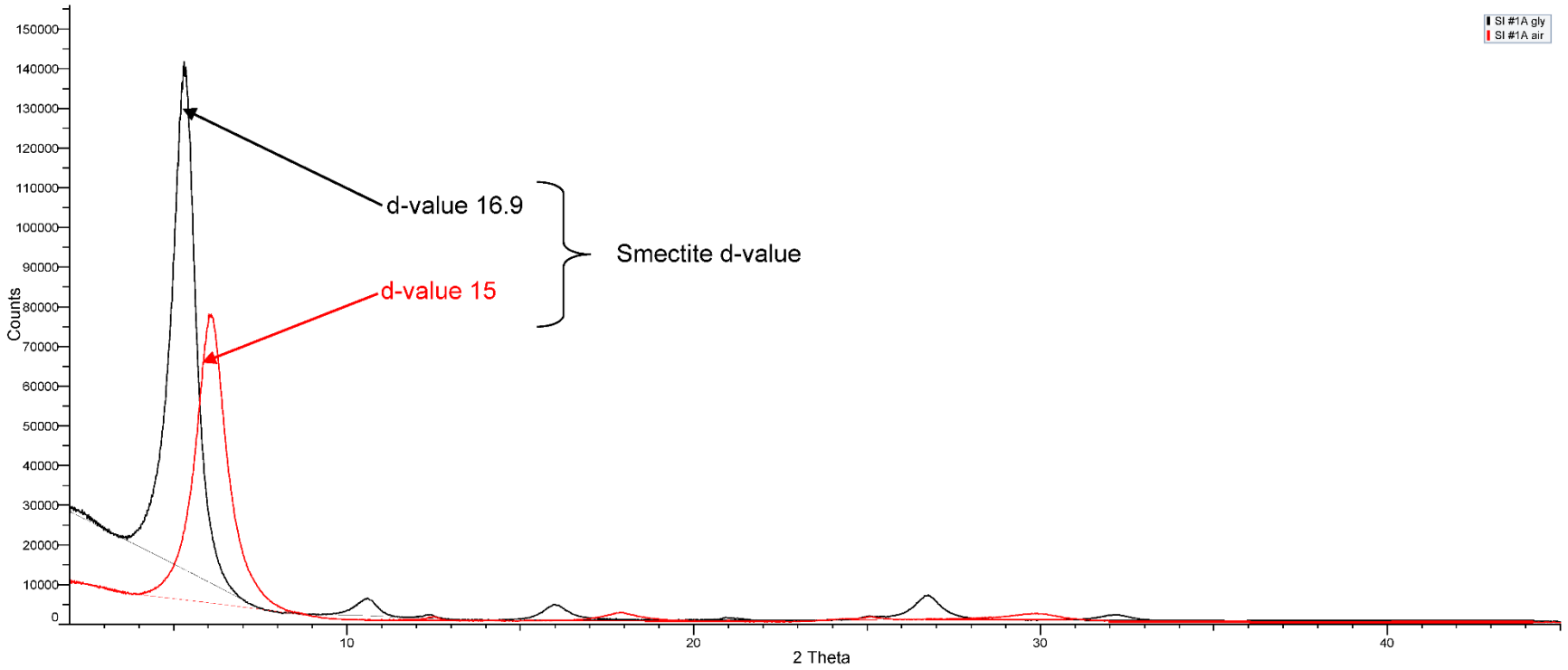

XRD pattern for SI 1B, air dried and glycolated samples.

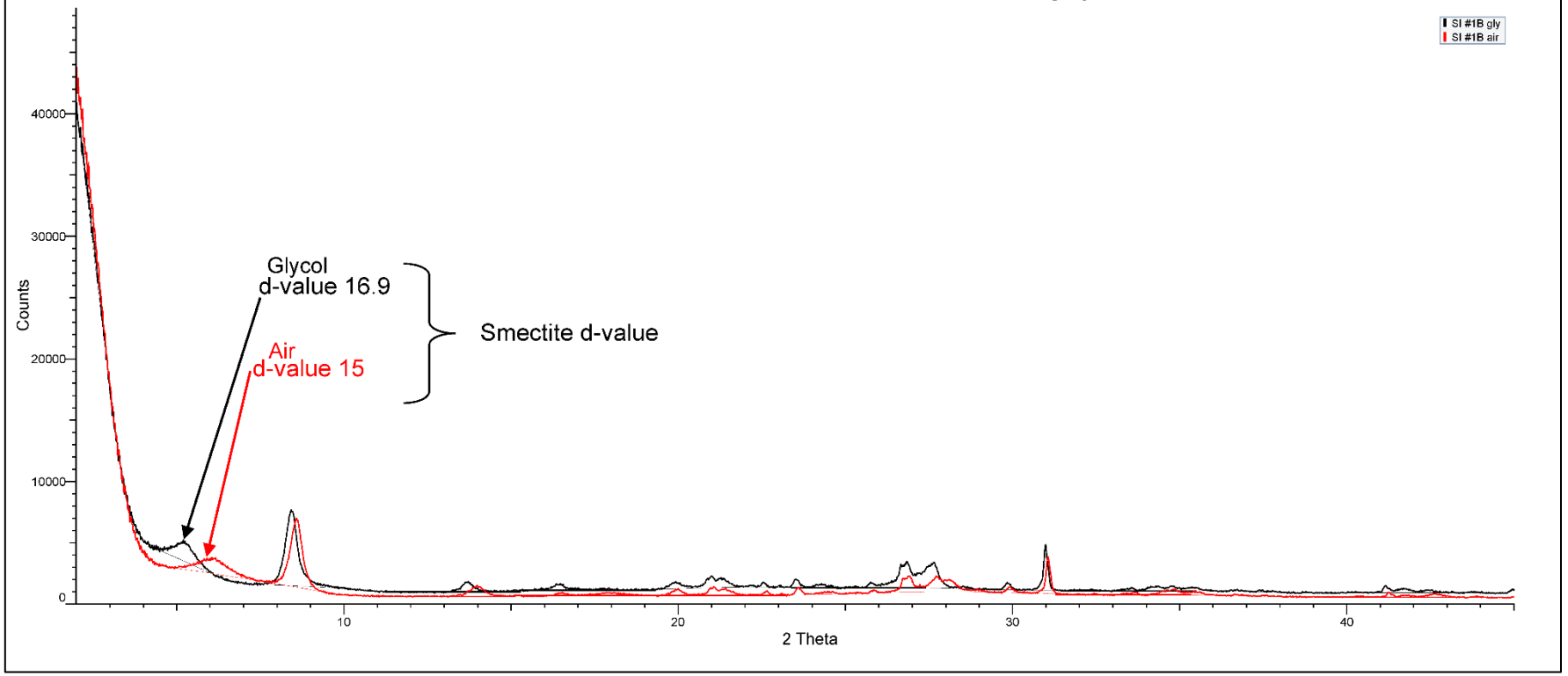

XRD pattern for SI 1C, air dried and glycolated samples.

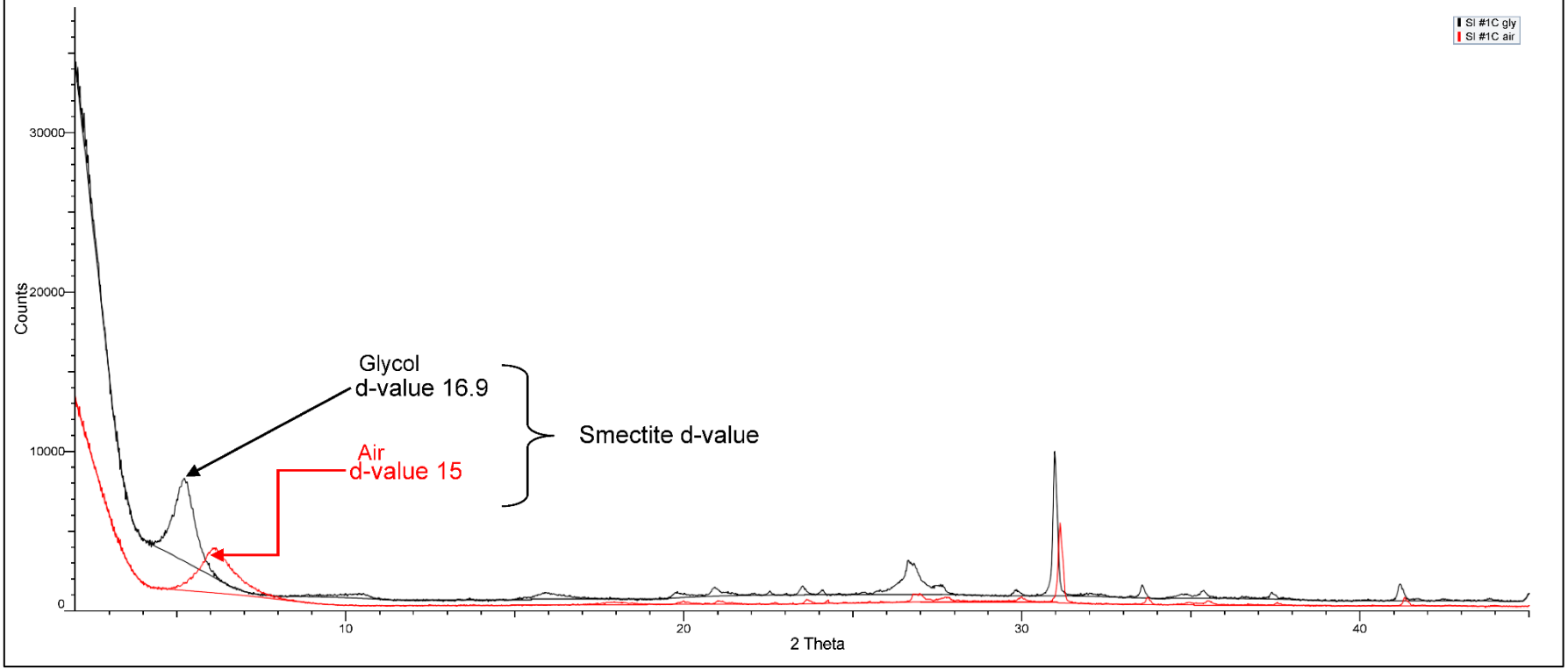

XRD pattern for TOU 2B air, dried and glycolated samples.

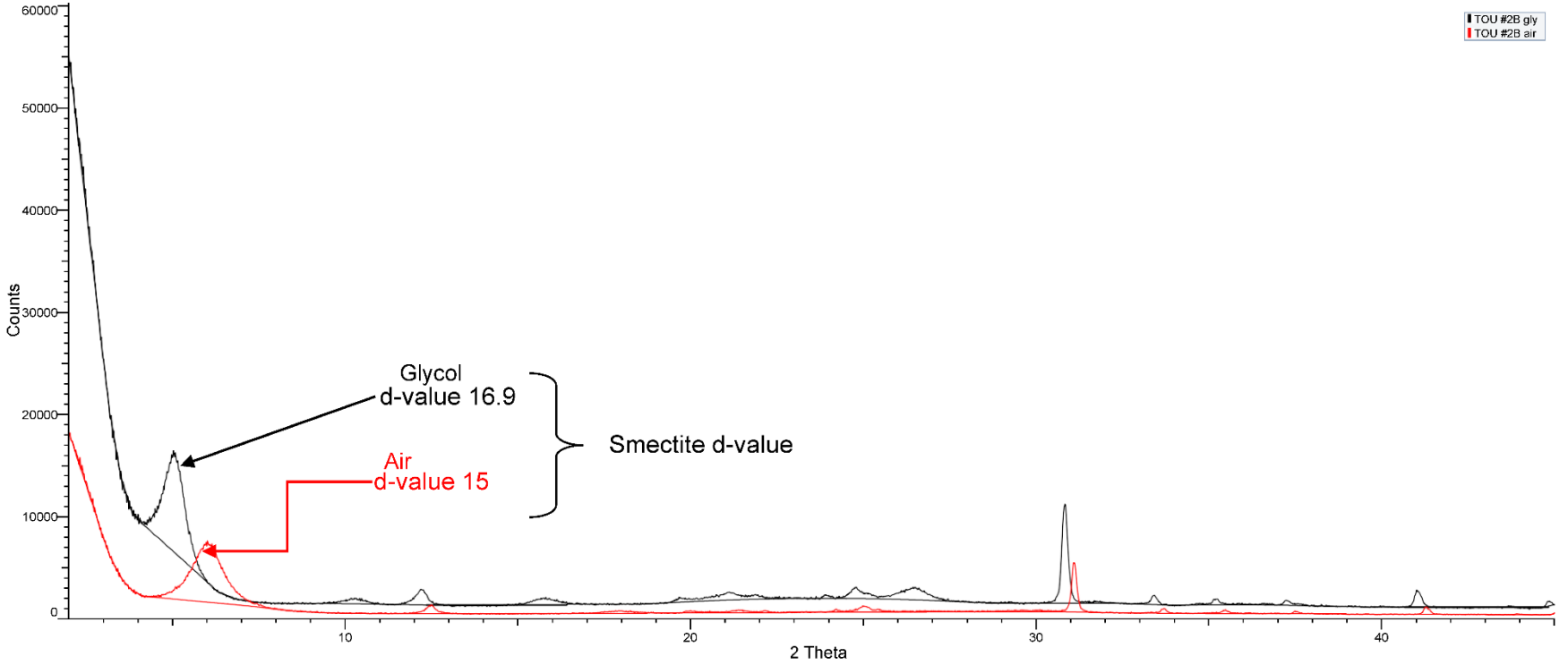

XRD pattern for TOU 2C ,air dried and glycolated samples.

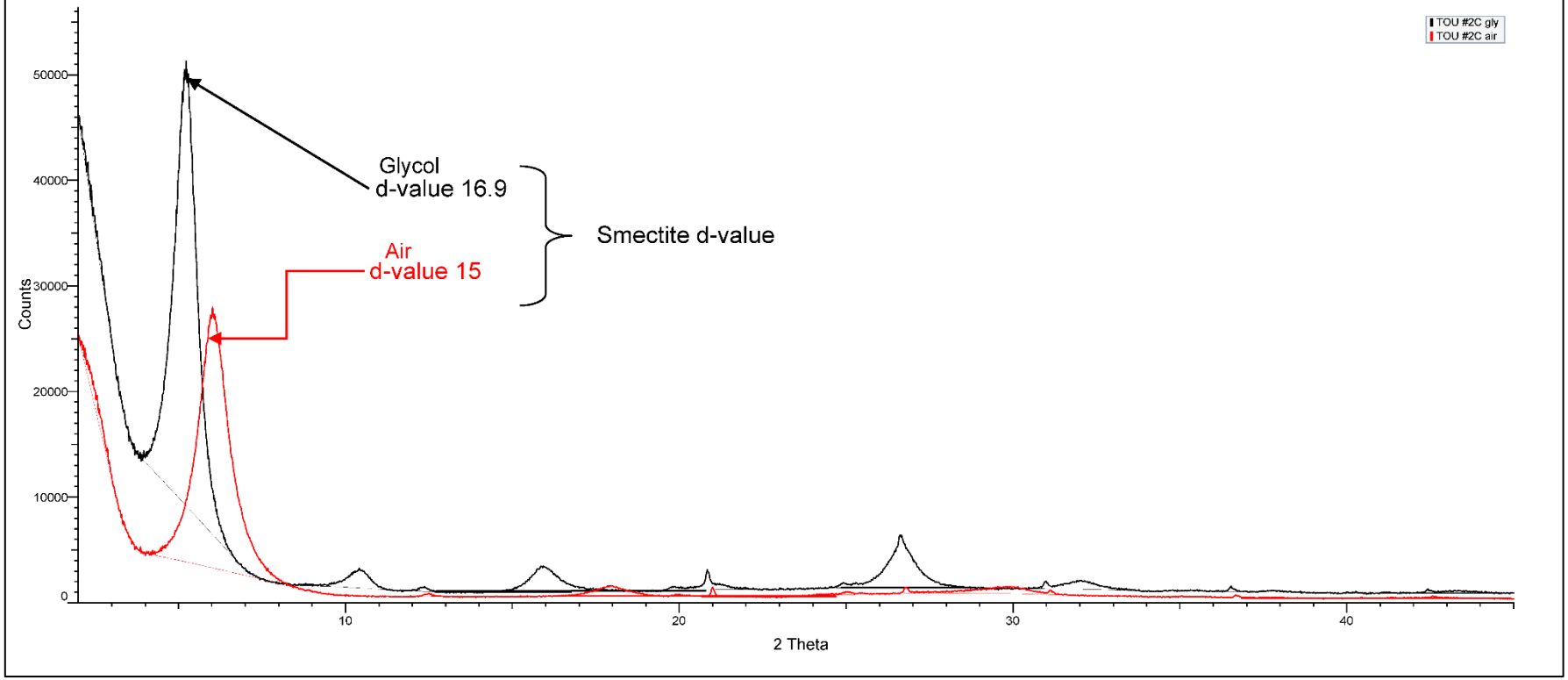

XRD pattern for VOP 2A, air dried and glycolated samples.

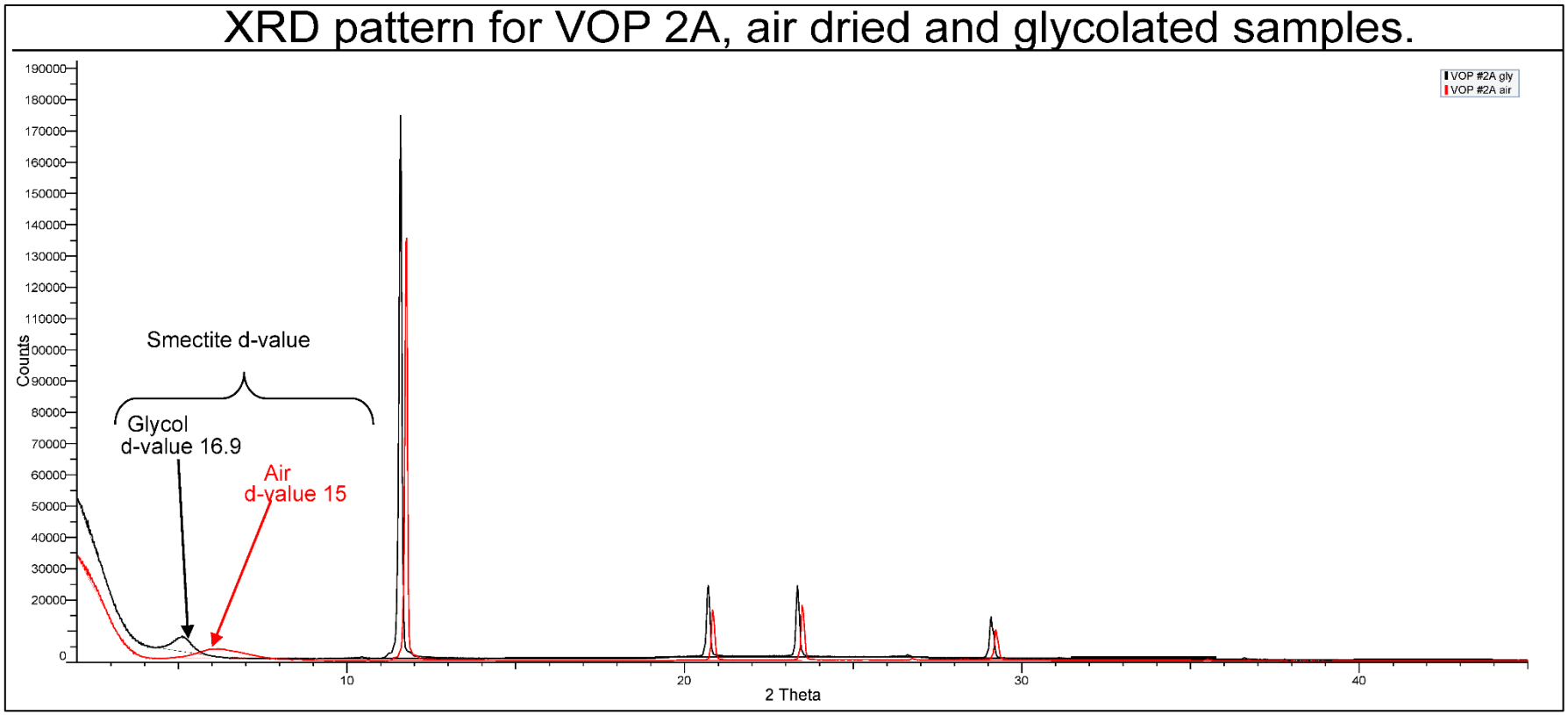

XRD pattern for VOP 2B, air dried and glycolated samples.

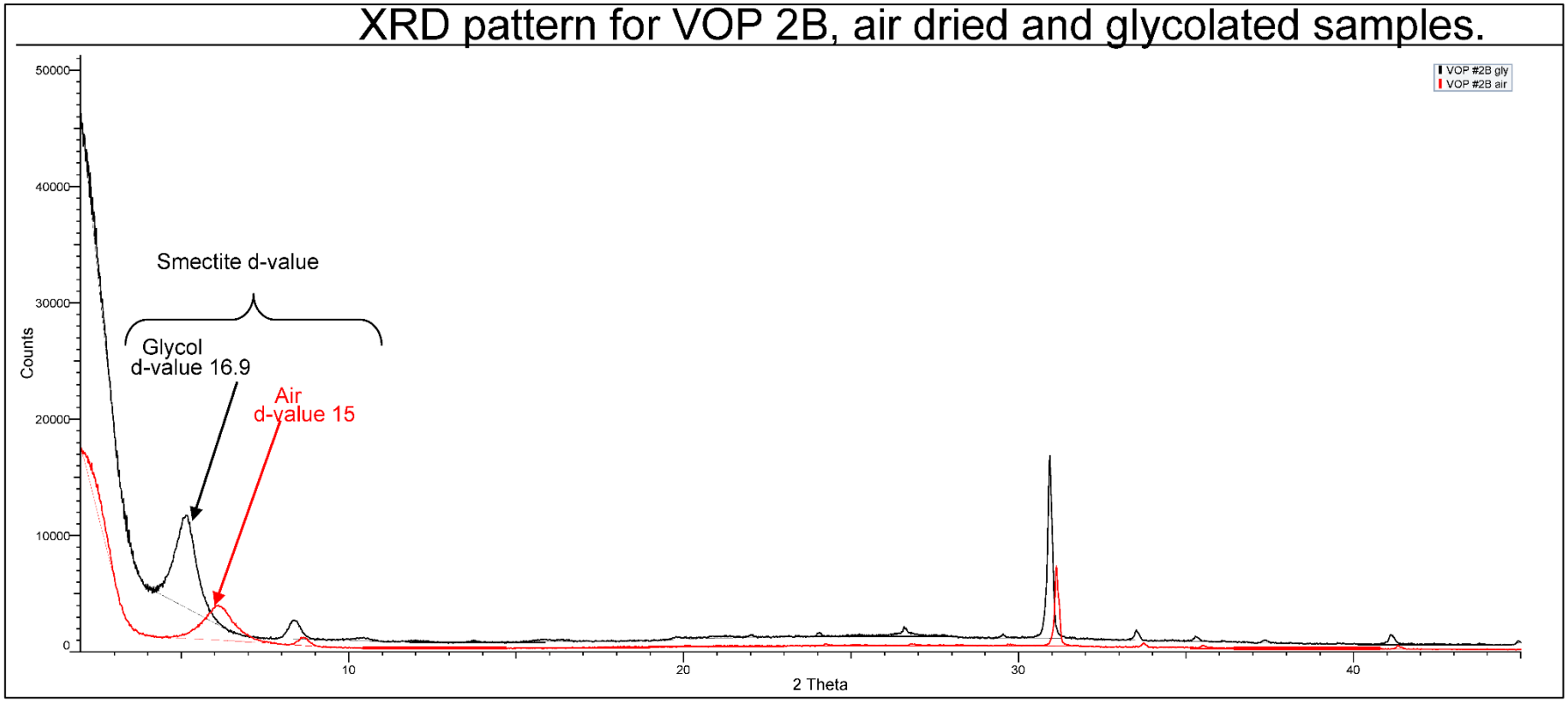

Appendix XII, Pictures of selected nannofossils identified from 11 samples. Images from Paleo Data, Inc.

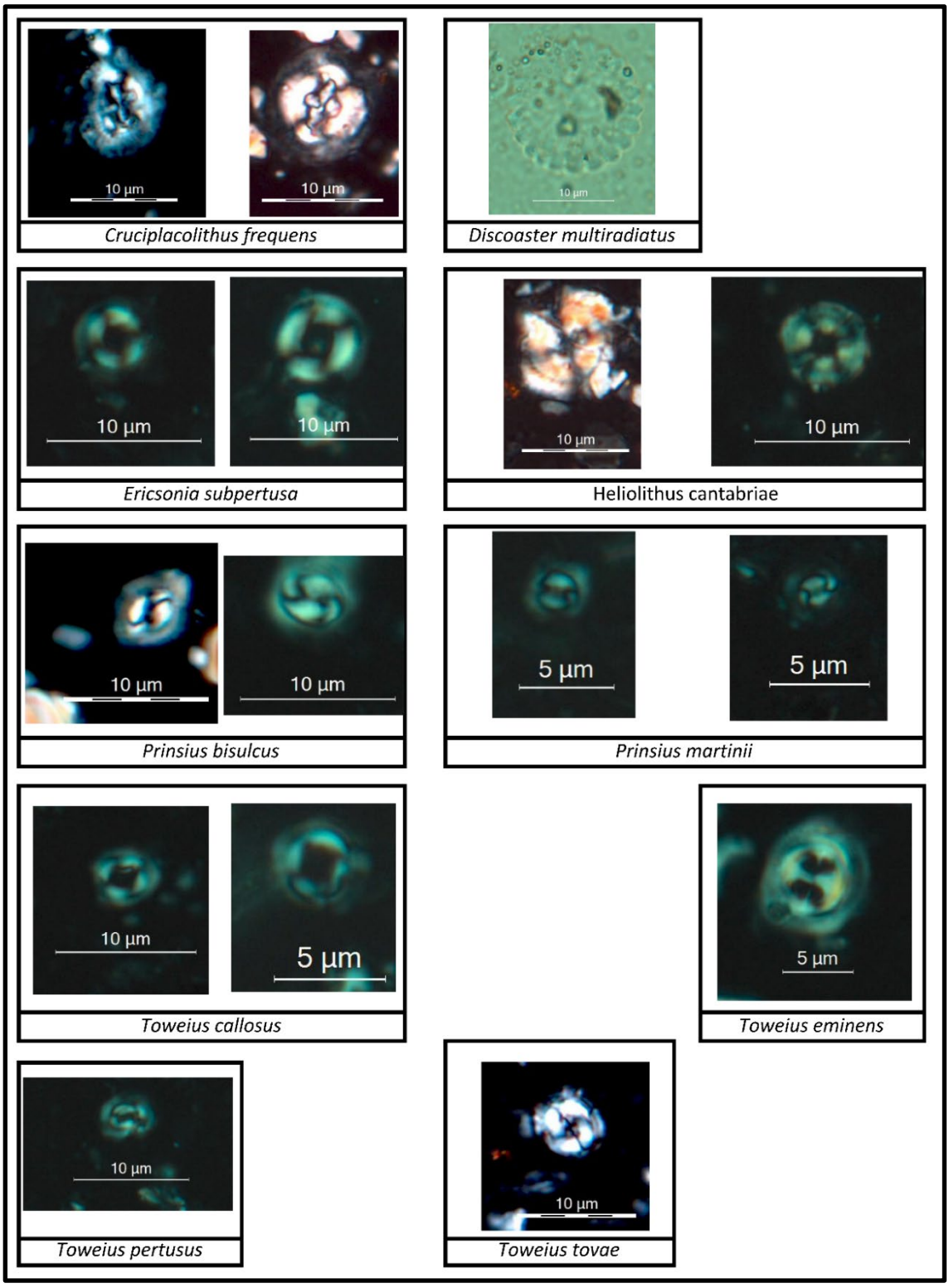

10 END NOTES

I. [i] All stratigraphic units in Belize are informal. Both the International Stratigraphic Guide, 2nd ed. (Salvador, 1994) and the North American Stratigraphic Code (NACSN, 2005) stated that formal units must be published in a recognized scientific medium and must include a statement of intent to designate that formal unit. On both points, all stratigraphic units in Belize fail to qualify as formal units. The original descriptions of Belize stratigraphic units whose names are in informal use today trace back to hand-typed (and subsequently photocopied) documents (i.e., not recognized scientific media) and they do not include statements of intent to designate. Therefore, all stratigraphic units in Belize are "provisional informal names," as discussed in the International Stratigraphic Guide, 2nd ed. (Salvador, 1994). Subsequent publications in recognized scientific media (e.g., King et al., 2004) have referred to these units, their descriptions, and in some instances their informal 'type localities,' but these publications have not formalized the units. Owing to these esoteric issues, the lower case "f" on formations and "g" on groups are used to make clear the continued informal status of these units and to be consistent with previous work (e.g., King et al. (2004) and references therein).

II. [ii] Data used in the image, tables and map was obtained from. Consent was requested and received from Geology and Petroleum Office Belmopan (GPO), Belize, to use and publish the data received, in this study.

III. [iii] The term 'type locality' is used here in tick marks ('') to indicate that this term was used in the original publication to refer to a place on the surface in Belize were the informal unit was well displayed. There are no 'type localities' for informal units (Salvador, 1994; NACSN, 2005) and these 'type localities' have not been published in a recognized scientific medium as required, therefore we are distinguishing this kind of 'type locality' from the requisite type locality or type section of formal units as described in the International Stratigraphic Guide, 2nd ed. (Salvador, 1994) and the North American Stratigraphic Code (NACSN, 2005), respectively.